CRANFIELD UNIVERSITY

KEVIN S. OPOKU

DETERMINING THE ONSET OF GRINDING BURN USING MAGNETIC BARKHAUSEN NOISE

CRANFIELD SCHOOL OF INDUSTRIAL AND MANUFACTURING SCIENCE

MRES INNOVATIVE MANUFACTURING - ADVANCED AUTOMATION AND DESIGN

CRANFIELD UNIVERSITY

CRANFIELD SCHOOL OF INDUSTRIAL AND MANUFACTURING SCIENCE

MRes INNOVATIVE MANUFACTURING – ADVANCED AUTOMATION AND DESIGN

Academic Year 2004 - 2005

KEVIN S. OPOKU

DETERMINING THE ONSET OF GRINDING BURN USING MAGNETIC BARKHAUSEN NOISE

Supervisors: Prof. D. J. Stephenson
Dr. I. Walton

Academic Year 2004 to 2005

This thesis is submitted in partial fulfilment of the requirements for the degree of Master of Research

ABSTRACT

A study of the quick non-destructive technique of Magnetic Barkhausen Noise (MBN) in detecting the onset of grinding burn in the absence of any microstructural changes during grinding has been undertaken.

51CrV4 Steel is a used in industry for manufacturing automotive parts (Nissan). Uniaxial tensile tests using a coarse surface whilst taking in situ MBN measurements were used to calibrate MBN to residual stress for hard and soft samples of 51CrV4. X-ray diffraction tests of some ground samples of hard and soft 51CrV4 samples were used to correlate the obtained calibration curves. A depth profile analysis was also carried out from results of MBN and XRD measurements of 51CrV4 soft and hard samples ground at different specific material removal rates.

The MBN Vrms and Vpeak parameters in the elastic deformation region were shown to behave linearly with total stress. A predictive model to calculate residual stress values showed good correlation in terms of the direction but the magnitude of the error was poor within its working limits. The Vrms and Vpeak and FWHM also showed a sharp change in the trend during the change from compressive to tensile stress.

The application of the MBN technique in detecting grinding burn before it happened meant that waste could be limited and grinding processes optimised without compromising the surface integrity of components.

ACKNOWLEDGEMENTS

I am grateful to my supervisors, Prof. D. J. Stephenson and Dr. Ian Walton for the availability, their guidance and for their technical expertise in the field of grinding and the Barkhausen Noise technique. Special thanks also go to the technicians who helped me with the different equipments during this thesis.

I am also grateful to my family, my girlfriend Lara, and my friends for all their encouragement and support.

Table of Contents

List of figures

List of Tables

Chapter 1 INTRODUCTION

Grinding is one of the most important processes of abrasive machining. It is used widely in industry, especially the aerospace and automotive, to manufacture highly accurate machine parts with very high form tolerances. In many cases, it is used as the finishing process and thus influences directly, the surface integrity of the part. Surface integrity is a term associated with the quality of a machined surface and it is defined in terms of properties such as fatigue strength, residual stress and wear resistance to mention a few. The surface integrity of components that are manufactured using the grinding process and indeed all the other manufacturing processes are very important due to the different environments they operate and the different conditions they are subjected to. Differing surface integrity properties will result in different performance, reliability and durability. A component failing under use can be so severe that it could result in a loss of life and multi-million pound lawsuits, hence the importance of ensuring that components that are manufactured by grinding are sound.

The Magnetic Barkhausen Noise technique is one of the many techniques which have gained importance in the machining industry as a way of non-destructively testing the surface integrity of machined components. In terms of surface integrity, this thesis will focus on residual stresses of components that have been manufactured using grinding. One of the most significant problems that affect the surface integrity of components manufactured using grinding is “grinding burn”. Grinding burn is caused by thermal damage during the process of grinding and it compromises the material being ground by reducing its service life and increasing its risk of failure by changing residual stress levels in the metal. Thermal damage, characterised as grinding burn may be in the form a discoloration of the surface (oxidation), a softening of the surface layers (temper burn), the formation of a white layer (hard brittle layer) during rehardening burn, the formation of tensile stresses and in severe cases microcracking.

Thermal stresses generated in the grinding process are the primary cause of tensile residual stresses (Chen et al., 2000). Grinding initially puts compressive

stresses into the workpiece as a result of mechanical deformation due to the normal grinding force (Snoyes et al., 1972). From Figure 1, it is seen that this mechanical deformation is superimposed with the thermal effects related to grinding.

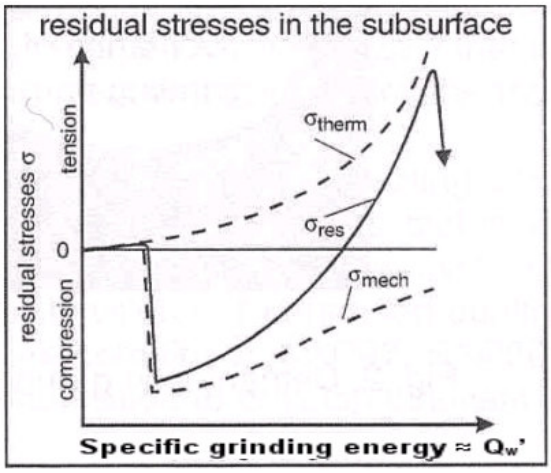

Figure 1: Change in residual stress of a ground part with increasing grinding power (Freimuth and Mandrysch 1999)

Increasing local temperatures causes an expansion and contraction of the workpiece which tends to change the initial compressive stresses to tensile ones. Compressive stresses are generally desirable as it increases fatigue life of the component being ground and its mechanical properties, whilst tensile stresses decreases it. Thus the occurrence of grinding burn can be detected by the change in residual stress.

Although a lot of techniques exist which are used to characterise the changes in ground parts such as X-ray diffraction (XRD), nital etching, ultrasonic, and eddy current testing, none have proved as easy to use, quick and functional among the non-destructive group than the Magnetic Barkhausen Noise (MBN) technique.

The key point in this thesis will be to map the grinding process in order to identity the stage during the change from compressive to tensile stresses that grinding burn occurs. This will be done by using different material removal rates and monitoring the residual stress changes using MBN. The information will then be used to develop a tool which will enable grinding burn to be detected before it

happens. To do this, different steel samples ground using different parameters will be compared and correlated with stress results from X-ray diffraction (XRD) methods and tensile testing methods. A stress depth profile (the behaviour of stress at different depths of a ground work piece) will also be analysed to characterise the effects of grinding burn at different surface depths of the samples.

1.1 Thesis Aims and Objectives

The aim of this study lies in characterising the onset of grinding burn in 51CrV4 steel samples using the Stresstech MBN apparatus and correlating measurements to X-ray residual test measurements and mechanical tensile test measurements. Changes in the output signal parameters of the MBN apparatus with changing grinding parameters will then be compared for any trends.

The main objectives are:

- Specially prepared 51CrV4 samples will be used to calibrate stress to the MBN parameters, investigating the relationships of the various MBN parameters and its effect on residual stress. This will be done using tensile testing techniques and the Stresstech MBN apparatus.
- Residual stress measurements taken with the X – ray diffraction (XRD) technique will also be used to help with the calibration by measuring the baseline residual stresses present in the tensile samples before they are used for mechanical tests needed for the calibration.
- The results from the calibration will be correlated to those from metallurgical examination of the surface and sub–surface microstructure and calibration of the MBN signal by the X – ray diffraction experiments.
- Results of stress measurements carried out in the Stresstech laboratories in Finland will be used to carry out a stress depth analysis to further test the correlation between the MBN parameters and XRD measurements.
- Further work if possible will be to investigate the impact of surface roughness on the MBN signal of the ground samples.

Chapter 2 LITERATURE REVIEW

2.1 Grinding

Grinding is an abrasive machining process together with honing, lapping and polishing. According to (Degarmo et al., 2003), abrasive machining is a material removal process that involves the interaction of abrasive grits with the workpiece at high cutting speeds and shallow penetration depths. Abrasive machining uses hard granular particles in changing the geometry and texture of the part by abrading or removing chips of the material with the abrasive. The abrasive refers to the hard granular particles which are often bonded to wheels of different geometries and sizes.

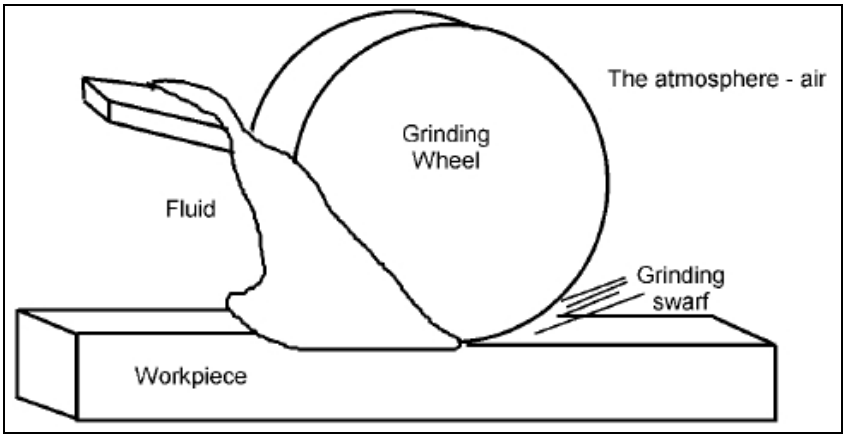

Figure 2: Elements of a typical grinding process (Marinescu, et al. 2004)

In grinding the abrasive is almost always in the form of a wheel rotating about its axis. Five main elements that affect the process of grinding are (Figure 2 (Marinescu et al., 2004)):

- Grinding wheel
- Workpiece
- Grinding fluid
- Atmosphere
- Grinding swarf

The grinding wheel does the machining and in the process it suffers wear. The grinding swarf is a combination of cut chips from the workpiece, the grinding fluid and worn abrasives grains from the wheel. The grinding fluid not only cools the workpiece by reducing the temperature but it also washes away the swarf and provides lubrication at the contact zone.

Marinescu, et al. (2004) also showed the interaction between the abrasive grain and the workpiece during grinding using Figure 3.

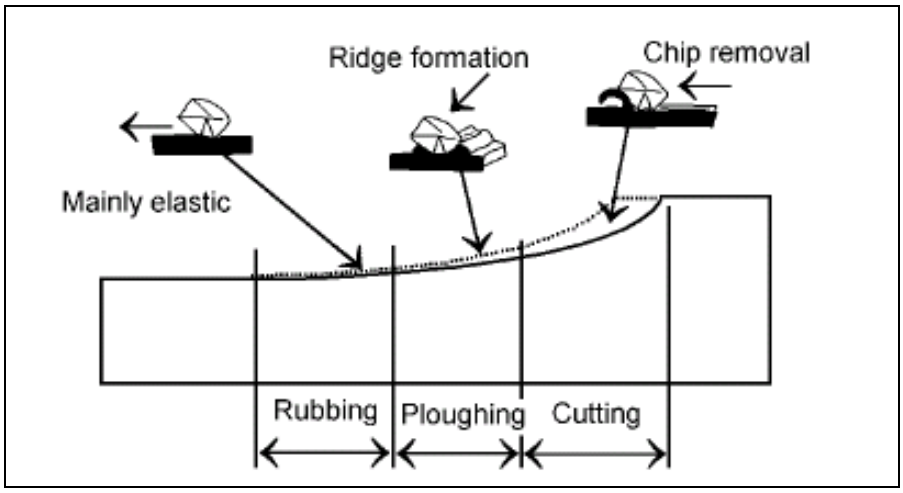

Figure 3: Material removal mechanisms (Marinescu et al., 2004)

Material removal was described by 3 mechanisms; *Rubbing, Ploughing and Cutting.*

Rubbing despite friction, causes some elastic and material deformation. Ploughing occurs when the penetration depth of the abrasive grain is increased causing ridges and scratches. Finally the Cutting action comes into play when penetration is further increased and material removal increases rapidly. Whereas the bulk of the energy from the Rubbing and Ploughing action goes into the workpiece in the form of heat, most of the energy from the cutting action is carried away in the form of grinding swarf (Griffiths, 2001).

The atmosphere also plays a part by reacting with the workpiece surface to form an oxide layer which helps by reducing friction and providing lubrication during grinding (Marinescu et al., 2004). However this effect is reduced with increasing wheel speed. The interacting layer in the contact zone is illustrated in Figure 4.

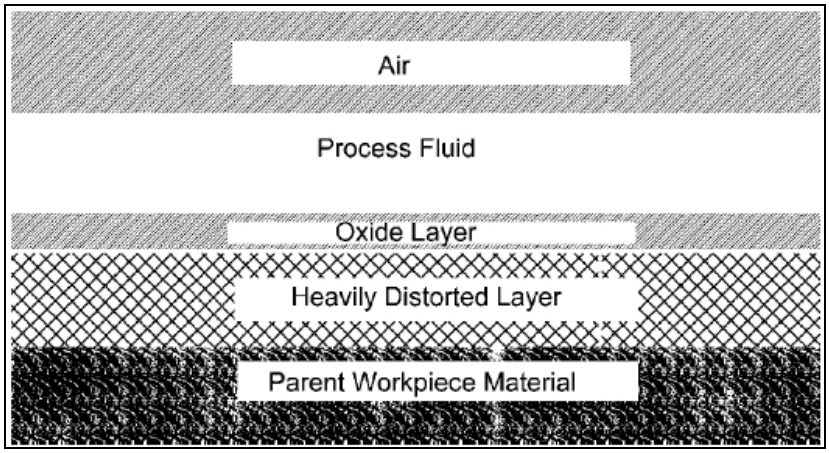

Figure 4: Interaction layers in contact zone during grinding (Marinescu, et al. 2004)

2.1.1 Grinding Wheel Specification

The various types of abrasives have different specifications however there are five main factors used in specifying a grinding wheel (Figure 5 (Marinescu et al. 2004)). That is;

- Abrasive type
- Abrasive grain sizes
- Grade
- Structure
- Bond

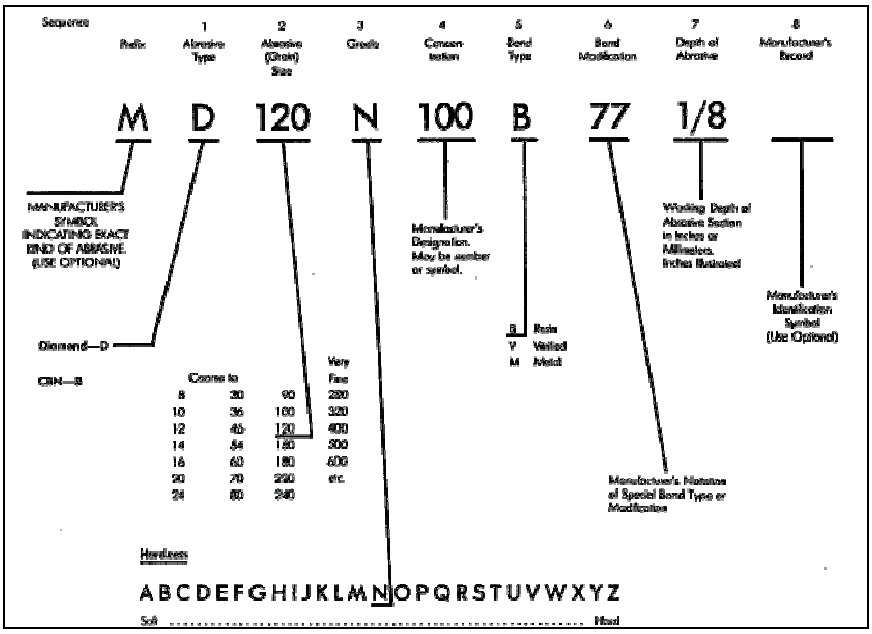

Figure 5: Standard naming system for diamond CBN wheel (Kutz, 2002)

2.1.1.1 Abrasives

In order to control wear, the grains of the abrasive must be harder than the material being ground even at high temperatures. The knoop hardness of the abrasives are summarised in Table 1. Common examples of abrasives are (Kutz, 2002):

Aluminium oxide (Al_2O_3): Also called Alumina and normally used commonly for the grinding of steels and not so hard materials because the grains dull prior to fracture. It is usually synthetic

Silicon Carbide (SiC): Silicon Carbide is normally used for low tensile strength materials such as cast iron, brass, stone and cemented carbides. They are synthetic and hard but brittle and this limits their use.

Cubic Boron Nitride (CBN): This is the second hardest natural or man – made substance to diamond but has superior thermal qualities to that of diamond. It is good for grinding hard, tough tools and die steels.

Diamond (C): Diamonds are the hardest abrasives known to man and it is normally used for tungsten carbide, glass and some die steels.

Table 1: Comparison of abrasives and their knoop hardness (Koshal 1993)

Abrasive	Al_2O_3	SiC	CBN	C
Knoop Hardness (kg mm^{-2})	2100	2400	4500	7000

CBN along with Diamond fall under the category of superabrasives. Marinescu et al., (2004) also attributed its popularity to its excellent thermal resistance (better than diamond), allowing work at 1900ºC and good chemical resistance to ferrous alloys. CBN delivers in terms of lower fluid temperatures**;** there is a reduced likelihood of oxidation and lower tensile stresses (Chen et al., 2002). It is very useful for cutting steels and has an excellent reputation in terms of durability (King and Hahn, 1986).

2.1.1.2 Grain sizes

For uniformity, wheel grain sizes are graded in various sizes by the numbers 4-600 depending on the kind of abrasives. Generally, grain sizes 4-24 are termed coarse; 30-60, medium and 70-600 fine. Fine grains produce smoother surfaces than coarse ones but are unable to remove as much metal (Kutz, 1998).

2.1.1.3 Grade

Grade refers to the strength of the bond holding the abrasive grains to the wheel. Wheel grade is defined as the resistance of the bond against abrasive grain extraction due to grinding forces (Marinescu et al., 2004).

2.1.1.4 Wheel Structure

The relationship between the abrasive grains, the bonding material and the space between them on the wheel is referred to as the structure. A close spacing is preferred for finishing operations and an open one for roughing due to its good self sharpening characteristics (Kutz, 2002). Open spacing also helps the fluid remove the cut chips from the wheel contact area which is essential when there is a risk of wheel loading or workpiece burn.

2.1.1.5 Bond type

Bond type demonstrates the kind of material used to hold the abrasive grains to the wheel in a specific shape. Examples of bonding materials used are: vitreous, resin, metal bonds etc.

2.1.2 Grinding Parameters

Important parameters that affect cutting conditions during grinding are the peripheral speed of the wheel, the workpiece speed, the depth of cut and the fluid used.

2.1.2.1 Peripheral speed of the grinding wheel (V_s)

The wheel speed is measured in meters per second (m/s) and can range from 20m/s to 250m/s depending on the grinding process and wheel type. The speed can be determined from Equation 1:

$v_s = \frac{\pi D n_s}{60 \times 1000}$	**Equation 1: Wheel speed formula**

where V_s is the peripheral speed of the wheel, n_s is the wheel rotation speed in rpm and D is the wheel diameter in mm.

2.1.2.2 Depth of cut (a_e)

Depth of cut is the advance of the grinding wheel in the direction perpendicular to the surface being ground. It has units in mm and rough operations normally have high depths of cut and finishing operations have lower values. *Sparking out*, is used to achieve very good surface finish and close tolerances by passing over the wheel on the surface without increasing the depth of cut until the sparks die out.

2.1.2.3 Workpiece speed V_w

This is the speed of the workpiece during grinding. It is normally expressed in m/min.

2.1.3 Grinding regimes

Different parameters for grinding have been grouped under different headings (wheel characteristics, removal rates and temperature traits (Figure 6)) to give a guide to the different characteristics associated with the surfaces when ground.

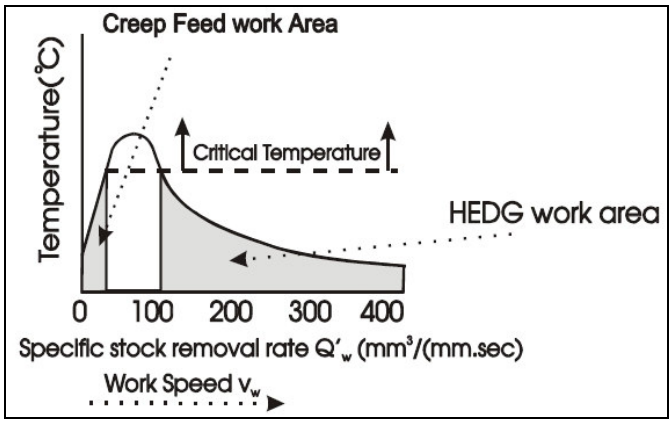

Figure 6: Different grinding regimes with their temperature and Q_w' traits (Tawakoli, 1993)

2.1.3.1 Surface (Reciprocating) grinding

Surface grinding involves the grinding wheel moving relative to a surface in a plane whilst a grinding wheel contacts the surface and removes a minute amount of material (Engineers Edge, 2007). The work reciprocates under the wheel and most machines provide cross-feed and automatic downfeed. Surface grinding is characterised by a low depth of cut at a high feed rate. Surface grinding is normally used for achieving very high tolerances on surfaces.

2.1.3.2 Creep feed grinding

Creep feed grinding emerged in Germany in the early 1960s and it is characterised by large depths of cut a_e and low work speed V_w. It is normally used in surface grinding together with Alumina wheels or CBN wheels. Another particular characteristic of creep feed grinding is the use of the fluid primarily as a coolant due to the high temperatures at the contact zone. Creep feed grinding with a CBN wheel increases productivity, improved surface integrity and decreased cost (despite the high cost of CBN wheels)

due to the good thermal characteristics of the CBN wheel (M. C. Shaw 1996).

2.1.3.3 High Efficiency Deep Grinding (HEDG)

HEDG combines high workpiece speeds, large depths of cut and high wheel speeds to produce high material removal rates. In this type of grinding regime, the fluid is used as a lubricant rather than as a coolant as the majority of the heat is taken away by the chips. Brinksmeier and Minke (1993) proposed that the fluid used in HEDG provided a hydrodynamic component of force which added to the force required for material removal. This hydrodynamic effect was evidenced as an increase in depth of cut a_e. Tawakoli (1993) also compared with creep feed grinding and HEDG (summarised in Table 2).

Table 2: Comparison between the different grinding regimes

	Reciprocating Grinding	Creep Feed Grinding	High Efficiency Deep Grinding
Depth of cut, a_e (mm)	LOW 0.001 – 0.05	HIGH 0.1 – 30	HIGH 0.1 – 30
Workpiece speed, v_w (mm/min)	HIGH 1 – 30	LOW 0.05 – 0.05	HIGH 0.5 – 10
Wheel speed, v_s (m/s)	LOW 20 – 60	LOW 20 – 60	HIGH 80 – 250
Specific material removal rate Q'_w ($mm^3/mm.s$)	LOW 0.1 – 10	LOW 0.1 – 10	HIGH 50 – 2000

2.2 Surface Integrity

Surface integrity is a subject covering the description and control of the many possible alterations (Figure 7) produced in a surface layer during manufacturing including their effect on the performance of the components in service (Koster et al., 1970). Increasing demands on component quality in terms of their life

cycle, mechanical properties, wear resistance and reliability among a host of factors means that effective ways of checking for the quality produced by grinding is imperative.

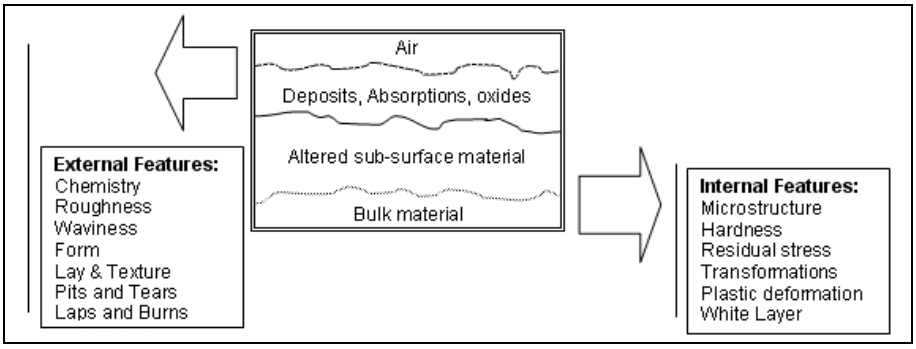

Figure 7: Schematic section through a machined surface (Griffith, 2001)

Relating this to grinding, a component with good surface integrity would probably have been machined under gentle conditions resulting in compressive stresses and with no thermal damage. Conversely, a low surface integrity would most possibly refer to a component which would have been machined under abusive conditions resulting in high tensile stresses and with thermal damage. Surface integrity can be evaluated under (Griffiths 2001):

- *Surface Topography*: Changes to the geometry of the workpiece such as surface roughness, waviness and lay, and
- *Surface Metallurgy*: Phase changes and hardness variations during treatment and machining and its impact on other properties of the workpiece such as fatigue, stress rupture and creep and tensile strength. It also includes chemical changes that occur during grinding such as the interaction of fluids, carbon content changes and the formation of oxides.

2.2.1 Surface Topography

Surface topography deals with the geometry of the surface of the ground surface. This is normally explained in terms of the surface finish or surface texture of the workpiece. Surface texture refers to the variation of a machined 3D surface from the nominal flat surface. This is due to the finishing operations

used for the finishing operation and irregularities linked to it. Surface texture is normally quantified in terms of roughness, waviness and lay (Figure 8).

- Roughness is a quantitative measure of the process marks produced during the creation of the surface and other factors such as the structure of the material. It is has the shortest wavelength.
- Waviness includes the variation from the nominal surface but within a longer wavelength.
- Lay refers to the Lay refers to the principal direction of the surface texture.

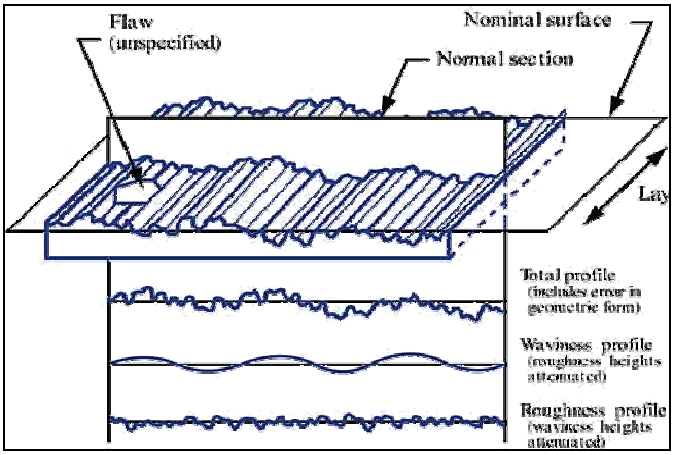

Figure 8: Surface texture characterisation (Rantala, 2004)

2.2.2 Surface Metallurgy

Surface Metallurgy is a study of the nature of the surface layer produced in machining. This includes microstructure changes such as the formation of oxides, phase changes, hardness changes, residual stresses and their effects on fatigue, distortion, tensile strength and stress corrosion. In the context of this thesis, the focus will be on phase change mechanisms that occur when grinding 51CrV4.

2.2.3 Grinding burn

Grinding burn was defined as metallurgical damage to the workpiece being ground as a result of high temperatures (Shaw, 1996). This can be seen as untempered martensite (UTM), overtempered martensite (OTM), and oxidation/decarburization and in some cases superficial microcracks. Grinding

burn compromises the surface integrity of a workpiece during grinding by introducing tensile stress and phase changes and sometimes cracks into the ground surface.

2.2.3.1 Oxidation burn

Oxidation occurs when oxygen reacts with the surface of the metal to form a thin oxide layer. This reaction is indicated by the free energy change ΔG. Some metals have a negative ΔG value causing the metal to readily oxidise (Small and Bishop, 1998). During grinding, the increase in temperature decreases the ΔG value causing oxidation at high temperatures. Oxidation burn causes a discoloration of the workpiece with colours ranging from light straw to dark blue at temperatures ranging from 450°C for conventional grinding (Marinescu, et al. 2004). This discoloration is usually just cosmetic and frequently occurs without the workpiece suffering any metallurgical damage. Oxidation burn is a poor indicator of grinding burn as it is unpredictable (Badger and Torrance 2000). Oxidation burn can also be removed by a spark out pass.

2.2.3.2 Temper burn (OTM)

A change of phase in the ground piece occurs when the surface temperature of the workpiece being ground reaches and exceeds the original tempering temperature of the steel (Guptha et. al, 1997). The surface is changed to overtempered martensite which is an unwanted soft layer (Figure 9).

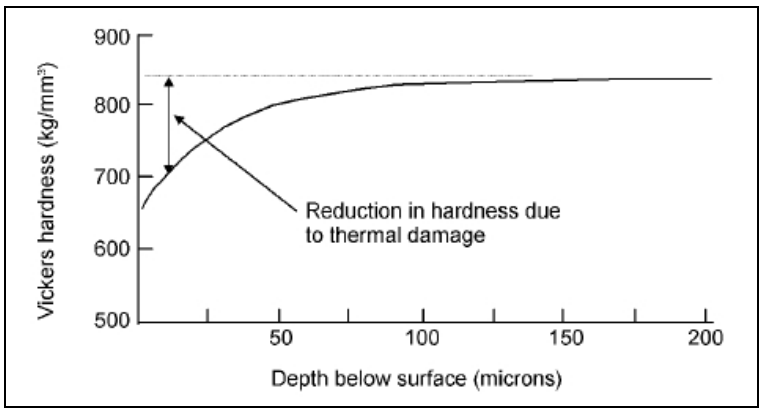

Figure 9: Softening of AISI 52100 steel due to temper burn (Marinescu, et al. 2004)

2.2.3.3 Re-hardening burn (UTM)

Re-hardening burn is characterised by a layer of untempered martensite (UTM). When the temperature of a Fe-C metal is increased above its austenizing temperature A_3 at 760ºC (Figure 10) its body-centred-cubic (BCC) structure changes to a face-centred-cubic (FCC) structure (reaustinization, γ). Decreasing the temperature rapidly from A_3 (due to the action of the grinding fluid) to temperatures below the M_s (martensite start) temperature (≈300ºC for 0.5% wt C) is sufficiently fast that transformation to any other phase than martensite will not occur (Walton et al., 2006). This transformation is a diffusionless process (so rapid the atoms have no time to intermix) with a metatstable material called untempered martensite (α') being formed (Figure 11, (Smith 1981)). This newly formed structure is a supersaturated solid solution of carbon in alpha (α) ferrite and it stops at a temperature M_f (≈150ºC for 0.5% wt C).

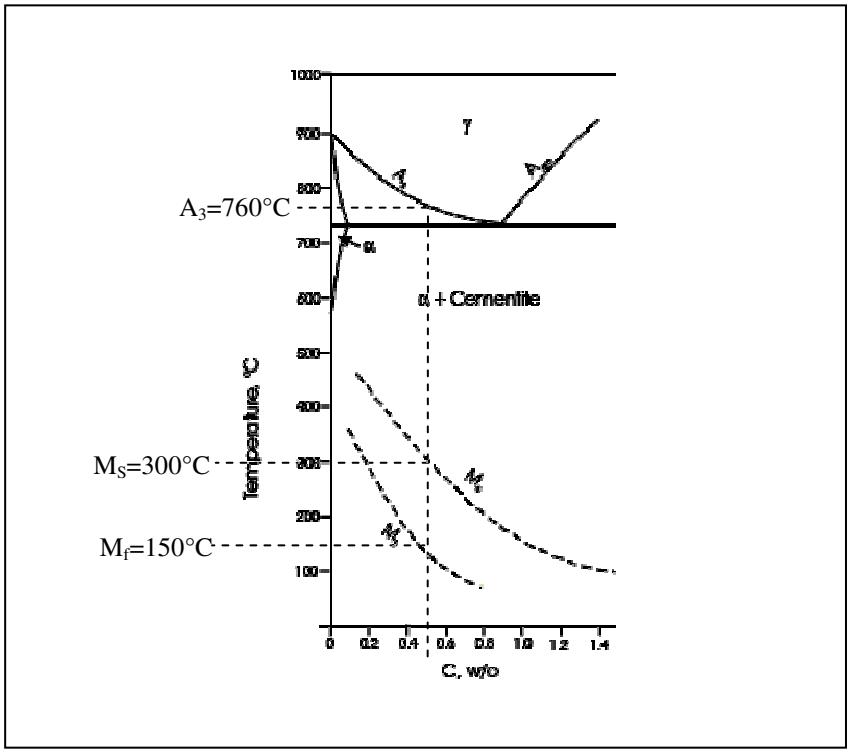

Figure 10: Fe - C phase diagram showing martensite start (M_s) and finish (M_f) curves when rapidly quenching from γ phase

Untempered martensite is a hard extremely brittle material which is undesirable and cannot be temper treated to obtain α plus Fe_3C.

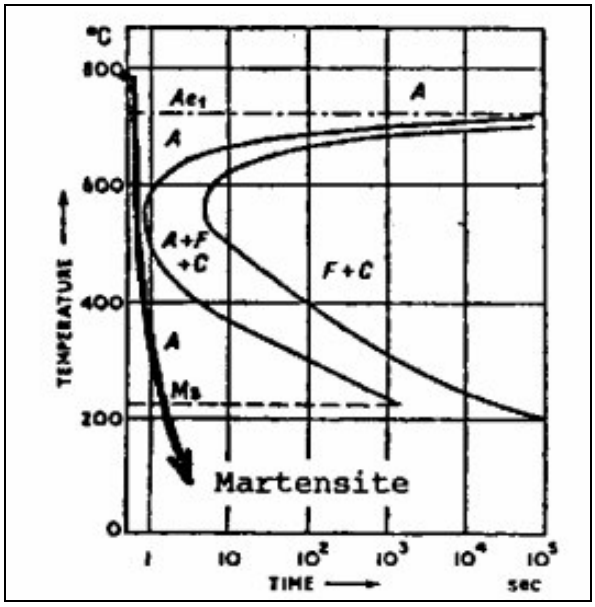

Figure 11: Isothermal transformation diagram for a eutectoid steel showing the cooling path for the formation of martensite (Smith 1981)

UTM shows up as a white later when etched using Nital. The presence of a small amount of OTM or UTM will cause a significant reduction in the fatigue strength of the material (Fields and Kahles 1971).

2.2.3.4 Tensile Residual stress

Residual stresses refer to tensional or compressive stresses present in a material in the absence of an applied force. In grinding, compressive residual stress formation is an important requirement for the surface integrity of stress sensitive components (Chen et al., 2000). Residual stress formation was during grinding was attributed to three mechanisms (Chen et al., 2000):

- thermal expansion and contraction during grinding,
- phase transformations due to high grinding temperature, and
- plastic deformation cause by the abrasive grains of the wheels.

Tensile residual stresses are caused by thermal expansion of the workpiece beyond its yield stress (Badger and Torrance, 2000). The most significant factor in the generation of tensile stresses was the expansion and contraction of the workpiece during grinding (Chen et al., 2000). Plastic deformation causes the production of compressive stresses as a result of mechanical deformation normal to the grinding source (Snoyes et al., 1972). Phase transformations results in tensile stresses.

Volumetric changes also induce compressive stress into the surface being ground, but generally mechanical loads cause compressive residual stress whereas thermal loads cause tensile residual stress (Figure 1, (Brinksmeier, 2003)).

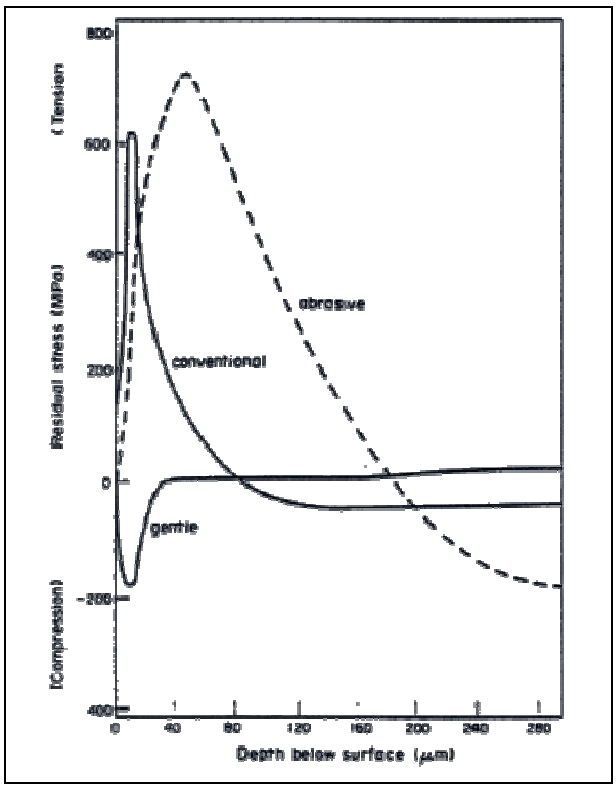

Figure 12: Variation of residual stress with different grinding regimes (Metcut Research Associates 1980)

During grinding, the parameters of grinding can be used to control the residual stresses produced. Figure 12 illustrates the residual stresses

produced under different severity of grinding regimes. Brinksmeier (2003) expanded on this point which is summarised as:

- Increasing the depth of cut increases the specific material removal rate and the grinding power which can cause thermal loading and a shift from compressive to tensile residual stress.
- The specification of the wheel can also affect the residual stress formed on the surface after grinding. Brinksmeier (2003) compared the a Cubic Boron Nitride (CBN) wheel with a Corundum wheel and found that the CBN wheel produced compressive stresses at the surface layer due to the good thermal conductivity and effective chip formation compared with the Corundum wheel.
- He also noted in the same experiments that residual stresses shifted from tensile to compressive stresses for increasing grain sizes.

Brinksmeier's (2003) findings were based on a series of experiments on 100 Cr 6 (AISI EN52100) using surface grinding with different parameters. Brinksmeier (2003) concluded that decreasing the depth of cut to decrease the specific material removal rate can reduce the thermal load on the surface being ground. However, decreasing the work speed will increase the thermal load. Hence, a decrease in the thermal impact on the workpiece can be achieved by increasing work speed which in turn decreases the specific material removal rate which will in turn result in a higher productivity.

2.3 Residual stress detection methods

Residual stresses can be classified under 3 categories according to the scale under which they are analysed. Type I stresses are defined over a few grains and Type II are evaluated over a single grain and Type III over an atomic scale (Figure 13).Type I stresses are called macrostresses and Type II and III microstresses.

Methods of evaluating macrostresses can be grouped generally under destructive and non-destructive. Non-destructive methods such as the MBN technique will be considered as well as destructive methods such as X-ray diffraction which is the industry standard and most trusted residual measuring technique.

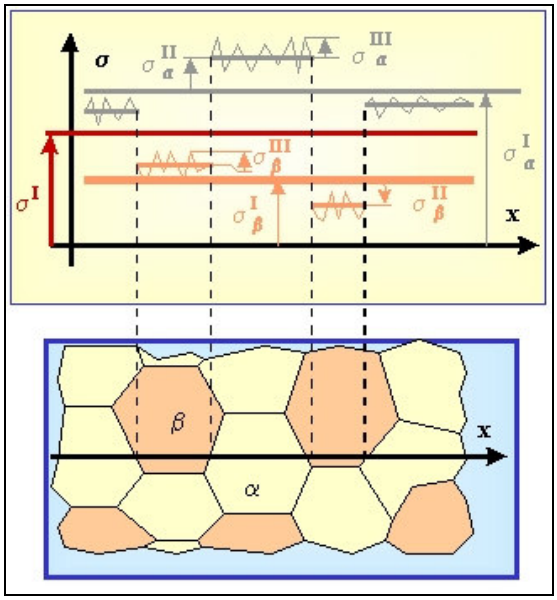

Figure 13: Type I, Type II and Type III residual stress characterisations (Physique & Industrie 2003)

2.3.1 X – ray Diffraction method (XRD)

X – ray diffraction is a powerful technique used to quantify and describe residual stresses and phase characterisations of materials (internal stresses, grain size, phase composition etc) (Toney, 1992). When macrostresses are present in a material, the lattice spacing between crystals change from their stress free values to new ones depending on the residual stresses and their elastic constant.

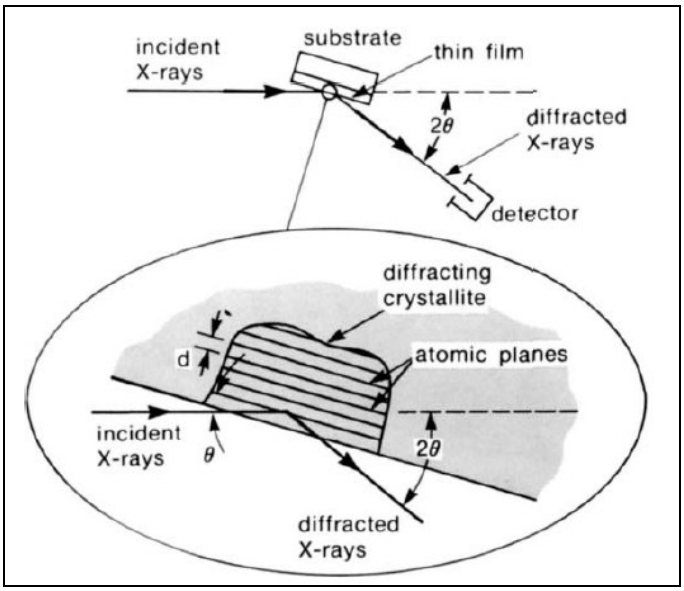

Figure 14: Basic features of a typical XRD experiment (Toney 1992)

This produces a shift in the position of the diffracted ray and thus a change in the Bragg angle (Figure 14). X – ray beams will be diffracted from a given family of beams as if the planes were being reflected. This diffraction is governed by Bragg's equation (Equation 2):

$n\lambda = 2d\sin\theta$	**Equation 2: Bragg's equation**

Where n is an integer corresponding to the order of diffraction.
λ is the wavelength of the diffracted x – ray radiation
θ is the angle of incidence of the crystal plane

The working equation (Equation 3) mostly used to relate strains (in the direction given by ϕ and ψ) and residual stress is (Brandes and Brook 1992);

$\sigma_\phi = \frac{d_{\phi\psi} - d_0}{d_0} \times \frac{E}{1+\upsilon} \times \frac{1}{\sin^2\psi}$	**Equation 3: Relation between XRD and Residual stresses**

where σ_ϕ is the stress tensor, $d_{\phi\psi}$ and d_0 the interplanar spacing of planes with normal parallel to the surface normal and at an angle ψ to the surface normal. E is Young's modulus and υ the Poisson ratio.

Though several methods are used, the most popular are the (a) two-exposure method and the (b) $\sin^2 \psi$ method. The $\sin^2 \psi$ is probably the most popular in use in today, its major advantage being that it uses a number of inclined angles ψ instead of one (Kandil, et al. 2001). The values of the lattice spacing $d_{\phi\psi}$ are plotted against $\sin^2 \psi$, and the stress σ_ϕ is derived from the slope of the line, or the elliptical fit.

2.3.2 Neutron Diffraction

The principle exploited in using neutron diffraction for residual stress measurements is very similar to X – ray diffraction, the main difference being that neutrons are used instead of X – rays. Neutrons have a bigger depth penetration (0.2mm to 25mm for steels) compared to X – rays (10mm) and the equipment used for neutron diffraction is very expensive with only a small number of manufactures in the world (ISIS in Didcot, ILL in Grenoble, Saclay in Paris and Chalk River in Canada) (Kandil, et al. 2001). Neutron diffraction relies on the changes in lattice spacing being used to calculate stress.
With translational and rotational movements of the component and high spatial resolution, neutron diffraction can also be used to generate complete three-dimensional strain maps of the components.

2.3.3 Ultrasonics

Residual stresses directly affect the velocity of ultrasonic waves (acoustoelastic effect). The acoustoelastic coefficients used to carry out the measurements are normally evaluated from calibration tests. This has the advantage of being able to measure the bulk of the material, but poor spatial resolution makes this method more suited to routine inspections (Kandil, et al. 2001).

2.4 Magnetic Barkhausen Noise (MBN) Technique

2.4.1 History

Prof. Heinrich Barkhausen, a German physicist, was born in 1881 in Bremen, Germany. He was educated in the Munich and Berlin universities and obtained

his doctorate in Gottingen. He worked on the theories of spontaneous oscillations and non-linear switching elements and developed electron-tube coefficients that are still in use today whilst working for Siemens and Halske laboratories. He also researched on acoustics and magnetism which led to the discovery of the Barkhausen effect.

2.4.2 Introduction

The Magnetic Barkhausen Noise (MBN) is a collection of noise-like signals (Figure 15), obtained when an alternating magnetic field is applied to a ferromagnetic material due to sudden changes in the magnetisation under an applied magnetising field.

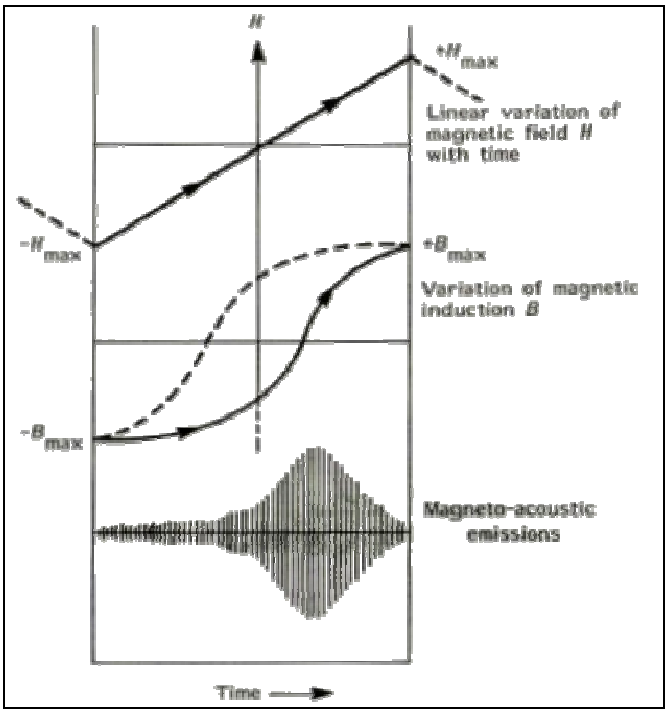

Figure 15: Magnetic Barkhausen Noise with associated magnetising field (Jiles, Review of Magnetic Methods for Non-destructive Evaluation 1988)

Ferromagnetic materials are made up of magnetic domains, with adjacent domains being separated by Bloch walls. These domains are magnetised along their easy direction when there is no applied magnetising field, and, as their overall magnetisation is the sum of all the domains, the magnetisation will be

zero. An applied magnetising field will cause the Bloch walls to move so that domains aligned close to the field direction grow at the expense of those that are less aligned. The movement occurs in sudden jumps as the domain walls break away from pinning sites such as dislocations, precipitates and grain boundaries (Stewart et al., 2004), also resulting in a change of magnetisation of the material. Prof. Barkhausen discovered that the change in magnetisation was not a continuous process but rather a series of single sudden jumps. This can be created by applying a magnetic field to the ferromagnetic material and "listening" for Barkhausen noise with the help of a conducting wire on the surface of the material. Figure 16 illustrates the generation of MBN under an applied magnetising field.

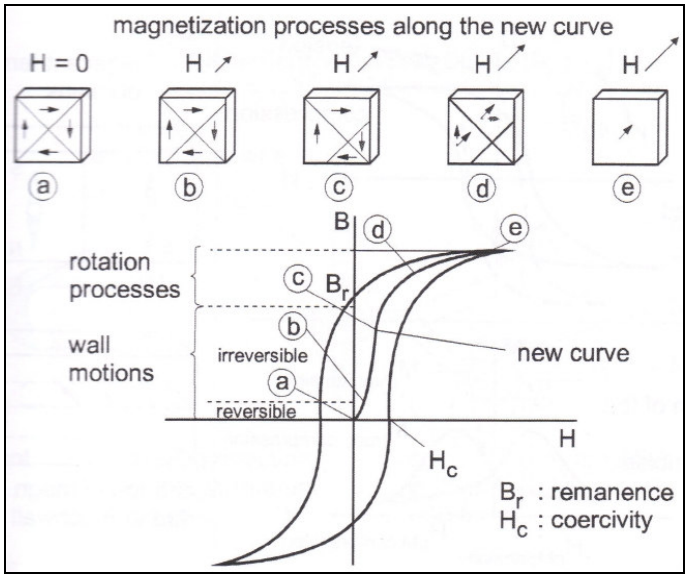

Figure 16: (a) no magnetising field, (b) – (e) applied field and change in magnetisation (B. Karpuschewski 1998)

The measuring principle employed by the MBN technique is based on the fact that the magnetic domain structure of ferromagnetic materials is influenced by stresses (residual and applied) and metallurgical parameters such as hardness in sub-surface zones (Karpuschewski and Mandrysch, 1998). The effect of stress on MBN is based on the magnetoelastic phenomenon (Jiles, 1988).

A demagnetised stress–free single crystal of a ferromagnetic material when analysed shows that under tensile stress, the magnetisation direction parallel to the stresses increases, whilst those perpendicular to it decreases until they

disappear. With compressive stresses the opposite happens with directions perpendicular to the magnetisation direction increasing whilst those parallel to the magnetising direction disappear (Figure 17) (Karpuschewski, 1998).

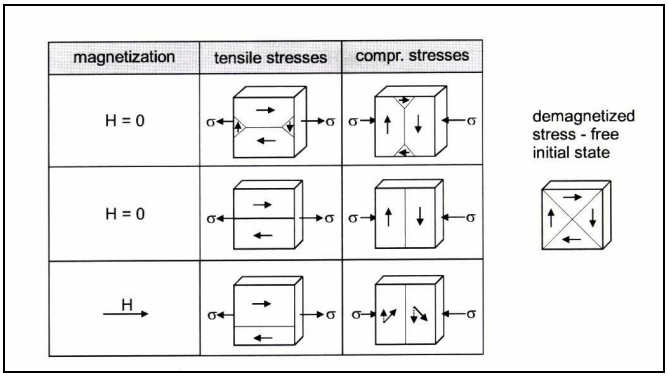

Figure 17: Domain wall movements under tensile and compressive stress and magnetising fields (Karpuschewski 1998)

The presence and distribution of elastic stresses in the material will influence the Bloch walls to find the direction of easiest orientation to the lines of the magnetic flux. Subsequently, a tensile stress will increase the value of the MBN signal and a compressive stress will decrease it (Tonshoff et al., 1998) (Figure 18).

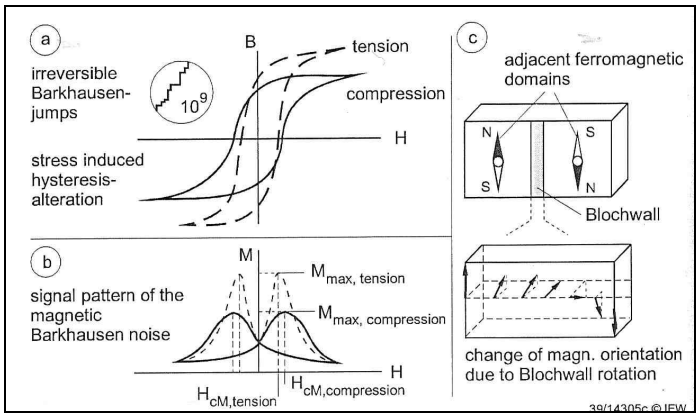

Figure 18: Magnetisation of a ferromagnetic material when (a) under compression and tension and (b) its corresponding MBN signal and (c) its Blochwall changes (Karpuschewski 1998)

Grain size, dislocation density and plastic deformation relates to the microstructure of materials and normally act as a form of barrier for Bloch wall movements. This means that MBN signals will differ between materials and change in microstructural properties (such as hardness) will affect the MBN signal.

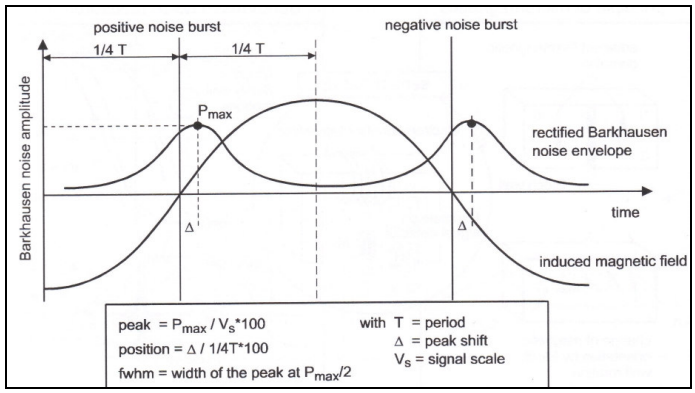

Figure 19: Measurement quantities (Tonshoff et al., 1998)

Tonshoff et al., (1998) noticed during their work on residual stress measurements on welds on deep drawing sheets that P_{max} was mainly used to quantify stress.

Donzella et al., (2003) detailed the effect of stress and microstructural changes on the different parameters derived from the MBN signal whilst carrying out stress and microstructure evaluation of steel specimens. They were able to acquire the MBN signal to lie between 2 consecutive zeros of the exciting coil voltage signal (the "burst"). The "positive burst" corresponded to the positive of the driving signal and the other the "negative burst". The absolute mean value of the burst was calculated and the consecutive bursts were averaged. They found that the Vrms voltage was the most sensitive to stress whilst the hysteresis loop parameters (B_r, H_c, μ_{max}) were almost insensitive to stress. The MBN envelope shape parameters (M_0, M_1, M_2) were also found to be sensitive to both stress and microstructure (Figure 20).

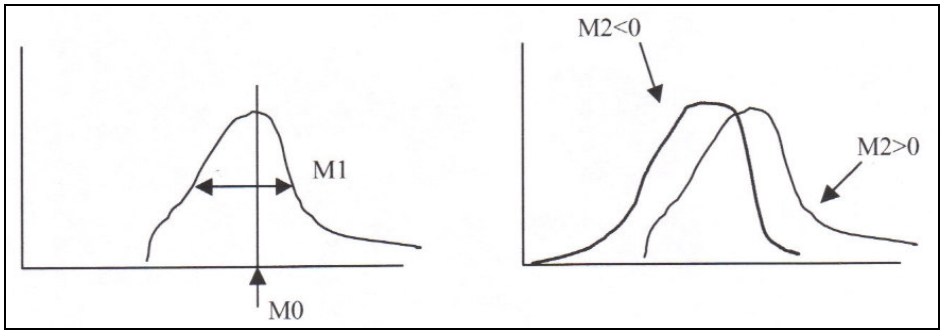

Figure 20: Mo specifies max MBN signal with respect to excitation signal, M_2 represents the spreading around M_0 and M_3 specifies if signal is concentrated more to the left or right of M0 (Donzella, et al. 2003).

Other results of their evaluation tied in with previous studies with the MBN signal increasing with tensile stresses and decreasing for compressive stresses. They also found out that the MBN envelope was higher and thinner (low M_1) for tensile stresses and lower and thicker for compressive stresses (high M_1). This finding was also consistent with the work of Gatelier-Rothea, et al. (1998) on carbon-iron binary alloys using MBN.

2.4.3 Influence of microstructure, applied and residual stress on MBN

Ng et al., (2003) correlated results of MBN measured signals to the microstructure and mechanical properties of low carbon steels (0.13% wt) and found that samples with small grain size had more intense MBN signals than those with larger grain sizes. This was due to the fractional volume of the grain boundaries acting as sites for domain wall unpinning. His experiment involved loading the samples annealed at different temperatures to a uniaxial tensile load until fracture, whilst taking in situ MBN readings. He also documented the behaviour of the MBN signal under the three regions of the stress – strain curve where the samples undergo elastic deformation, plastic deformation and necking/fracture. For elastic deformation, there was an initial sharp increase in the MBN Vpeak as applied stress was increased in the tensile direction. Upon yielding, there was still an increase in the MBN Vpeak, though with a gentle and steady slope as applied stress was increased in the tensile direction. Upon necking, the MBN Vpeak exhibited a gentle declining slope until fracture (Figure 21).

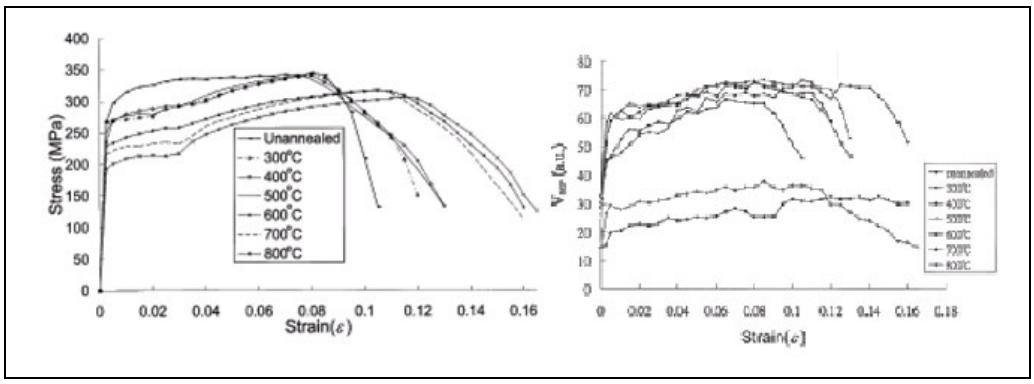

Figure 21: Stress-Strain curve with corresponding MBN-strain curve

Stefanita et al., (2000) found that during plastic deformation, the behaviour of MBN with stress departed from the linear trend reported earlier.

Kleber and Vincent (2004) also investigated the impact of elastic and plastic deformation achieved in tension and compression using Armco iron and a low carbon steel. A tensile plastic deformation showed an increase for Armco iron while it was a steep decrease in the low carbon steel. A comparison between the tensile and compressive trends, as well as between the elastic and plastic deformation region enabled them to attribute these effects to two mechanisms. That is, the effect of residual internal stresses through magneto-elastic coupling and dislocation–domain wall interaction. In Armco iron, the latter mechanism seems to have the strongest influence on the Barkhausen noise, while in the low carbon steel the influence of residual internal stresses prevails (Kleber & Vincent, 2004). Their work also showed that plastically deformed work parts can be detected using MBN.

V. Moorthy et al., (1999) studied the use of the MBN technique to study 0.2% carbon steel and 2.25Cr-1Mo Steel under different tempered conditions. The samples were subjected to an increasing uniaxial tensile load up to its maximum, unloading after each load to measure its MBN signal. Moorthy et al., (1999) split the effect of the stress-strain on the magnetic parameters into four stages. That is;

1. Perfectly elastic: The MBN signal stayed fairly constant as in the virgin state of the sample.
2. Microplastic yielding: There was a significant decrease in the MBN V peak as a result of dislocation pile-ups reducing the mean free path of the domain wall displacement.
3. Macroyielding: A sharp increase of the MBN signal amplitude, and
4. Progressive plastic deformation: A fairly linear decrease of the MBN signal as a result of the combinational effect of the introduction of compressive residual stresses on the surface and the increase of dislocation density during plastic deformation.

Moorthy, et al. (1999) only took their measurements after loading the samples with a specific load and unloading before taking the MBN reading.

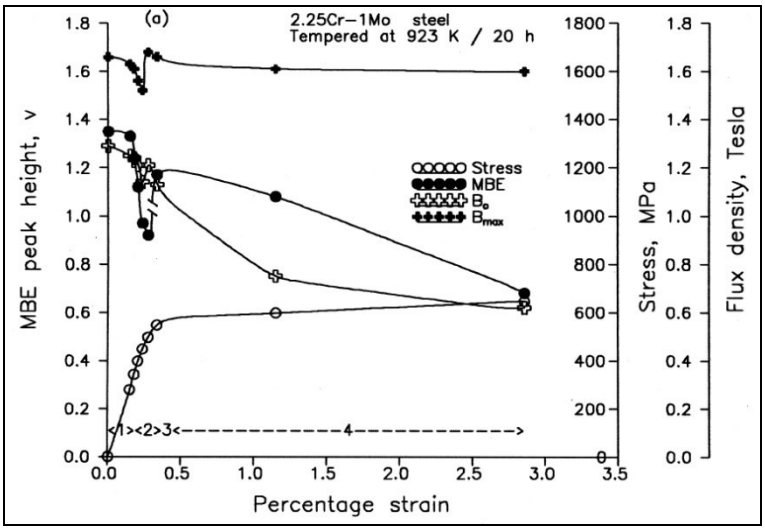

Figure 22: Variation of MBN Vpeak with the stress-strain curve showing 4 mechanisms.

Moorthy, et al. (1999) showed that the MBN profile showed the different stages much more distinctly than the hysteresis curve. This further confirmed that the stress-strain curve and the MBN technique can be used to isolate the different effects of residual stress and dislocation density.

Dhar A. et al., (2001) investigated the influence of uniaxial deformed hot-rolled steel samples on MBN signals when subjected to different magnitudes of plastic strain. They found that the MBN energy initially increased with increasing plastic strain followed by a decrease at higher plastic deformations. Further increase resulted in an independent relationship between plastic strain and MBN energy.

The effective depth of the MBN signal was reported as 30% – 50% of the value calculated from the Equation 4 given by (Jiles and Suominen, 1994);

$\delta = \sqrt{1/(\pi . f . \sigma . \mu_o \mu_r)}$	**Equation 4: MBN depth equation**

Where f is the frequency in Hz, σ the conductivity in $\Omega^{-1}m^{-1}$, $\mu_o = 4\pi \times 10^{-7}$ $H.m^{-1}$ the permeability of space, and μ_r the relative permeability. From

Equation 4, residual stress can be investigated at different depths under the surface of the metal.

Work by Ng. et al. (2001), focussed on using the parameters obtained from Barkhausen noise, in particular the root mean square voltage (rms), and the half maximum width (FWHM) of the profile in evaluating the amount of carbon in fabricated steel parts. Their evaluation was because of the advantages of the Barkhausen noise had over infra red spectroscopy which was the common technique of evaluating carbon contents. They concluded that the MBN technique was a possible alternative in evaluating the microstructure of plain carbon steel since the values of FWHM and Vrms increased with increasing carbon content.

Work by Gathlier –Rothea et al., (1998) investigated the use of the MBN technique in characterising the microstructural states of carbon – iron binary alloys using 130 p.p.m. carbon-iron alloys in various physical and metallurgical forms. They found that the Vrms of the MBN signal decreased with grain size due to the Bloch walls and pinning sites. They also discovered that the rms signal is not the same in tension and in compression due to magnetostriction.

2.4.4 Grinding burn detection using MBN

There has been extensive work in the application of the MBN technique in evaluating residual stresses and surface integrity imperfections such as burn and softening after machining and heat processes. This is primarily as a result of the advantages associated with the MBN technique as a non-destructive tool. Desvaux, et al., (2004) concluded that the MBN technique was quick and well suited to industrial imperatives connected to the on-line measurement when they carried out work on using the MBN for surface residual stress evaluation of aeronautic bearings.

The MBN technique is a comparative tool and hence the need for a conventional stress detection method to calibrate it. X-ray diffraction, simple

cantilever beam experiments, 4-point bending and uniaxial and biaxial tensile tests are all examples of calibration methods.

Shaw, Hyde and Evans (1998) based their research on MBN on using it to detect grinding damage in gear steels. En36 case carburised steels were used in making specimens. The specimens were then treated to simulate 3 scenarios; no grinding damage, temper burn (softening) and rehardening. Residual stress measurements to a depth of 8 µm were then taken using an X-ray analyser and a Vicker's hardness reading. A load was applied to the specimens with the aid of a cantilever arrangement to calibrate the MBN readings to stress. The load was increased after MBN measurements, without unloading to give a range of -1200 to +1200MPa. The results from the calibration showed an almost linear region and a saturation effect at high applied loads. The linear region of the calibration curve pointed to a direction where it could be used as a prediction tool in detecting the onset of grinding burn by detecting the level of residual stresses in the surface of the component.

Stefanita et al., (2000) worked on the effects of elastic and plastic deformation on Barkhausen noise using hot rolled mild steel plate with a yield point of ~190 MPa. Their work reiterated the fact that applied tensile stress increases the Barkhausen signal due to a strong magnetic easy axis in the stress direction whereas compressive stresses decrease this signal due to a magnetic easy direction perpendicular to the stress direction. Stefanita et al., (2000) also showed that the elastic region affected the MBN signal far greater than the plastic deformation region. This was attributed to an increase in dislocation density which reduces the domain wall movement and in turn reduces the MBN signal irrespective of whether the applied stress was increasing or decreasing. Hence as a predictive tool, the MBN technique would have to be used within the elastic deformation region.

Gauthier et al., (1998) reiterated the importance of calibrating the MBN technique with a known trusted technique during their work on cold formed

steel. They used a cantilever beam set-up to apply varying loads uniaxially whlist taking MBN readings on the inside and the outside of the sample. The calibartion curves that were produced from the data were found to be in good agreement with conventional methods. This was further correlated to cutting and sectioning methods and X-ray diffraction with good correlation results.

Gupta et al. (1997) investigated the technique of MBN in detecting grinding damage in ground samples of 52100 steel using different conditions of fluid conditions. That is normal flow (100%), half flow (50%), quarter flow (25%) and no flow (0%) corresponding to various degrees of grinding burn. Under the same grinding conditions, micrographs of the samples from the four flow conditions showed that the 25% flow and the 0% flow samples had undergone overtempered martensite and untempered martensite thermal damage respectively. The 0% fluid sample had a white layer at the surface followed by a layer of overtempered martensite before the bulk material. Analysis of the samples with the Barkhausen technique showed that the V peak (related to V rms) gave a good relation with the change in residual stress in the ground samples (Figure 23).

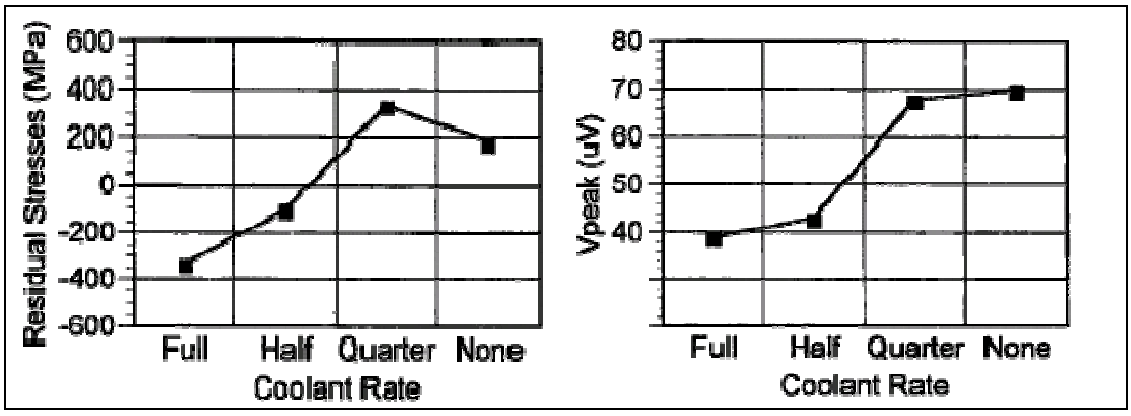

Figure 23: Measured residual stress and measured V peak of the same sample (Gupta et al, 1997)

Gupta et al. (1997) also showed that peak width of the Barkhausen technique (also cited as the full width half maximum) was effective in showing change in microstructure as impurities tend to pin the magnetic Bloch walls obstructing its movement (Figure 24). The conclusion of the work from Gupta et al. was that

Barkhausen noise was a viable tool in the determination of surface damage of ground components.

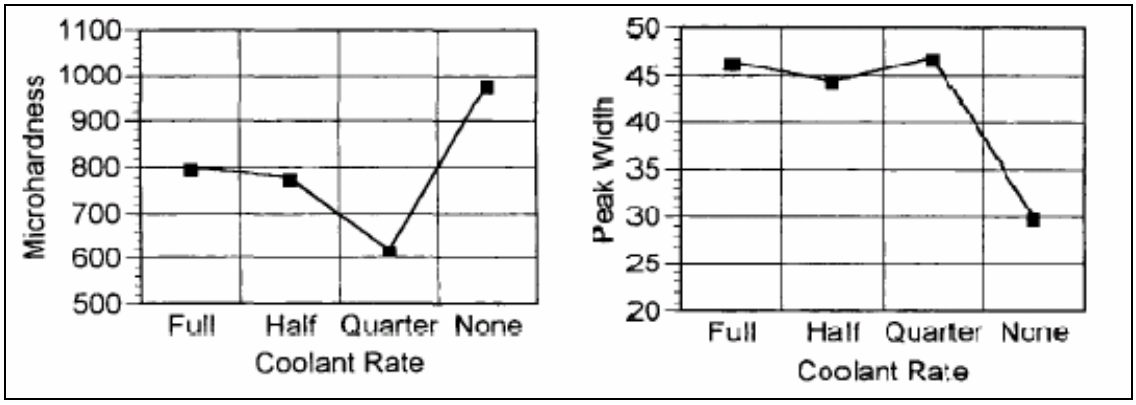

Figure 24: Peak width correlation with hardness changes (Gupta et al., 1997)

The SAE ARP 4462 (1991) paper also reinforces the use of the Barkhausen technique in the detection of grinding burn in high strength steels. The report sets out guidelines on the calibration, measurement procedure and general guidelines as to the adoption of the Barkhausen technique as a tool in detecting grinding burn. Though very generalised with no theory on how it works, it classifies grinding burn into “sound surface”, “minor defect”, “moderate defect” and “severe defect” and gives typical signal responses (Figure 25) as to rejection guidelines. It also suggests the Barkhausen technique as a first test method during quality checking with further checks by the nital etch method.

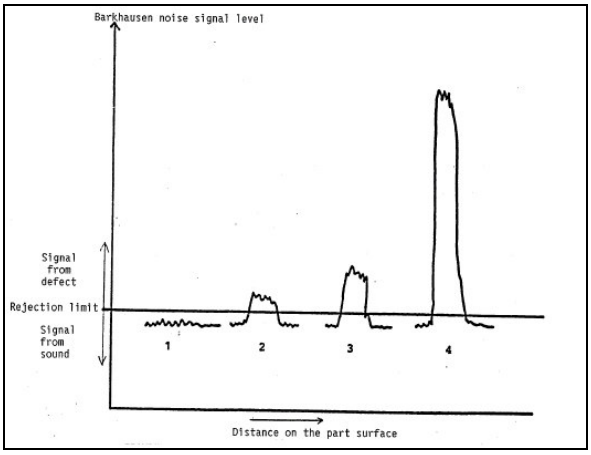

Figure 25: Acceptance criteria for defects (1 = sound, 2 = minor defect, 3 = moderate defect, 4 = severe defect) (SAE ARP 4462)

The report also illustrated the signal shapes in the presence of microstructure damage such retempering and rehardening (Figure 26).

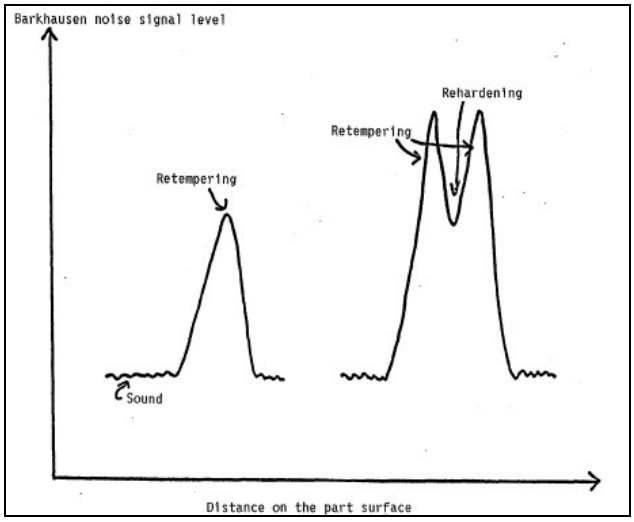

Figure 26: Retempering and Rehardening burn signal characteristics (SAE ARP 4462)

Comparisons of other testing techniques used to evaluate grinding burn are given below in Table 3. This compares a number of popular residual stress measurement techniques.

Table 3: Comparison of grinding burn detection methods (Wojitas et al, 1998)

Features	Nital Etch	Eddy Current	X-ray Diffraction	MBN
Non destructive	No	Yes	No	Yes
Standardised	Yes	Yes	Yes	Yes
Chemical Use	Yes	No	No	No
Automated	No	Yes	Yes	Yes
Quantitative	No	Yes	Yes	Yes
Reliable	No	Yes	Yes	Yes
Coating Proof	No	Yes	No	Yes
Both Stress and Hardness	No	No	Yes	Yes
Fast	No	Yes	No	Yes
Large Areas	Yes	Yes	No	Yes

Nital etching uses a controlled corrosion process and metallography to characterise the microstructure of a metal. It selectively corrodes or stains particular phases present in the metal to allow observation of the phases being investigated. Nital etching is a very laborious process involving several stages of cleaning, polishing, coating and drying. Recent government environmental directives also mean that the process is expensive in the light of installations costs and waste disposal considerations of the dangerous chemicals involved.

Eddy current is another thermal damage detection method that relies on a metallurgical (phase) transformation taking place in the ground metal. It has the merit over its peers of being a non-contact method but its results are sometimes misleading.

X-ray diffraction has for a long time been the trusted way to measure residual stress. Though it is a long process (typical measurement times being 8 hours for conventional apparatus) and expensive it is accurate with good reproducibility.

From the comparison of these methods to the MBN technique using Table 3, it is seen that MBN is a non destructive novel way of detecting grinding burn which can be exploited after it has been calibrated and set up. It is quick, quantitative, and reliable and can be used for large areas through coatings.

2.4.5 MBN Summary

Though it may seem from the literature presented here that the use of MBN as a detection tool for grinding burn has been quite researched, there is a very important difference in what is being researched and the work that exists. At the moment, grinding burn is applied by setting thresholds as to sound and unsound components. Thus as a control measure, an unsound component will already have been machined and would have to be disposed. This study aims to use MBN to detect grinding burn ***before*** it happens, and thus limit waste and optimise manufacturing processes.

Chapter 3 EXPERIMENTAL PROCEDURE

3.1 Material

All the work carried out as part of this thesis used 51CrV4 steel in hard and soft forms. Vickers hardness values for the 51CrV4 hard and soft was measured as 600 and 300 H_V respectively using the Vickers hardness machine. 51CrV4 is used in the mechanical and automobile industries for components such as gear parts, pinions and shafts. The material specification is shown in appendix A. The composition of 51CrV4 is shown in Table 4 below.

Table 4: Chemical composition of 51CrV4

Chemical composition (Typical analysis in %)	C	Si	Mn	Cr	V	Other
	0.50	0.25	0.90	1.10	0.12	(Pb)

3.2 Grinding

The samples used in this thesis can be grouped into two sets depending on their use.

- The first sets of specimens were used to obtain a baseline MBN reading and also, a residual stress measurement using the X-ray diffractometer. This first group of samples were ground using different grinding parameters.
- The second sets of specimens, the tensile specimens, were used to calibrate the MBN readings to residual stress measurements. These specimens were cut using the EDM process from a plate of 51CrV4 which had been surface ground. The Edgetek SAM (Super Abrasive Machine) at Cranfield University was used for all the grinding tasks. A typical grinding set-up of the Edgetek SAM is shown in Figure 27. The Edgetek SAM grinding centre is a 5-axis CNC grinding centre with a 27kW spindle. All the grinding tasks were carried out using an electroplate CBN B252 wheel.

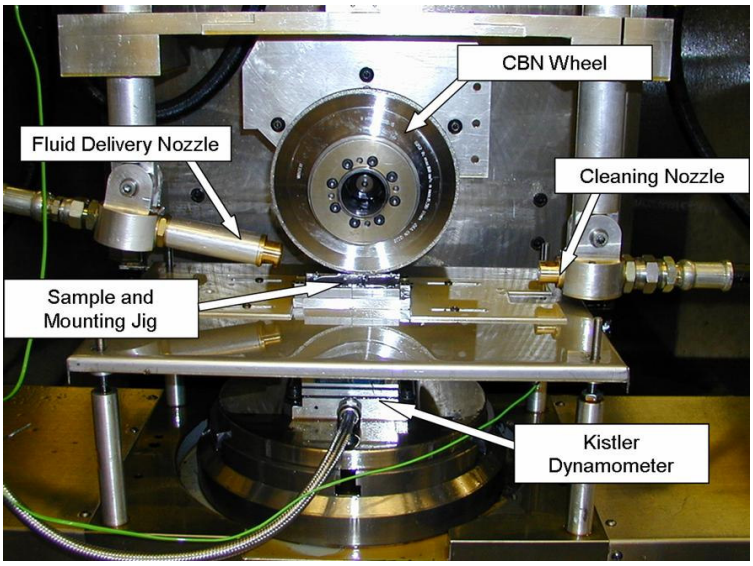

Figure 27: Grinding set up in the Edgetek SAM grinding centre

Table 5 lists the samples that were ground on the Edgetek SAM along with the relevant grinding parameters. M01 to M05 are soft 51CrV4 samples ground using mineral oil and samples PL1 to PL6 are soft 51CrV4 samples ground used a water based emulsion with an additive.

Table 5: Ground samples with their relevant grinding parameters

Sample	MBN File	Q'_w(mm^3/mm.s)	a_e(mm)	V_s(m/s)	V_w(mm/s)	Comments
Hard creep	Hard Creep	5	4	50	1.25	Creep grinding
Soft creep	Soft Creep	5	4	50	1.25	Creep grinding
MO1 0.4	m01	0.4	0.4	50	1	Mineral oil fluid
MO2 0.8	m02	0.8	0.4	50	2	Mineral oil fluid
MO3 1.6	m03	1.6	0.4	50	4	Mineral oil fluid
MO4 3.2	m04	3.2	0.4	50	8	Mineral oil fluid
MO5 8	m05	8	0.4	50	20	Mineral oil fluid
PL1	PL01	0.4	0.4	50	1	Water based fluid
PL2	PL02	0.8	0.4	50	2	Water based fluid
PL3	PL03	1.6	0.4	50	4	Water based fluid
PL4	PL04	3.2	0.4	50	8	Water based fluid
PL5 Hard	PL05	500	4	146	125	Water based fluid
PL6 Hard	PL06	500	4	146	125	Water based fluid

For the tensile tests, the samples were machined to produce a uniform stress region within the gauge length of the sample. Another important consideration was to make the gauge length large enough to fit the probe of the MBN equipment and a strain gauge at the same time. Historical data showed that the biggest change in residual stress due to grinding was approximately 800MPa and the maximum load of the tensile test machine selected to be used was 30kN. The cross – sectional area A, was derived using Equation 5 below.

$\sigma = \frac{F}{A}$	**Equation 5: Cross - sectional calculation**
$A = \frac{F}{\sigma} = \frac{30000N}{800 \times 10^6 Pa} = 37.5mm^2$	

To make the cross – sectional area approximate to 37.5 mm^2, a width by thickness of 9mm by 4mm was used. The geometry for machining of the tensile specimen was decided as in the Figure 28.

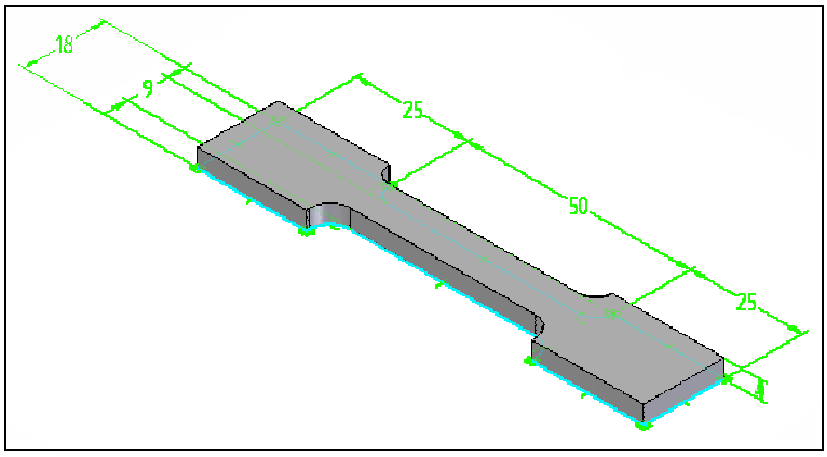

Figure 28: Tensile specimen geometry

The tensile specimens were machined using wire electro-discharge machining (EDM) in order to minimise the occurrence of stress raising features along the profile of the specimen. Twelve samples each were machined in the hard and the soft samples.

A typical ground surface finish of R_t = 4.5 μm (R_a = 0.42 μm) was put on one side of the sample by grinding on the Edgetek using a B252 wheel with the following

parameters: work speed, V_w=100mm/min: peripheral wheel speed, V_s=146m/s: depth of cut, a_e = 30 µm.

The thickness of the specimen was reduced to 3mm without any change in the microstructure and no significant change in the residual stress in the sample. This meant that the surface on the ground side had an $R_t \approx 4.5$µm and the as-received surface, an $R_t \approx 1.8$ µm (typical surface finish of a surface ground by an alumina wheel as the as-received specimen were) (Figure 29). The surface roughness profile was measured with a Taylor Hobson Talysurf 120L with a 2µm radius diamond tip stylus. This produced a trace with roughness parameters such as R_a and R_t (Result traces are shown in Appendix B).

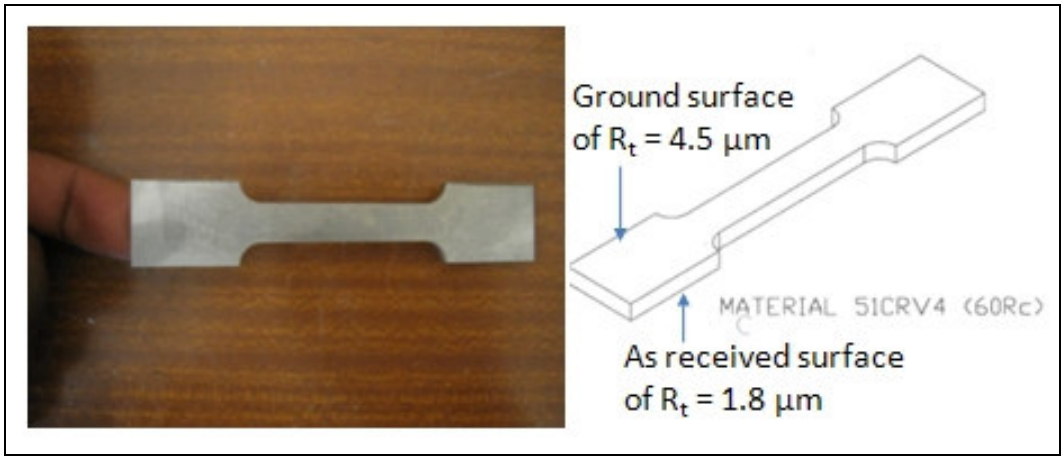

Figure 29: Tensile specimen with different surface roughness

The hard 51CrV4 samples were referenced as HG01 to HG12 (hard – ground – number). The soft samples were labelled in a similar way, from SG01 through to SG12 (Soft – ground – number).

3.3 Mechanical Testing

The Instron 3300 and 5500 series Universal Testing Machines with 30kN and 100kN load cells respectively were used for the uniaxial tensile tests to characterise the elastic region where the MBN measurements were to be taken. Initial calibration tests were done to determine the suitability of the tensile testing machines to the calibration tests. Both a hard and soft tensile specimen of 51CrV4 was incrementally loaded till fracture on the 3300 and 5500 series Universal Testing Machines. Their resultant stress-strain curves were analysed to determine

which tensile testing machine was to be used. The results showed that the maximum load of the 3300 series 30kN tensile testing machine was too small to produce a complete calibration curve for the mechanical properties of the hard condition 51CrV4. The accuracy of the results was also questioned due to the signal containing a lot of noise and thus the Instron 5500 series (Figure 30) with the 100kN load cell was used for the testing.

Figure 30: Instron 5500 series tensile tester

The test set up shown in Figure 31 was used for the mechanical tensile tests. The software for the Instron 5500 series, Merlin, was used to set the parameters of the test. A strain rate of 0.2mm/min was used in order to generate enough points to give a good description of the behaviour of the tensile samples under an applied load. The direction was set as downward to load the specimen in tension. After the test parameters had been set up, the tensile specimen was loaded into the jaws of the tensile tester upper jaw first before the lower jaw and the extensometer loaded as shown in Figure 31.

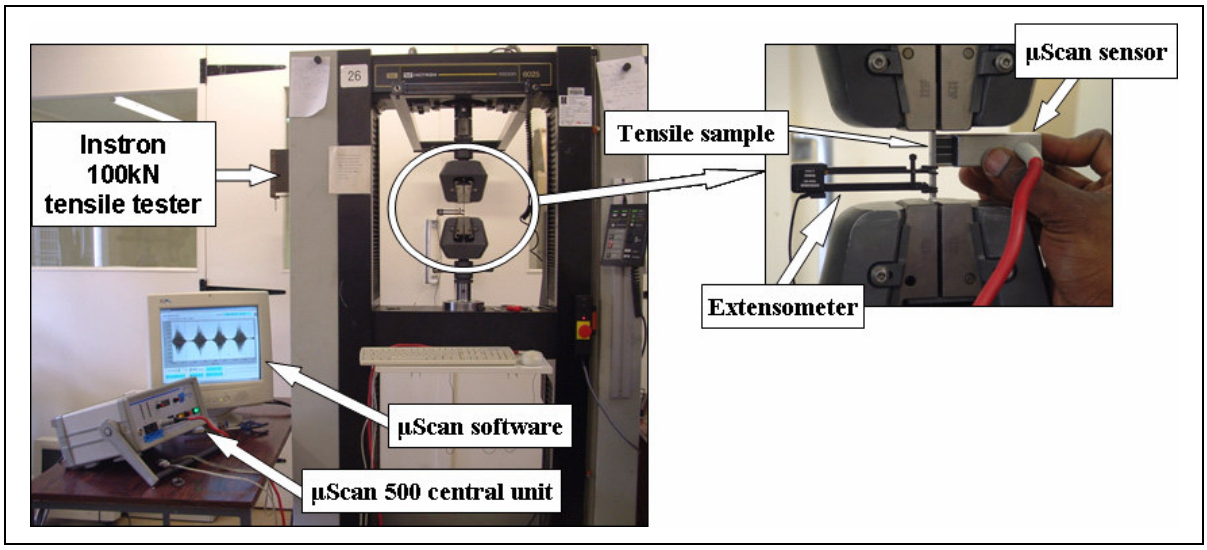

Figure 31: Tensile test set up for calibration experiment

After the securing pin of the strain gauge had been removed and the strain gauge and extension length balanced using the Merlin software, the test was started and the data of the test logged.

The Instron 5500 tensile tester had a maximum load limit setting. This allows the load to be held at the value set. This was used during the MBN calibration tests in order to give enough time to take an MBN reading at a specific load value. For the tensile tests, their load and strain values were recorded together with their MBN readings at discrete load points in order to get the comparison needed. It was important to keep the sensor of the µscan MBN flat on the tensile specimen without applying too much force on it to affect the applied stress (Figure 32).

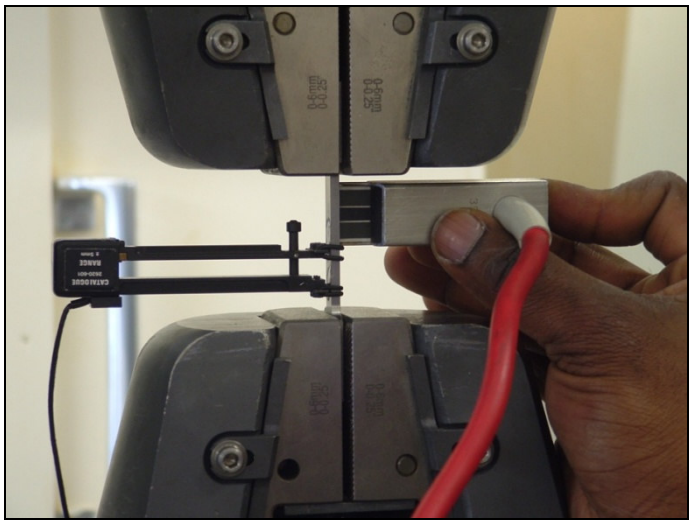

Figure 32: Measuring the MBN signal of a strained sample

Two loading strategies were employed.

- Strategy 1: Loading the tensile specimen, taking MBN readings and unloading it before the increasing the load for the next MBN reading.
- Strategy 2: Loading the tensile specimen, taking the MBN readings and increasing its load without unloading it.

Strategy 1 had a calibration method similar to that used by Shaw et al., (1998), where the load was reduced to zero before an increase to the next load value occurred. This aided an analysis of what happened to the zero load points as the load was increased. Strategy 2 was also used by Stefanita et al., (2000). Table 6 summarises the different tensile specimens and the different loading strategies applied to them.

Table 6: Loading methods for calibration tests

Soft 51CrV4	*SG03*	Loaded (0kN to 12kN in 1.2kN increments) and MBN measured at each increment and unloaded before increasing load value to next load value (increment).
	SG04	Loaded (0kN to 12kN in 1.2kN increments) and MBN measured at each increment and unloaded and MBN measured again before increasing load value to next load value (increment).
	SG05	Loaded, measuring MBN and increasing load without unloading. Load values from 0kN, 1.5kN, 3.0kN, 4.5kN, 6.0kN, 7.5kN, 9.0kN, 10kN, 11kN, 12kN, 13kN and 14kN.
	SG06	Loaded and MBN measured increasing load value without unloading. Load values from 0kN, 1.5kN, 3.0kN, 4.5kN, 6.0kN, 7.5kN, 9.0kN, 10kN, 11kN, 12kN, 13kN and 14kN.
Hard 51CrV4	*HG08*	Loaded (0kN to 24kN in 2.4kN increments) and MBN measured at each increment and unloaded and MBN measured again before increasing load value to next load value (increment).
	HG09	Loaded (0kN to 24kN in 2.4kN increments) and MBN measured at each increment and unloaded and MBN measured again before increasing load value to next load value (increment).

	HG11	Loaded and MBN measured increasing load value without unloading. Load values from 0kN, 1.5kN, 3.0kN, 4.5kN, 6.0kN, 7.5kN, 9.0kN, 10.50kN, 12kN, 13kN, 14kN, 15kN, 16kN, 17kN, 18kN, 19kN, 20kN, 21kN, 22kN, 23kN, 24kN, 25kN and 26kN.
	HG12	Loaded and MBN measured increasing load value without unloading. Load values from 0kN, 1.5kN, 3.0kN, 4.5kN, 6.0kN, 7.5kN, 9.0kN, 10.50kN, 12kN, 13kN, 14kN, 15kN, 16kN, 17kN, 18kN, 19kN, 20kN, 21kN, 22kN, 23kN, 24kN, 25kN and 26kN.

3.4 MBN measurements

Magnetic Barkhausen noise is the technique being investigated as to its ability to detect grinding burn. The equipment used to measure the MBN signal was the μScan 500C manufactured by Stresstech, Finland.

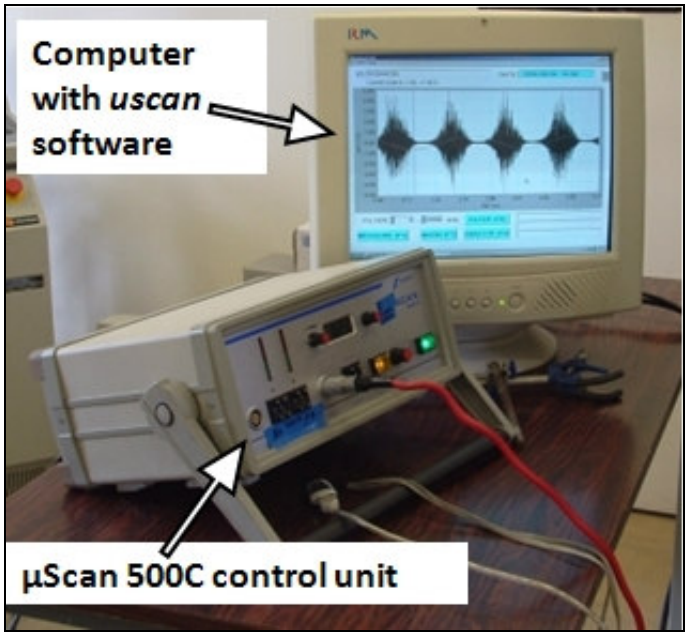

Figure 33: Stresstech μ500C showing control unit and screenshot of *uscan* software

Information from the μ500C operating instructions (Stresstech, 1999) details the features and the capabilities of the equipment in exploiting the Magnetic Barkhausen Noise technique in;

- Non destructive testing applications
- Estimating near surface gradients such as stress, plastic deformation, hardness etc
- Correlating different microstructural parameters to the Barkhausen signal
- Optimising different conditions for the analysis, and
- General research work

The parameters for the MBN readings had to be set up using the control unit of the μScan 500C and its software the *υscan*. The parameters used for setting up the μScan 500C control unit are shown in Table 7.

Table 7: Control unit parameters for μScan 500C

μScan 500C Function	**Setting**
Mode	μS EXT
MAGN	99%
GAIN	**20** for soft 51CrV4 and **50** for hard 51CrV4

The software measurement parameters used for both samples (hard and soft 51CrV4) is shown in Figure 34.

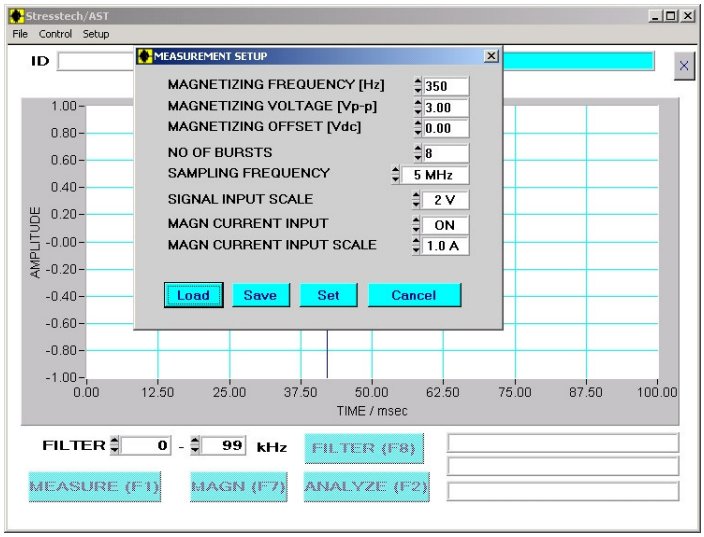

Figure 34: Measurement setup for μScan software

After the measurement parameters on the control unit and the software had been set up, the readings could be taken. The sensor was pressed firmly on the surface of the specimen making sure that it was flat and that complete contact was made by the sensor surface to the sample (Figure 35). Readings were taken using the **F1** function key on the keyboard. The resultant MBN signal is then displayed in the window of the µScan software (Figure 36) where it can be saved for subsequent analysis within the software.

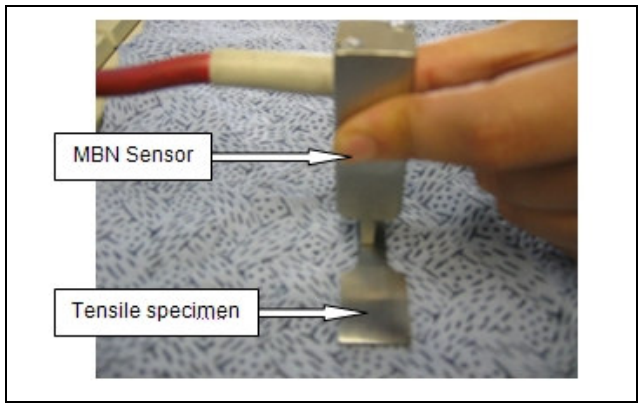

Figure 35: Measuring the MBN signal of a sample specimen

The negative and positive parts of 4 bursts are displayed (Figure 36). The green sine curve is the magnetising current and the red curve is a parabola fitted to the first half of the cycle. The red curve not fitting into the magnetising current curve means a saturation of the sensor's magnetising circuit and the reading should be taken again.

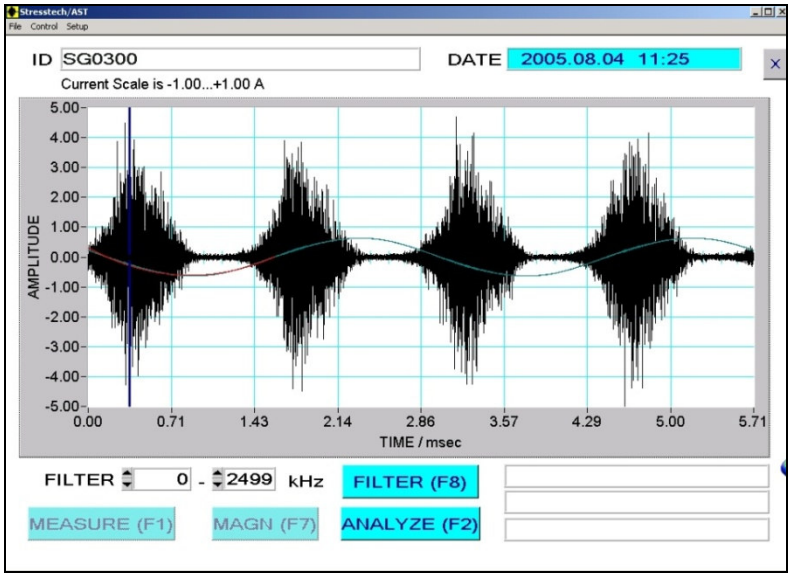

Figure 36: Main window of µScan with captured MBN signal

The µscan software allowed for the analysis of the measured MBN signal. The data considered for this study are (Figure 37):

- RMS Voltage of the Barkhausen noise (V rms)
- Peak Voltage (V peak)
- Peak Position
- Full Width Half Maximum (FWHM)
- Permeability

These parameters can be analysed in the range 0 to 2499 kHz making it possible to characterise the required parameters at different depths using the MBN depth equation (Equation 4).

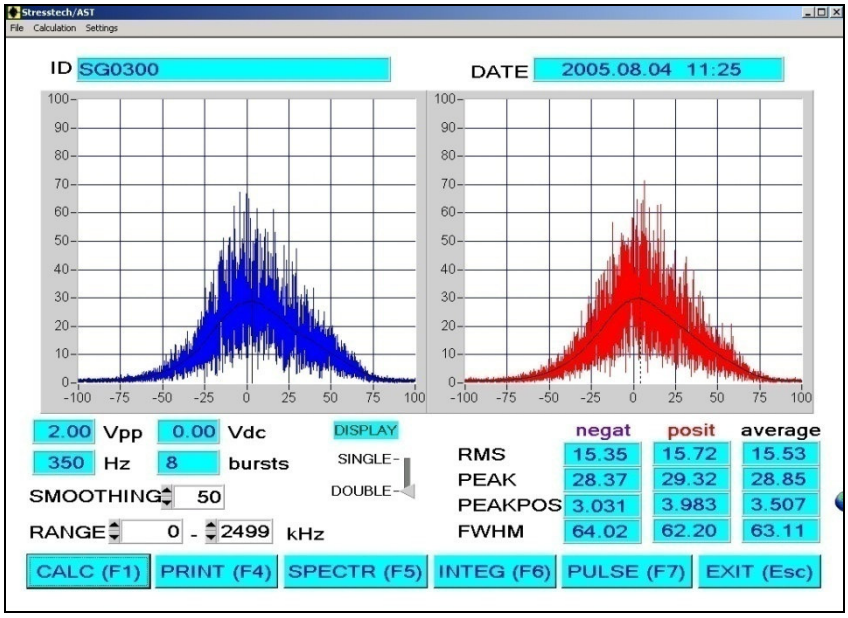

Figure 37: Analyse window with some calculated parameters

MBN readings were taken from the tensile samples during the calibration with the mechanical tests and also of the ground samples of different material removal rates. The samples were demagnetised due to the influence of the magnetic chuck but also due to the grinding process which can generate magnetisation of the component. All the files were saved as µScan data files in order to aid analysis without doing the measurement again. In the analysis window of the µScan software, information of the signal envelope can be saved as a text file to aid further analysis using the Microsoft Excel software.

3.5 X – ray Diffraction (XRD) Measurements

X-ray diffraction (XRD) is an industrially accepted method for measuring residual stress. A creep feed ground sample with a Q'_w of 5mm^3/mm.s was evaluated in terms of its residual stress and used to represent the residual stress present in the tensile specimen after it had been ground (spark out to obtain a course surface roughness). This was used as a representation of the residual stress values present in the tensile specimens before the mechanical tests. XRD tests were also used on as received samples of the hard and soft 51CrV4. This gave the residual stress values of the samples after their manufacture.

A Siemens D500 diffractometer was used for the all the XRD analysis. It had the Bragg-Brentano geometry and used Cr – Kα radiation.

Figure 38: Siemens D500 diffractometer

The Bruker EDSTRESS program was used to set up the parameter files for the measurement. Two parameter files were set up, one for the hard 51CrV4 and another for the soft 51CrV4 sample. The Bruker XRD commander program was used for the measurement tasks and the Bruker STRESS^{PLUS} software to calculate the stress.

The residual stress values were measured of samples M01 to M05 and samples PL1 to PL6. These results were used in correlating the results from the calibration tests and verifying the validity of the MBN technique in measuring residual stresses to determine grinding burn.

The ground samples were sectioned using Electro discharge machining (EDM) in order to fit the samples into the diffractometer after grinding (Figure 39).

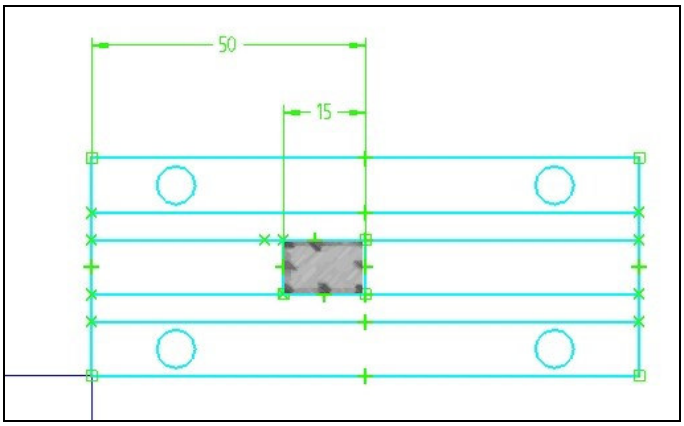

Figure 39: EDM section of sample for X - ray diffraction.

X-ray analysis was also carried out in the Stresstech facility in Finland for ground samples at material removal rates (Q'_w) of 5, 500 and 1000 $mm^3/mm.s$ at different depths for both the hard and the soft samples. The depth of penetration of the X – ray diffraction technique is about 10 µm and so in order not to change the residual stresses the surface of the samples had to be electropolished in order to remove a depth off the surface and evaluate the residual stress values below the surface. These were also used to find a correlation with the MBN measured signals.

Chapter 4 RESULTS

4.1 Baseline Measurements

Baseline measurements were carried on the following samples;

- As received tensile samples: The tensile samples before the coarse surface were ground into them. These were tested with XRD and the MBN.
- Coarse surface tensile samples: The tensile samples after the coarse surface had been ground into them. These were measured using the MBN.
- Ground samples: Soft 51CrV4 samples ground under different grinding parameters and using either mineral oil or a water based emulsion as the fluid. These were measured using the MBN and XRD.

4.1.1 XRD Baseline Measurements

Residual stress for an unground sample of 51CrV4 hard and 51CrV4 soft were measured and their values assumed to be the same for the tensile specimens in their "as received" state. The residual stresses of the coarse surface tensile samples were taken from XRD measurements of a hard and soft sample 51CrV4 ground using creep parameters. The results are summarised in Table 8.

Table 8: Baseline Residual Stress XRD Measurements of Hard and Soft 51CrV4

	XRD residual stress	
	As received	**Coarse surface**
Soft 51CrV4	-179MPa	-209MPa
Hard 51CrV4	-195MPa	-389MPa

The XRD plots are presented in appendix C.

4.1.2 Tensile Testing Baseline Measurements (Elastic region characterisation)

The stress – strain relationship of the tensile samples had to be deduced in order to characterise the elastic and plastic deformation regions. This was done by straining a soft and a hard tensile sample of 51CrV4 till fracture on the Instron 3300 and 5500 tensile testing machines. This enabled uniaxial tensile tests to be

carried out on the samples and extrapolation of the results into the compressive region in order to get a total stress versus MBN parameters relationship.

4.1.2.1 Soft 51CrV4

The result of straining the soft 51CrV4 tensile specimen is illustrated in Figure 40. The Young's modulus was calculated as the slope of the linear elastic region which was from an applied stress of 0 to about 445 MPa (12kN). The result was 104.97 GPa.

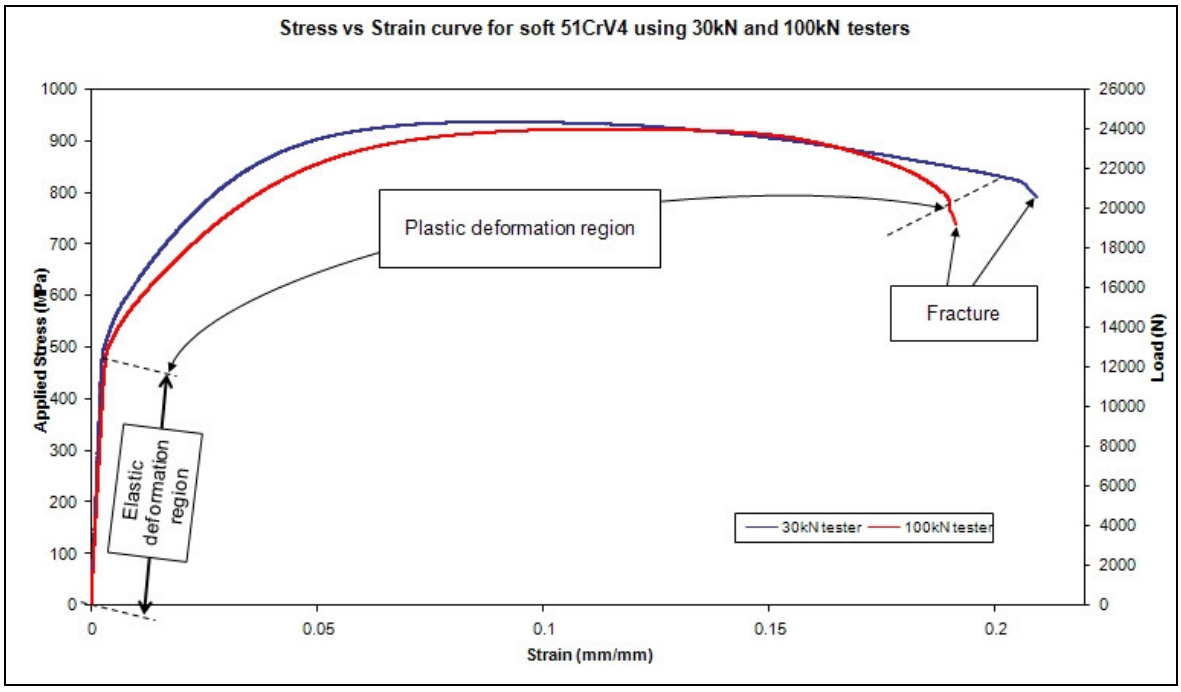

Figure 40: Stress - strain relation for soft 51CrV4 till fracture on 30kN and 100kN tensile Instron testers

4.1.2.2 Hard 51CrV4

From the stress – strain curve of Figure 41, (corresponding load axis on the secondary axis) the elastic region was deduced as the region between an applied stress of 0 to about 889 MPa (24kN). The Young's modulus was calculated as 110.124 GPa.

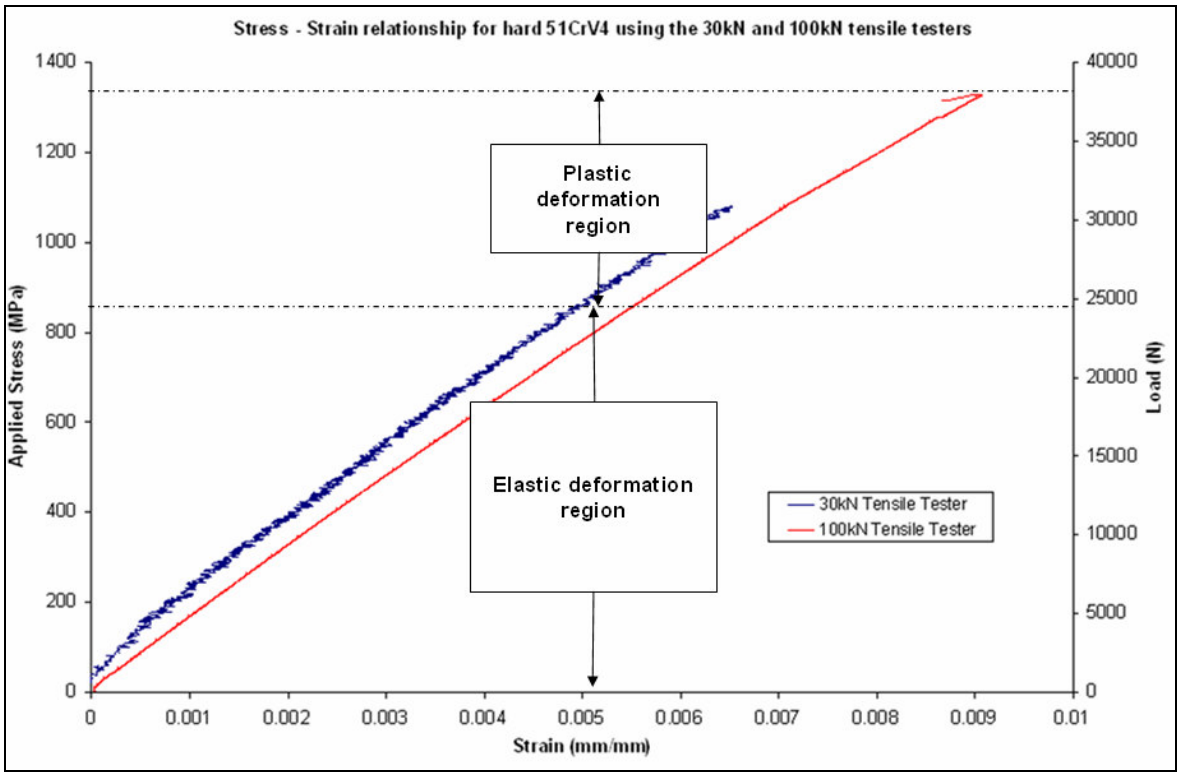

Figure 41: Stress - strain chart for 51CrV4 hard till fracture on 100kN and 30kN tensile testers

From Figure 41, it can also be seen that the hard 51CrV4 had a virtually unnoticeable plastic deformation region. The curve from the 30kN had a lot of noise because of the circuitry used to calibrate the extensometer to the DOS based software and the maximum load of 30kN was also too small to fracture the hard sample and hence the decision was made to use the Instron 5500 100kN load tensile tester for the calibration tests.

4.2 Correlating MBN to Applied Stress

The calibration of the MBN readings to residual stress using the mechanical tensile tests gave an approach of correlating the MBN readings to residual stresses. All MBN readings were taken on the coarse surface of the tensile specimen.

4.2.1 SG03 Soft 51CrV4 Calibration

SG03 was calibrated to the MBN technique by loading the tensile sample, taking an MBN reading, unloading and increasing it to its next load value. Load

increments of 1.2kN were used and the elastic limit of 12kN was used as the maximum point.

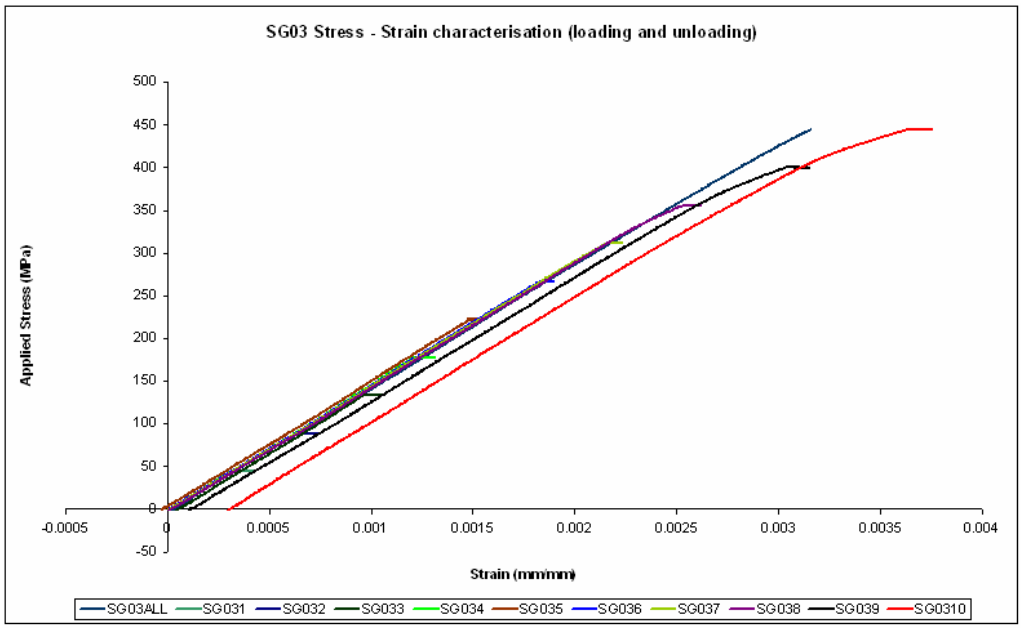

Figure 42: Stress - Strain chart for 51CrV4 Soft (SG03) tensile sample, unloading after each load until 448 MPa

In Figure 42, SG03ALL is the first run of the tensile tester from 0kN to 12kN to characterise the sample and to set the baseline in order to check deviations during the test. After SG038 (9.6kN), the SG03 sample becomes plastically deformed as the deviation from 0mm/mm strain is significant.

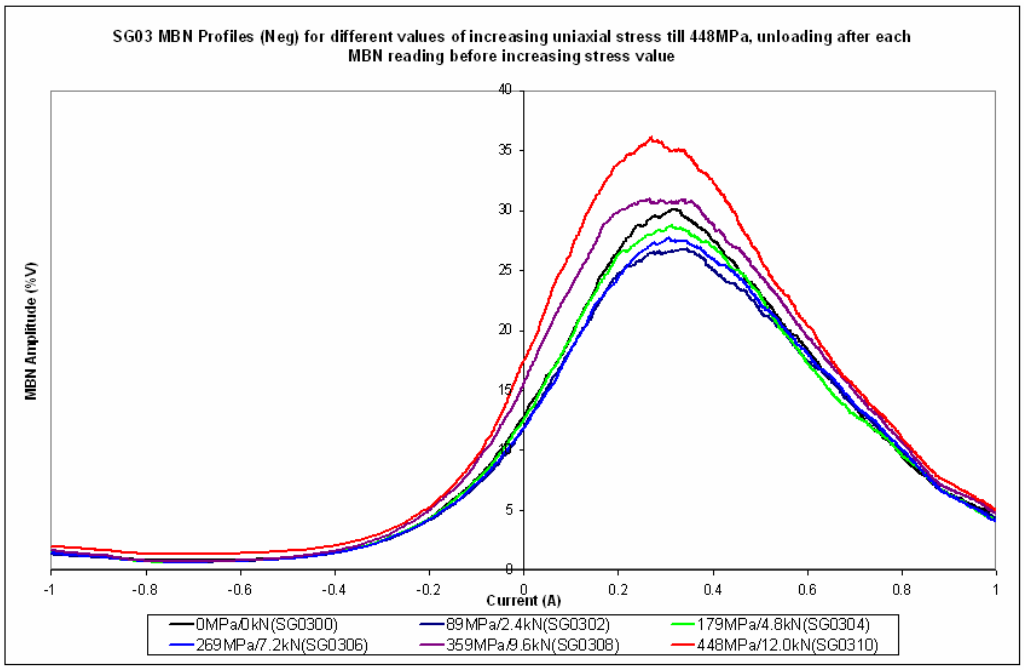

Figure 43: MBN Profiles of SG03 with increasing applied stress

The MBN profiles of the incremental load values are shown in Figure 43. There is a general increase in MBN profiles from 0kN (SG0300) until about 400MPa where there is a significant rise. This trend can be seen more clearly from Figure 44. The variation of MBN parameters Vrms, Vpeak, Peak Posn and FWHM can also be seen in Figure 44.

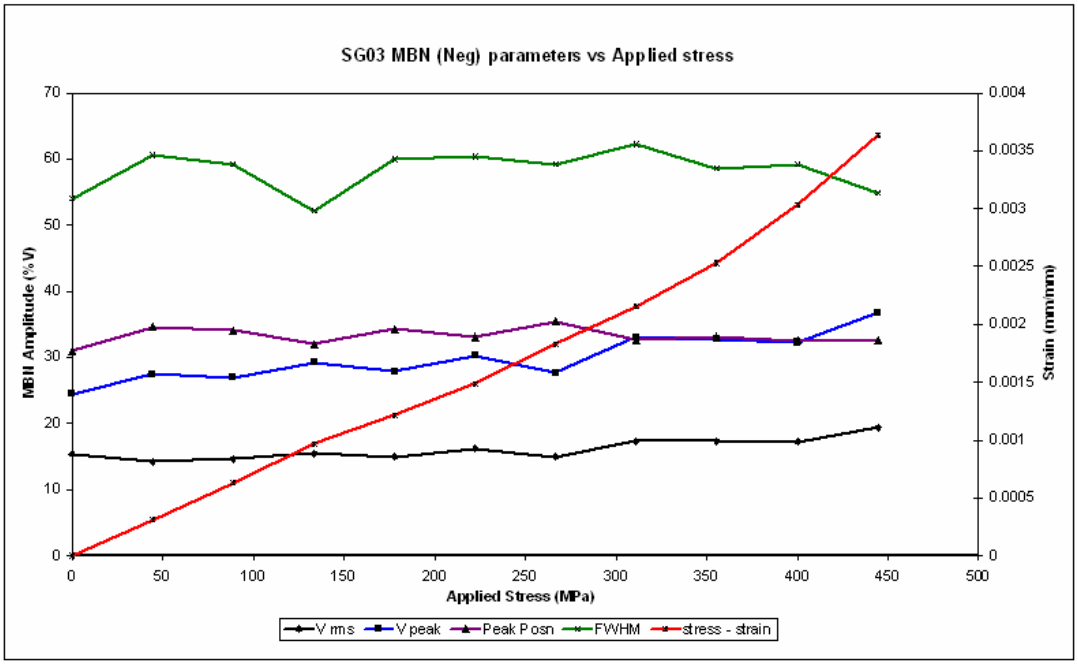

Figure 44: MBN Parameters changing with Applied Stress for SG03

The experiments were uniaxial in tension and so to extend it into the compression region, the applied stress was added to the residual stresses present in the tensile sample as in Shaw et al. (1998). In his paper, the macroscopic residual stresses σ_R were related to the applied stress σ_a by equation 5 in order to consider the effect of biaxial stresses. The total stress was calculated as;

$\sigma = \sigma_a + (1-\upsilon)\sigma_R$	Equation 6: Total stress equation

The residual stress was taken from the baseline XRD measurements. The soft sample was found to have an average value of -209MPa after being ground. This was taken as the residual stress present on the surface of the soft samples. The Poisson ratio was 0.3 (0.3 for most steels) and was used to compensate for the

biaxial stresses present during uniaxial loading. A chart of both the compressive and tensile regions of stress inferred from the baseline measurements and the calibration experiment is shown in Figure 45.

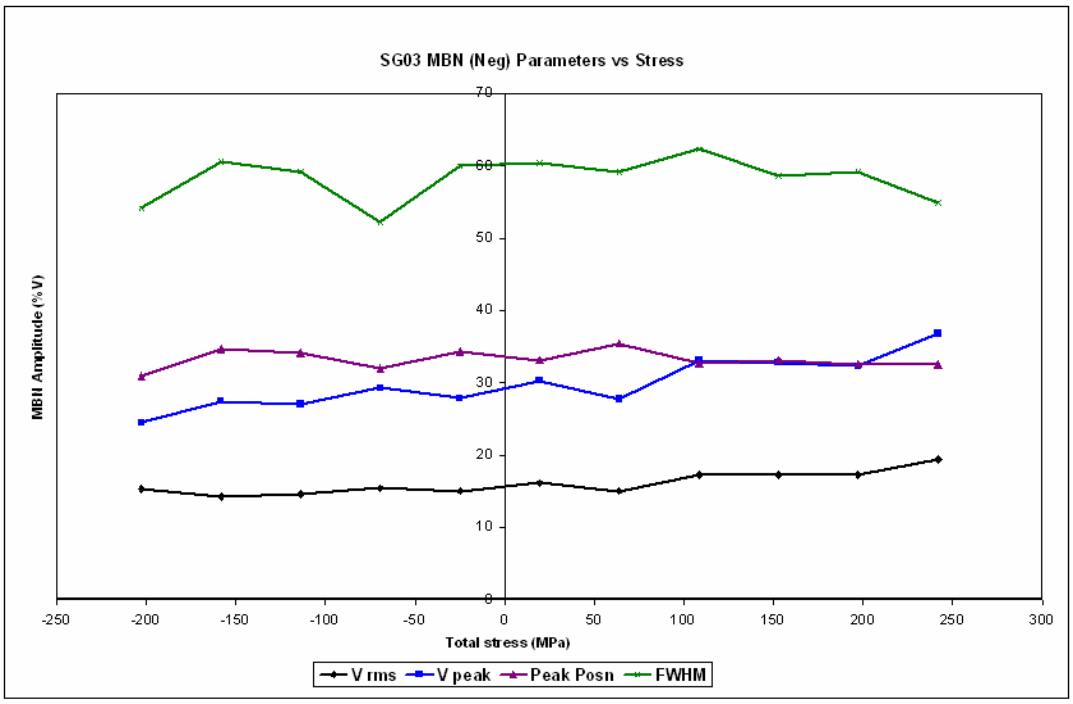

Figure 45: Total stress versus the MBN parameters

The results of the stress – strain curves for SG04 is presented in Appendix D together with its MBN profiles and calibration curves. SG04 was calibrated in the same way as SG03. That is the load was taken off after each load point before going to the next incremental load point. The results from SG04 concurred with that of SG03. Vpeak and Vrms generally increased with increasing applied stress until about its yield point and FWHM having a sharp change just before the change to tensile stresses.

4.2.2 SG05 Soft 51CrV4 Calibration

Tensile specimen SG05 was loaded continuously from 0kN till the start of the plastic deformation region at 14kN (518.5 MPa). The applied stress chart is illustrated in Figure 46. The chart shows a linear elastic region till about 480 MPa, when the plastic deformation region starts. SG05ALL shows the stress – strain curve after the first calibration run. The tensile specimen doesn't take its original path because of elastic hysteresis.

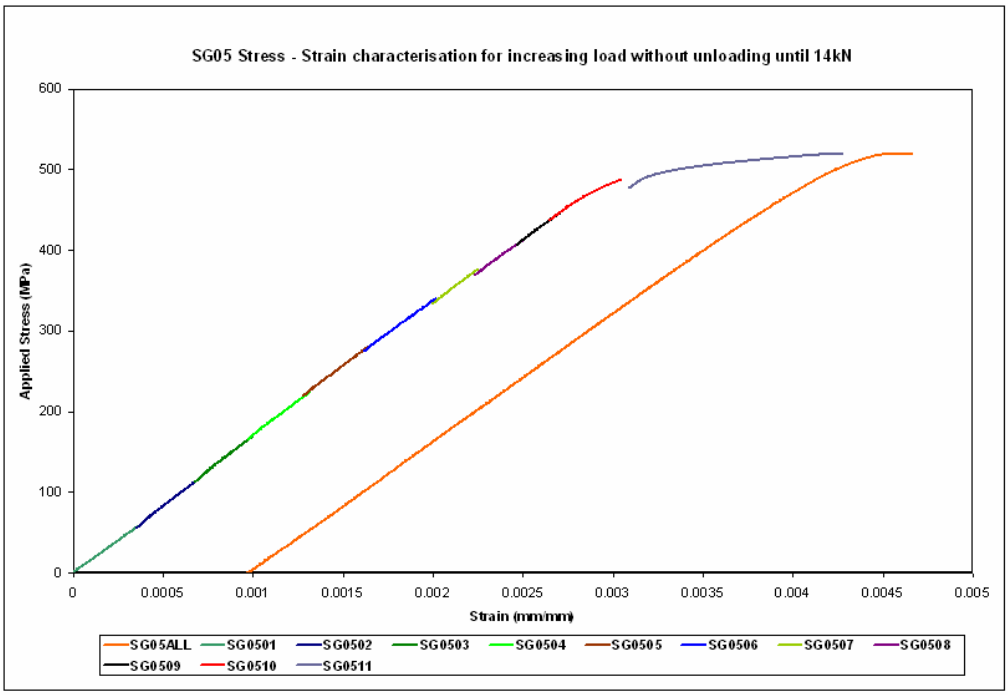

Figure 46: Stress - Strain chart for 51CrV4 Soft (SG05) tensile sample, unloading after each load until 518.5 MPa/14kN

Figure 47 shows the MBN profile at selected load points.

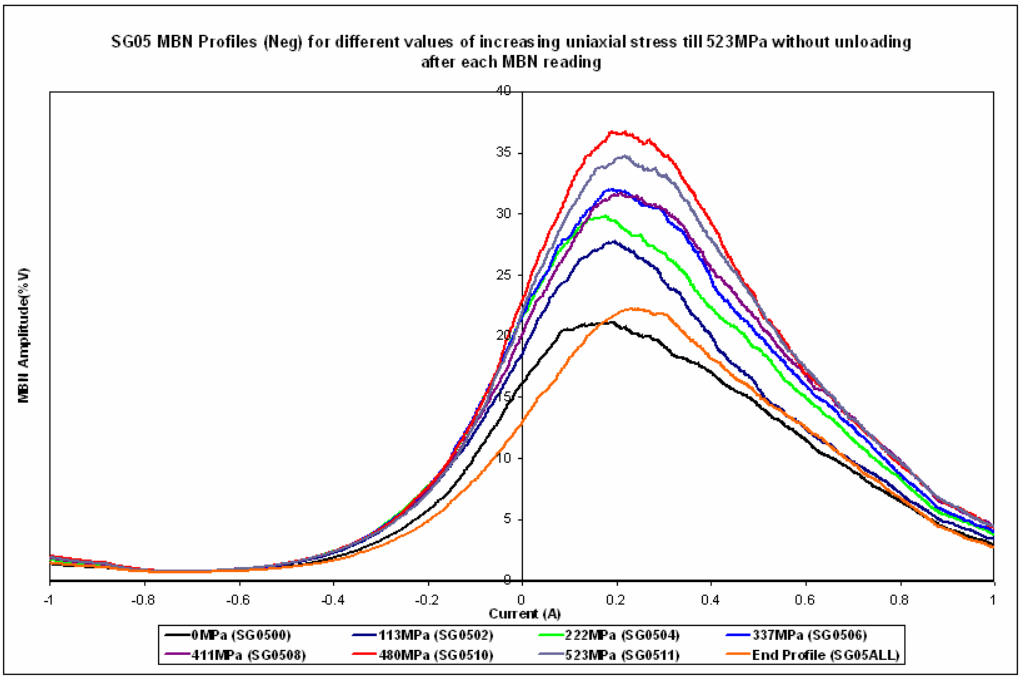

Figure 47: MBN profile of SG05 tensile specimen loaded without unloading until 14kN

Figure 47 shows a gradual increase in MBN profiles with the peaks positions in the same position except after the load had been taken off after 14kN where a shift

towards the right is seen. A residual stress value of -209 MPa measured from XRD baseline experiments was taken as the residual stress in the sample before the test and used to extend the graph into the compressive region.

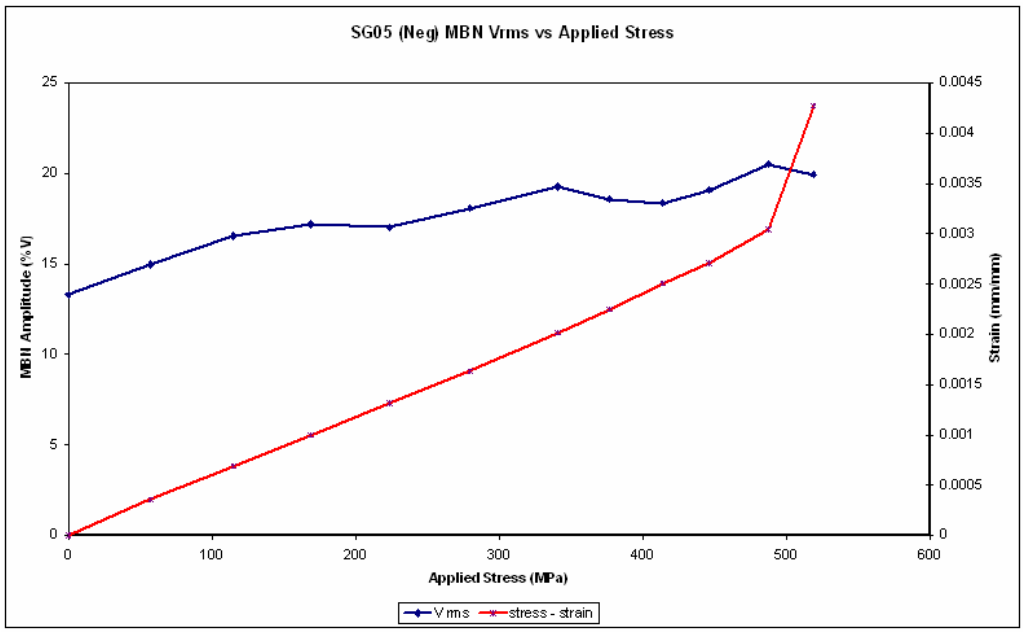

Figure 48: Variation of total stress with MBN Vrms for SG05

Figure 48 shows the gradual increase of Vrms with increasing applied stress. At the limit of elastic deformation, there is a sharp increase of the stress-strain curve and a decrease of the Vrms. The shift in peak position of SG05ALL can be seen more clearly in Figure 49.

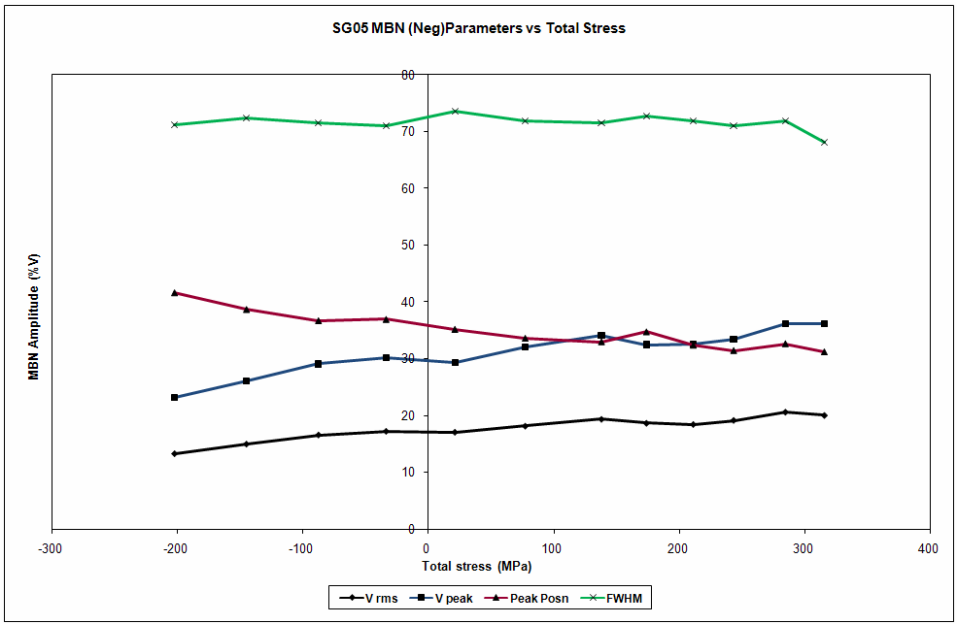

Figure 49: Variation of MBN parameters with applied stress for SG05

Results of SG06 loaded in the same way as SG05 is presented in Appendix E and all the findings concur.

4.2.3 HG08 Hard 51CrV4 Calibration

The HG08 tensile specimen was calibrated loading the specimen to the required load value, taking an MBN reading and then unloading to 0kN and then taking another MBN reading before increasing by 2.4kN. This was increased till the maximum load at 24kN.

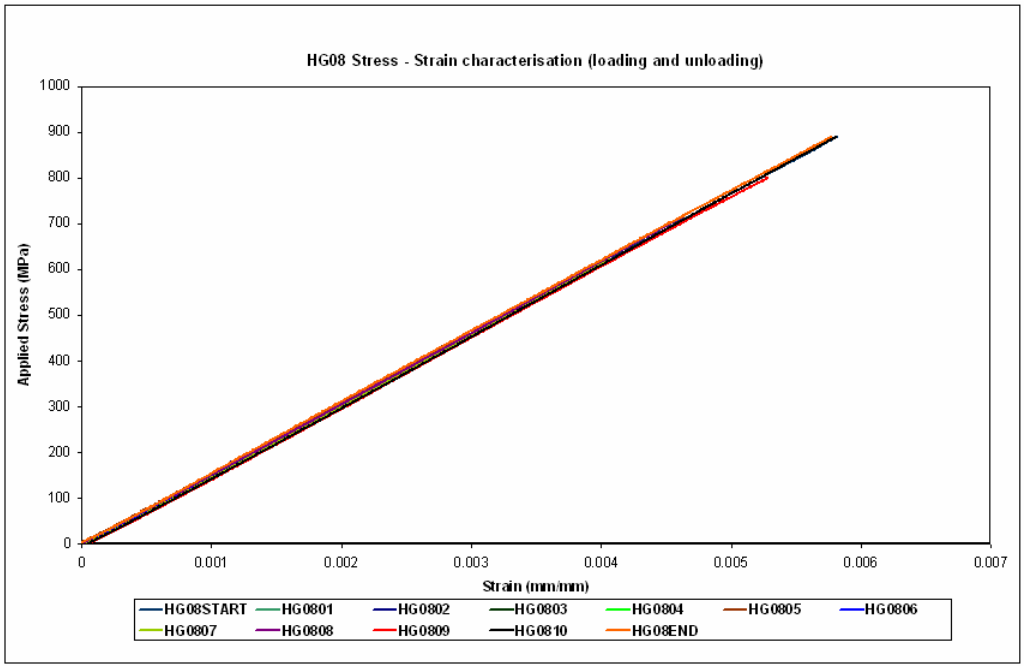

Figure 50: Stress - Strain curve for HG08 showing loading paths

The stress-strain curve with the equivalent load scale (on the secondary axis y-axis) is shown in Figure 50. The equivalent MBN profiles at selected load increment values from 0kN load till 24kN is shown in Figure 51.

The results of the increasing load points and the equivalent MBN parameters were plotted on the same graph to extract any relationships or trends. The result is shown in Figure 52. Apart from the general increase in MBN profile with increasing applied stress and a shift to the right of the last MBN profile at around the yield point, it is seen that the range and magnitude of the MBN amplitude of the hard

51CrV4 sample is higher and bigger (ranges from about 10 to 60 %V) compared to the soft 51CrV4 samples (20 to 40 %V).

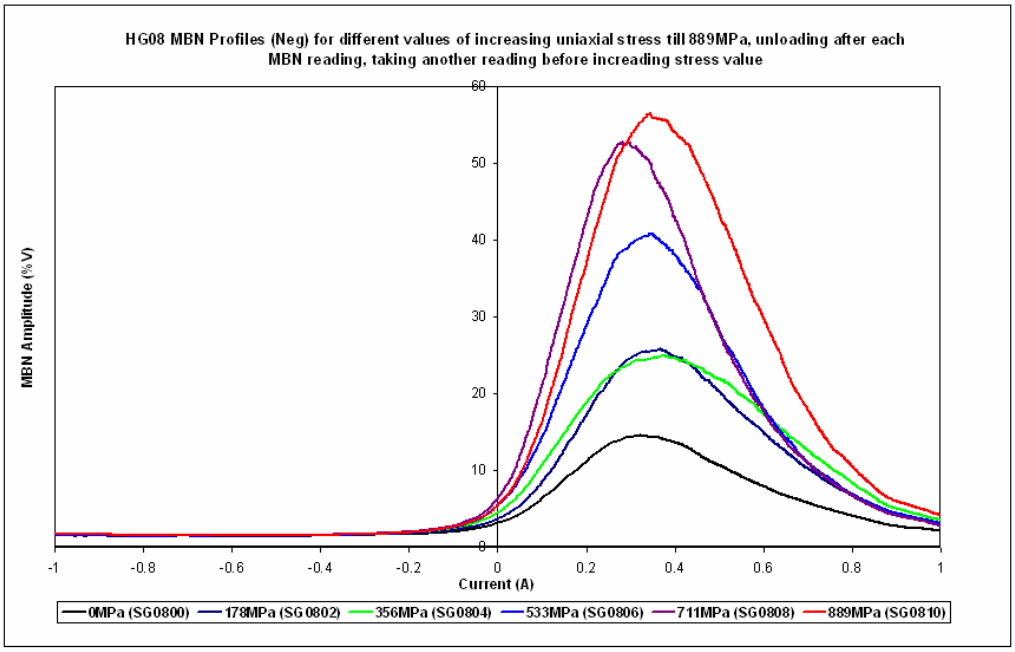

Figure 51: HG08 MBN profiles of selected load point of calibration test

The residual stress was added to the applied stress of Figure 52 to get the total stress using Equation 6. The residual stress value (-389MPa) was obtained from an XRD measurement of a hard 51CrV4 sample with coarse ground surface. The result obtained is shown below in Figure 53.

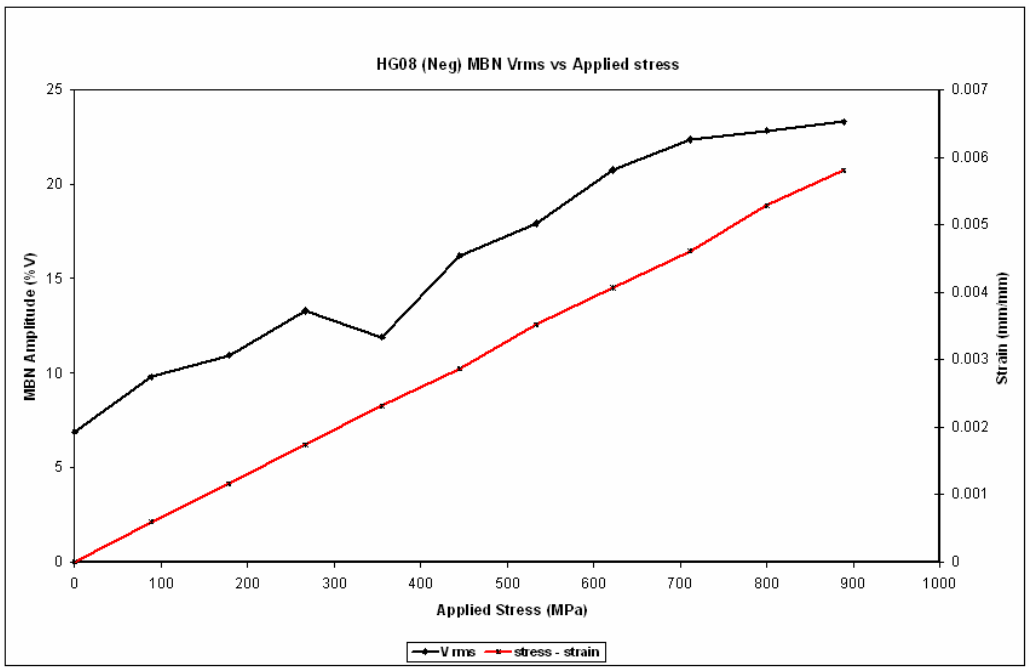

Figure 52: Variation of MBN Vrms with applied stress for HG08

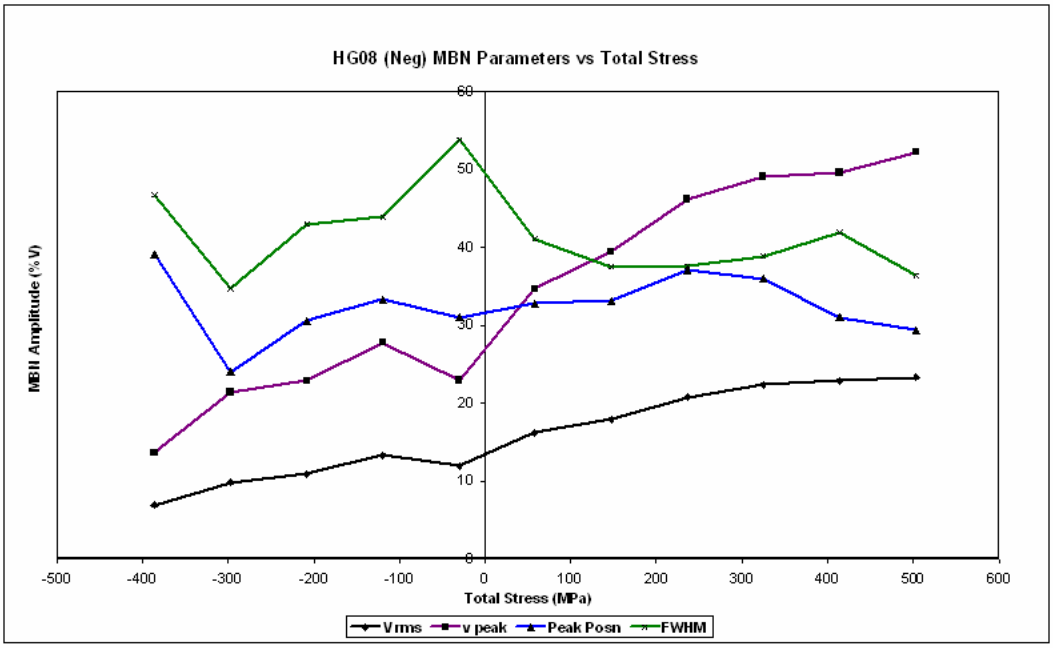

Figure 53: Variation of total stress with MBN parameters for HG08

Vrms and Vpeak generally increase with increasing applied stress till the end of the elastic region at about 750MPa (24kN load). There is a sharp decrease and increase decrease of Vrms and Vpeak just before the change from compressive to tensile total stresses (Figure 53). This has an opposite reaction with the FWHM reading. It has a sharp increase and decrease occurring at the same total stress value (-30MPa).

Tensile sample HG09 was loaded in the same way as HG08 and its results are shown in appendix E. Its Vrms and Vpeak also show the significant dip before a change from compressive to tensile stress (-100MPa, Figure 94) though the equivalent but opposite increase in the FWHM parameter doesn't happen till about a total stress of about 300MPa.

4.2.4 HG11 Hard 51CrV4 Calibration

The HG11 tensile specimen was loaded in tension by increasing the load value continuously without unloading it from 0kN in 2.4kN steps until 26kN. This was beyond its elastic limit in order to investigate the effect of plastic deformation on the MBN parameters. The stress – strain curve is shown below in Figure 54.

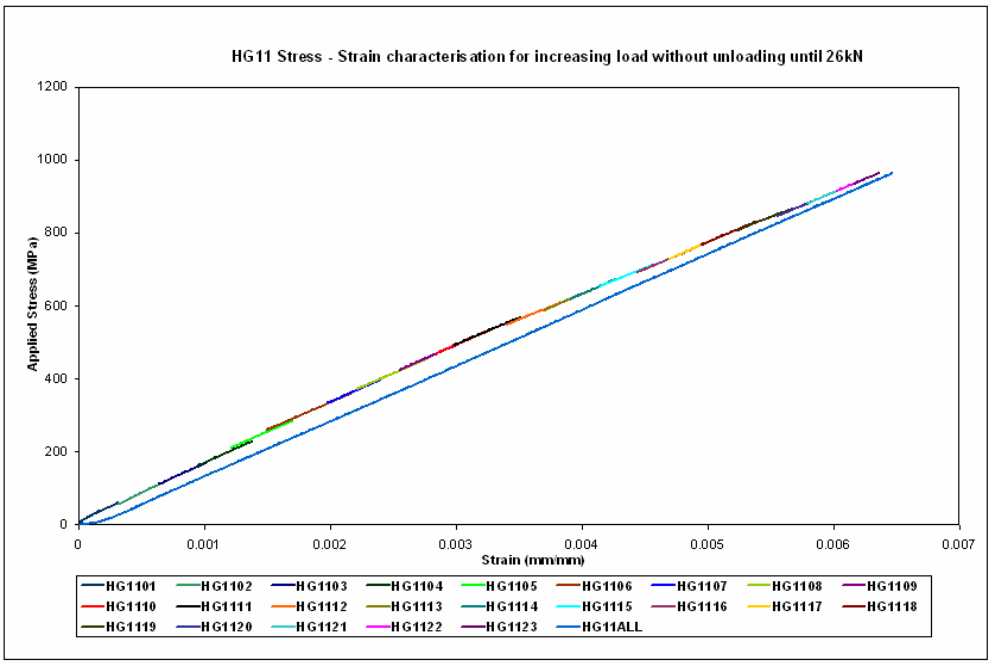

Figure 54: Stress - strain chart for HG11, increasing load continuously till 26kN.

HG11ALL is a plot of after the first calibration run has been made. It is seen that it's zero strain point moves because of plastic deformation mechanisms and elastic hysteresis.

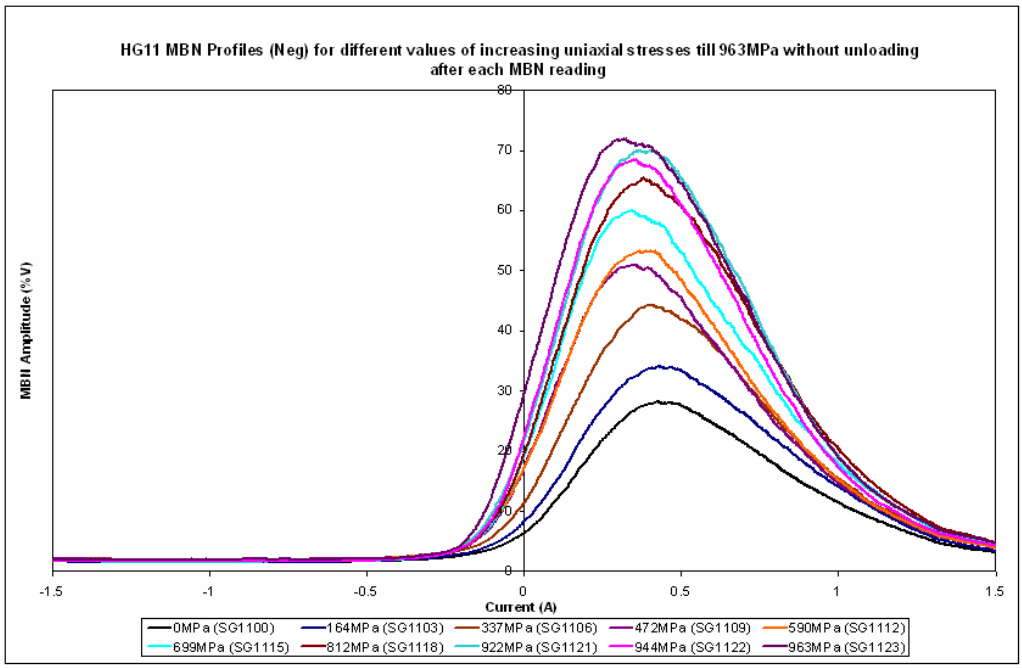

Figure 55: Selected MBN profiles taken at load points during HG11 calibration

Vrms is almost linear up until a sharp increase at about the start of the plastic deformation region at about 980 MPa (Figure 56).

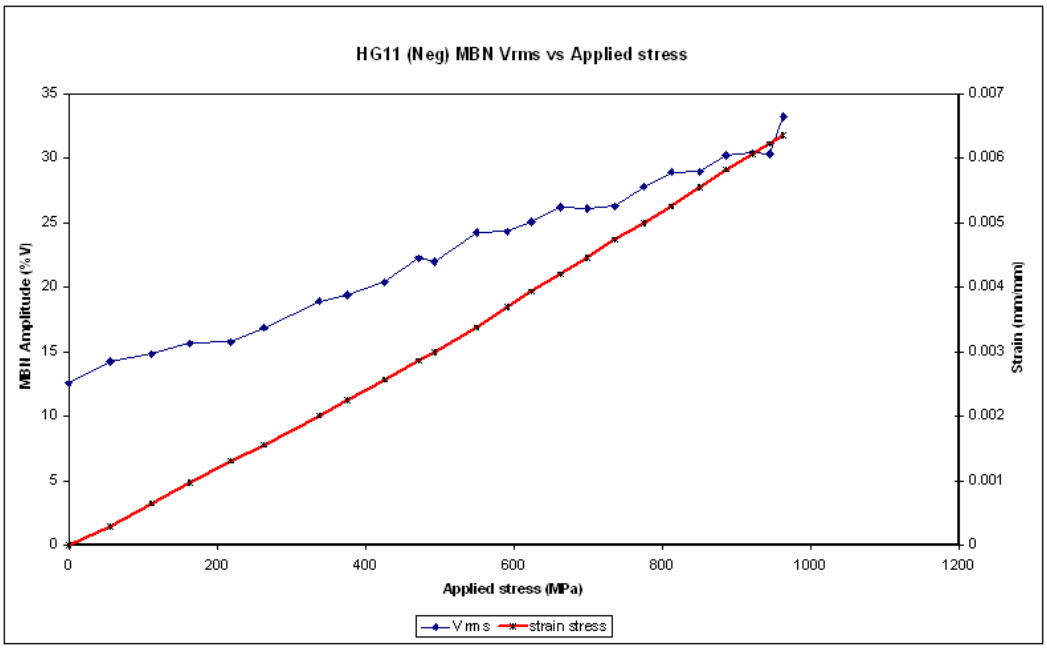

Figure 56: Variation of MBN Vrms with applied stress for HG11

The sharp peak in the plot of FWHM just before the transition from compressive to tensile stresses can also be seen in Figure 57.

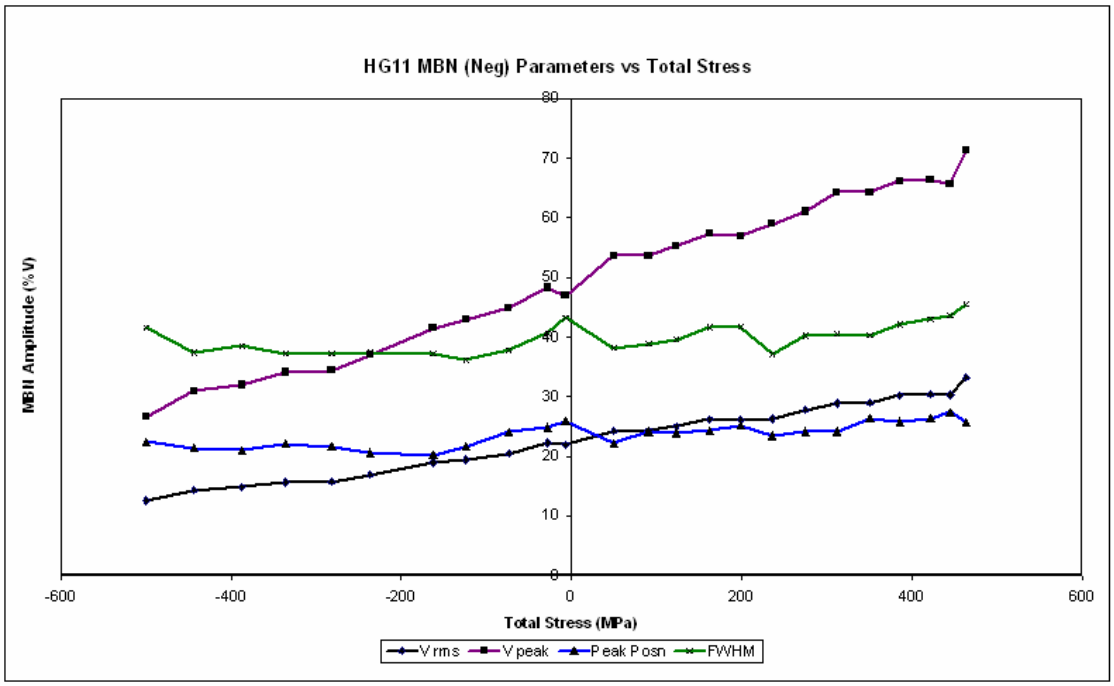

Figure 57: Variation of MBN parameters with total stress for HG11

4.2.5 Burn Threshold Prediction

Vrms voltage of the MBN signal from all the results showed that in the elastic region it behaved linearly with changes in stress. The results were used to build a model to estimate the residual stresses present in a soft 51CrV4 sample. It enabled the calculation of the residual stresses present in a sample of 51CrV4 knowing the measured MBN Vrms. The model would only apply in the linear elastic region as this linearity deviates at high stress values (plastic deformation). The linear relationship for the soft 51CrV4 was taken from the calibration of the SG05 and SG06 samples and is shown in (Figure 58).

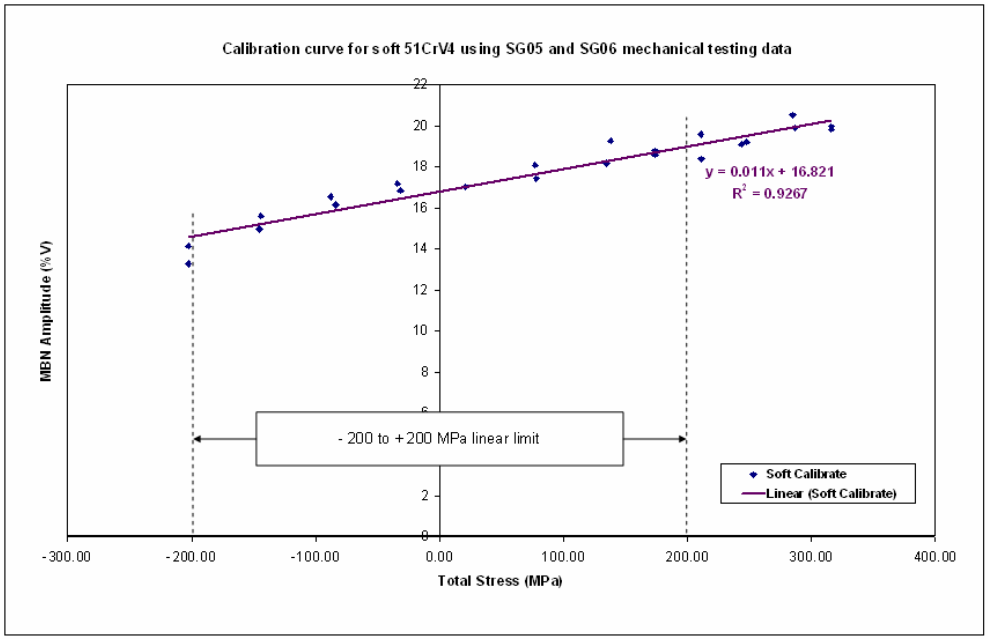

Figure 58: Linear function for predictive tool for soft 51CrV4

The linear function relating the MBN V rms voltage was derived from Figure 58 as;

$\sigma_{mbn} = \frac{V_{rms} - 16.821}{0.011}$	**Equation 7: Linear function for MBN predicted residual stress for soft 51CrV4**

Where σ_{mbn} the predicted residual stress is calculated from the measured MBN rms voltage V_{rms}. The limits of the linear function were also set as -200 to +200MPa.

The same steps were repeated for the hard 51CrV4 samples using samples HG11 and HG12 and the calibration curve is shown in **Error! Reference source not found.**.

$\sigma_{mbn} = \frac{V_{rms} - 22.102}{0.0195}$	**Equation 8: Linear function for MBN predicted residual stress for hard 51CrV4**

To verify the validity of the equation in predicting the residual stresses within the limits imposed for each, it was used to predict the stresses of a selection of samples ground with different parameters and having different known values of residual stress.

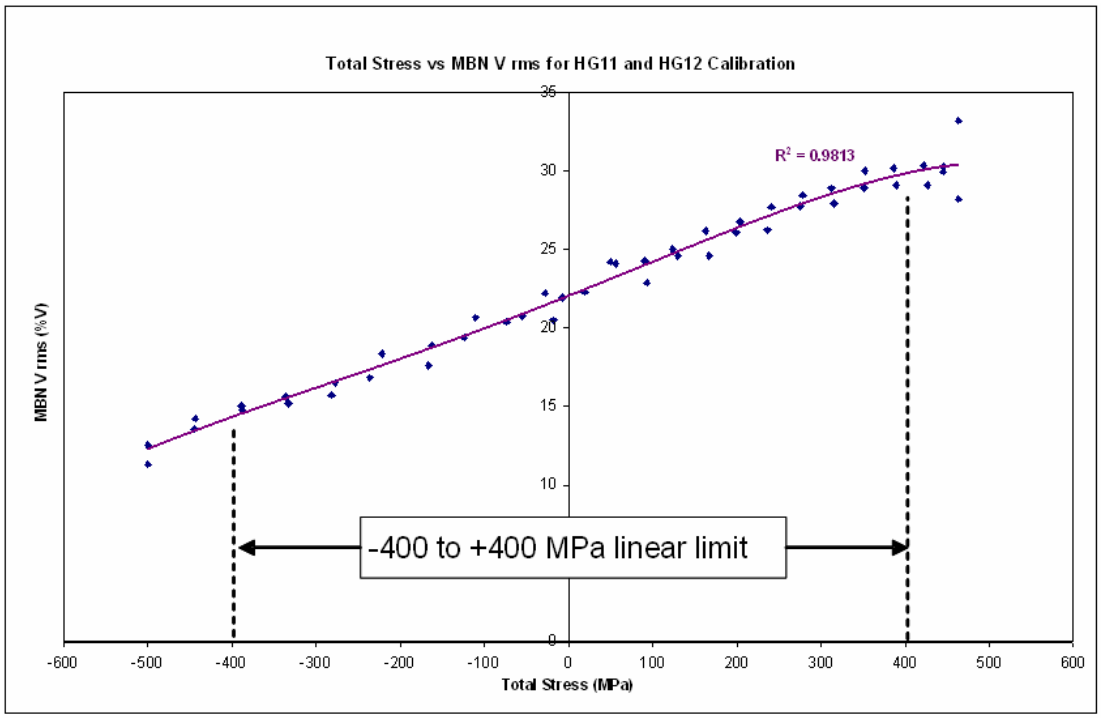

Figure 59: Linear function for predictive tool for hard 51CrV4

The soft samples ground at different Specific Material Removal Rate (M01 to M05 and PL1 to PL4) and the samples sent to Stresstech for the XRD analysis were used for the validation. The measured MBN Vrms of the samples were used to calculate the predicted stresses using Microsoft Excel and is presented in Table 9 below.

Table 9: Table of values for validation of soft prediction equation

	XRD Measured Stress (MPa)	MBN measured V_{rms} (%V)	MBN measured V_{rms} adjusted by 30% (%V)	Predicted Stress (MPa)	Overall Error (%)
Q5S	-133	22.37	15.87	-112	16
Q500S	503	17.72	11.22	-276	45
Q1000S	32	11.31	4.81	-502	1468
M01	-295	20.4	13.9	-182	38
M02	-488	22.2	15.7	-118	76
M03	-244	20.26	13.76	-187	24
M04	-476	24.06	17.56	-53	89
M05	-478	18.98	12.48	-232	52
Creep	-209	20.55	14.05	-176	15
PL1	-452	21.55	15.05	-141	69
PL2	-235	19.13	12.63	-226	4
PL3	-191	19.03	12.53	-230	20
PL4	-322	19.75	13.25	-205	36

The results are plotted below in Figure 60. From the chart, it is seen that a better prediction is only valid when the residual stress is within the limits of the predictive tool (elastic deformation region).

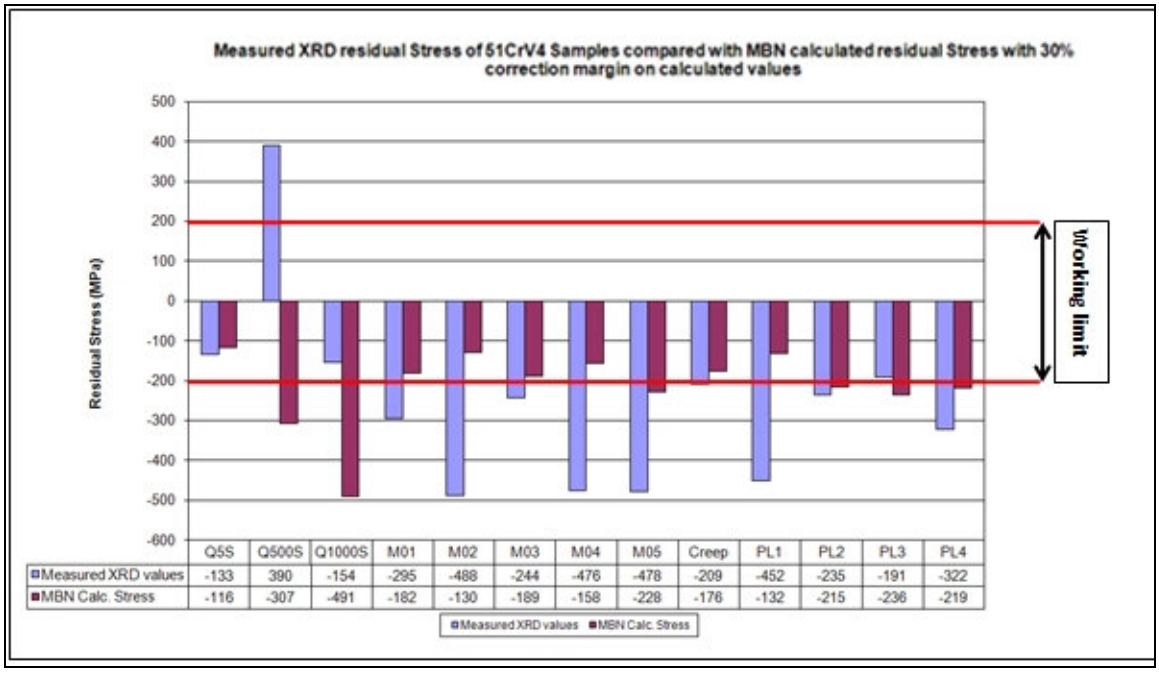

Figure 60: Comparison chart between XRD measured and MBN calculated residual stress

Samples M01, M03, Creep, PL2 and PL3 were either within the limits or near enough to give a good correlation. The biggest error with these samples was 24% for M03 and the least was 4% with PL2.

4.3 Depth Profile Investigation

The depth profiles studies were carried out using soft and hard samples of 51CrV4 of the as received samples and samples ground at Q'_w values of 5, 500 and 1000 $mm^3/mm.s$. The depth of the X – ray diffraction method is about 10µm for steel and thus controlled etching had to be used on the surface in order to access further depths under the surface. The MBN readings of the samples ground at different Q'_w values were also analysed to different depths by varying the frequency variable of Equation 4l. The depth function of a typical 51CrV4 sample of permeability 350 is shown in Figure 61.

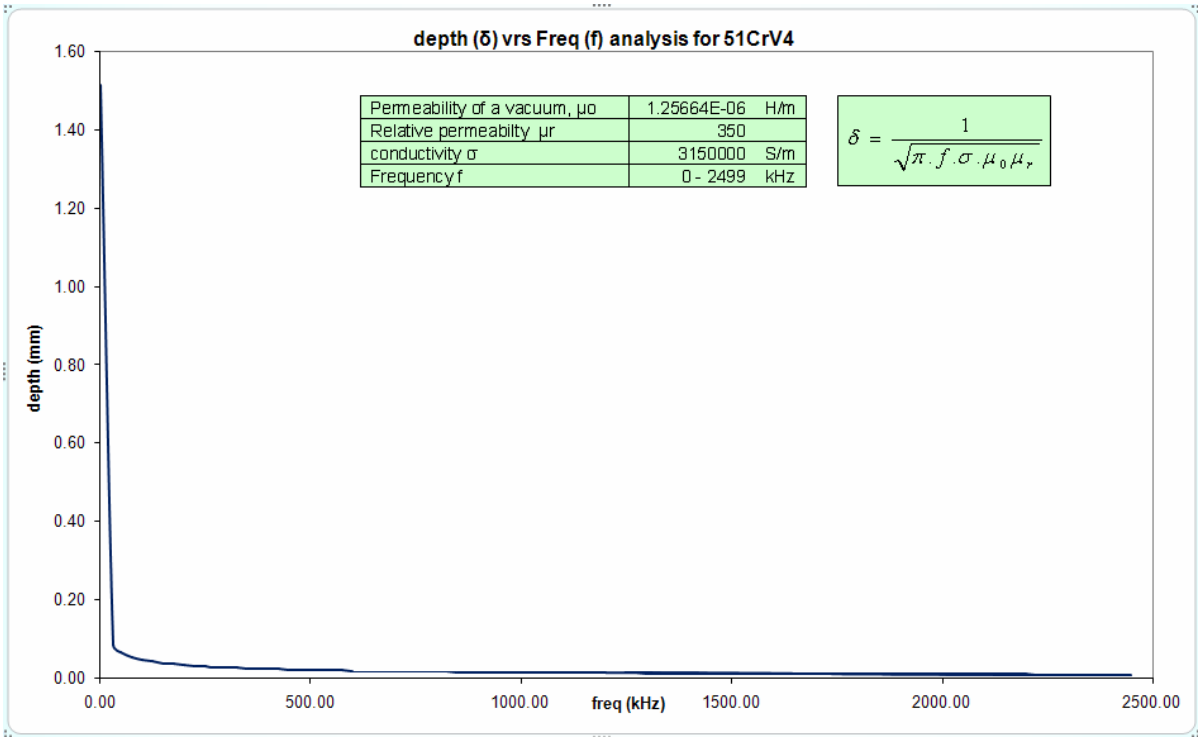

Figure 61: Calculated depth of MBN signal of a typical sample of 51CrV4

4.3.1 Soft 51CrV4 Residual Stress Profile

A table of the MBN parameters of ground samples of soft 51CrV4 together with the depth and equivalent frequencies are presented in Table 10.

Table 10: Measured XRD and MBN parameters for soft 51CrV4 at Q'_w = 5, 500 and 1000 $mm^3/mm.s$

Q5S01				XRD	MBN			
Removed depth /mm	Effective Depth /mm	Upper MBN freq. /kHz	Lower MBN freq. /kHz	Stress 0 /MPa	V rms	V peak	Peak Pos	FWHM
0	0.01	2499.00	2297.53	-252	0.136	0.27	28.63	41.87
0.006	0.016	2297.53	897.47	-250	5.664	10.1	28.04	68.69
0.01	0.02	897.47	574.38	-249	8.294	15.47	28.4	61.1
0.025	0.035	574.38	187.55	-133	16.06	30.45	30.22	59.62
0.11	0.12	187.55	15.96	-93	11.89	21.93	33.3	59.79
Q500S01				XRD	MBN			
Removed depth /mm	Effective Depth /mm	Upper MBN freq. /kHz	Lower MBN freq. /kHz	Stress 0 /MPa	V rms	V peak	Peak Pos	FWHM
0	0.01	2499	2297.53	390	0.083	0.157	25.24	38.22
0.011	0.021	2297.53	520.98	401	8.417	14.57	27.81	68.36
0.048	0.058	520.98	68.30	503	14.41	25.35	32.66	67.91
0.197	0.207	68.3	5.36	542	4.402	7.826	32.97	77.21
Q1000S01				XRD	MBN			
Removed depth /mm	Effective Depth /mm	Upper MBN freq. /kHz	Lower MBN freq. /kHz	Stress 0 /MPa	V rms	V peak	Peak Pos	FWHM
0	0.01	2499	2297.53	-154	0.084	0.077	26.89	27.7
0.013	0.023	2297.53	434.32	84	6.186	11.08	29.63	61.92
0.048	0.058	434.32	68.30	32	9.015	17.17	33.08	57.14
0.096	0.106	68.3	20.45	241	2.981	5.593	36.16	54.21
0.201	0.211	20.45	5.16	501	0.627	0.968	47.72	69.56
0.409	0.419	5.16	1.31	451	0.081	0.109	54.7	28.45

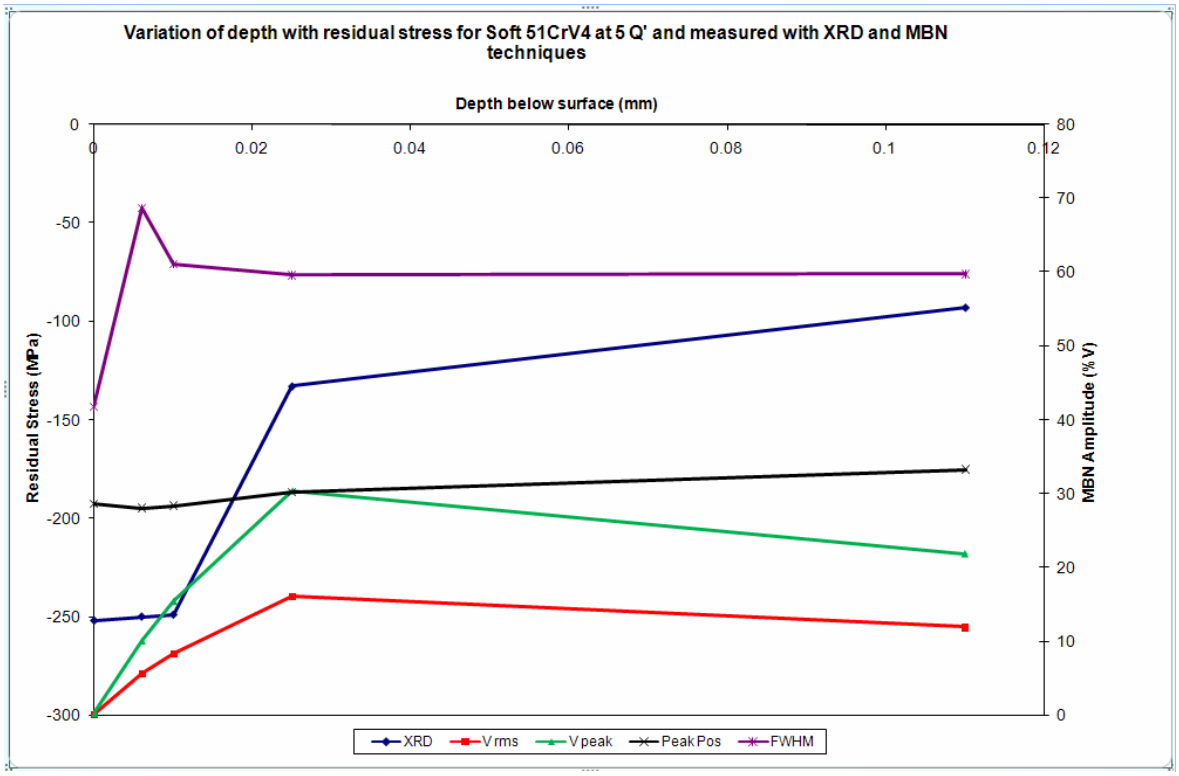

Figure 62: Variation of depth with residual stress of soft 51CrV4 using MBN and XRD techniques for Q'_w of 5 $mm^3/mm.s$

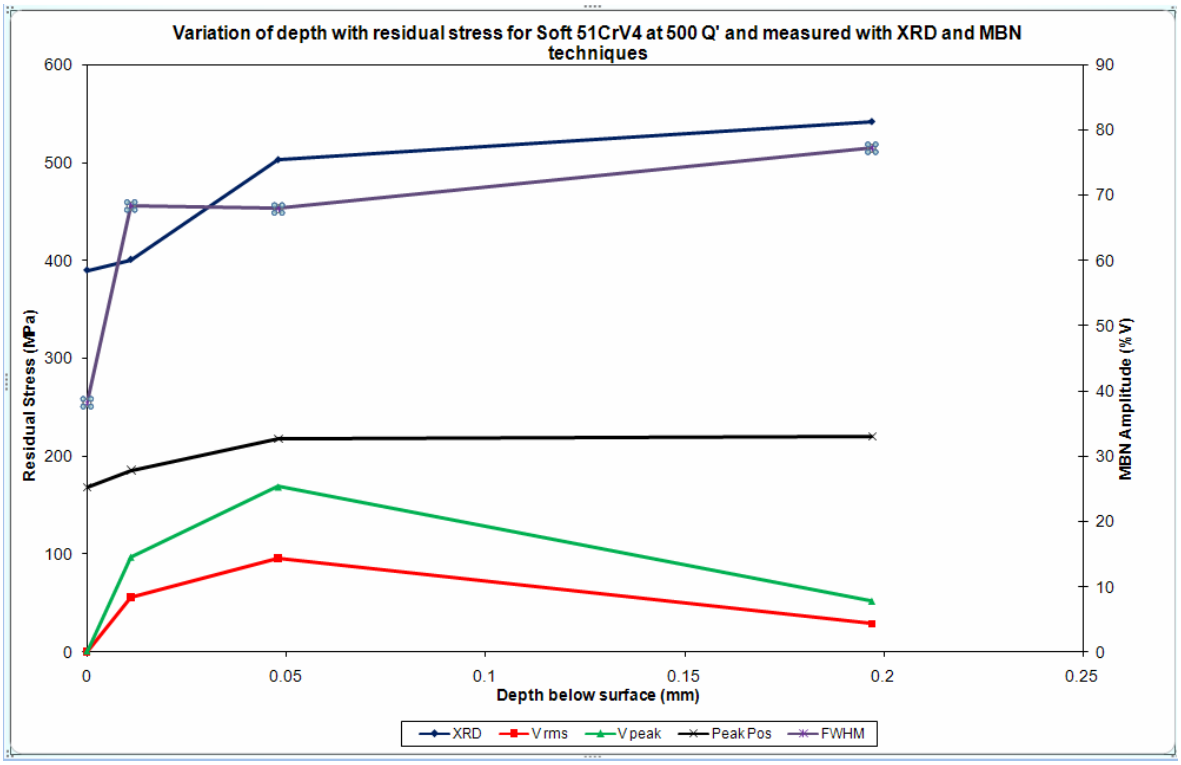

Figure 63: Variation of depth with residual stress of soft 51CrV4 using MBN and XRD techniques for Q'_w of 500 $mm^3/mm.s$

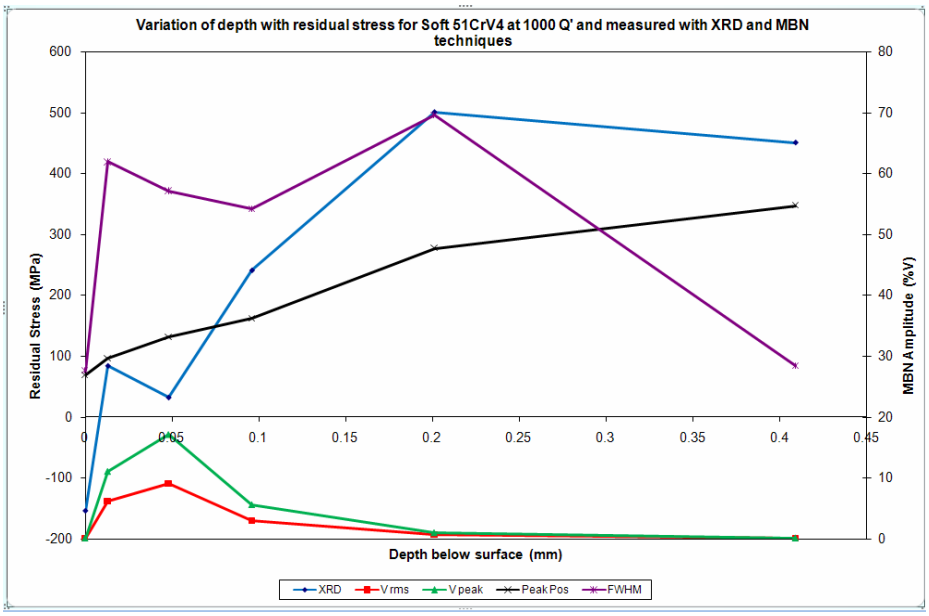

Figure 64: Variation of depth with residual stress of soft 51CrV4 using MBN and XRD techniques for Q'w of 1000 mm3/mm.s

The Q'_w of samples of 5 and 500 had a very good correlation between the XRD values and the measured MBN parameters of Vrms and Vpeak. $5Q'_w$ samples had compressive and the $500Q'_w$ was all tensile (Figure 62 and Figure 63). The $1000Q'_w$ had compressive residual stresses nearer the surface and tensile residual surfaces further deeper in the sample. The 1000 Q'_w sample also had a very good correlation between the XRD and the MBN peak position due to the change in microstructure at very such a high Q'_w (Figure 64).

4.3.2 Hard 51CrV4 Residual Stress Profile

The steps used for section for the soft sample was repeated for the hard sample. The tables and the results are summarised below for the different Q'_w in Table 11.

Table 11: Measured XRD and MBN parameters for hard 51CrV4 at Q'w = 5, 500 and 1000 $mm^3/mm.s$

Q5H01				XRD	MBN			
Removed depth /mm	Effective Depth /mm	Upper MBN freq. /kHz	Lower MBN freq. /kHz	Stress 0 /MPa	V rms	V peak	Peak Pos	FWHM
0	0.01	2499.00	2297.53	-759	0.129	0.263	22.33	34.64
0.008	0.018	2297.53	709.11	-782	7.87	15.76	23.33	44.44
0.011	0.021	709.11	520.98	-713	6.781	14.32	23.36	41.39
0.024	0.034	520.98	198.75	-314	11.49	24.68	23.67	40.74
0.102	0.112	198.75	18.32	-10	7.914	16.31	23.14	40.18

Q500H01				XRD	MBN			
Removed depth /mm	Effective Depth /mm	Upper MBN freq. /kHz	Lower MBN freq. /kHz	Stress 0 /MPa	V rms	V peak	Peak Pos	FWHM
0	0.01	2499	2297.53	-274	0.072	0.137	41.9	34.44
0.011	0.021	2297.53	520.98	-84	7.655	14.66	43.22	52.11
0.054	0.064	520.98	56.09	544	11.42	22.53	47.19	50.99
0.202	0.212	56.09	5.11	785	2.278	4.309	54.39	55.17
0.505	0.515	5.11	0.87	385	0.147	0.217	66.77	44.5
Q1000H01				XRD	MBN			
Removed depth /mm	Effective Depth /mm	Upper MBN freq. /kHz	Lower MBN freq. /kHz	Stress 0 /MPa	V rms	V peak	Peak Pos	FWHM
0	0.01	2499	2297.53	-314	0.062	0.131	36.16	29.91
0.009	0.019	2297.53	636.43	-214	6.088	12.19	36.89	46.49
0.046	0.056	636.43	73.26	-181	10.34	21.48	37.22	45.45
0.104	0.114	73.26	17.68	41	2.313	4.478	43.52	41
0.248	0.258	17.68	3.45	785	0.409	0.651	62.87	46.51
0.498	0.508	3.45	0.89	630	0.325	0.573	-92.38	53.71

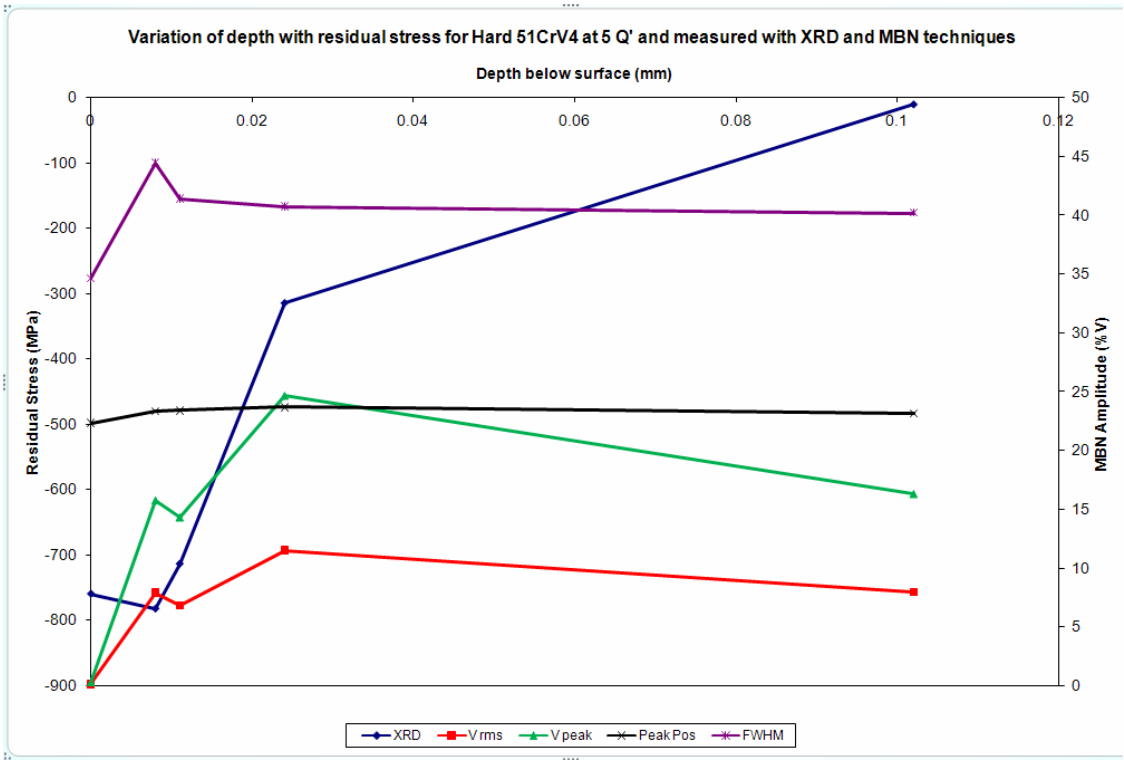

Figure 65: Variation of depth with residual stress of hard 51CrV4 using MBN and XRD techniques for Q'w of 5 mm3/mm.s

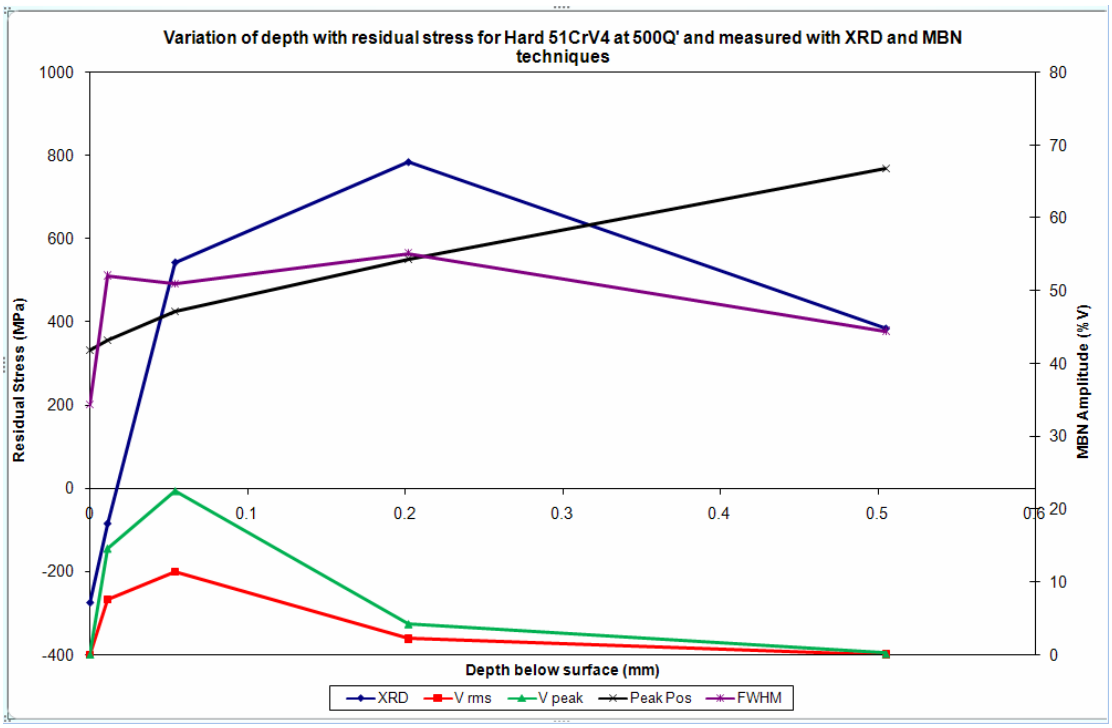

Figure 66: Variation of depth with residual stress of hard 51CrV4 using MBN and XRD techniques for Q'w of 500 mm3/mm.s

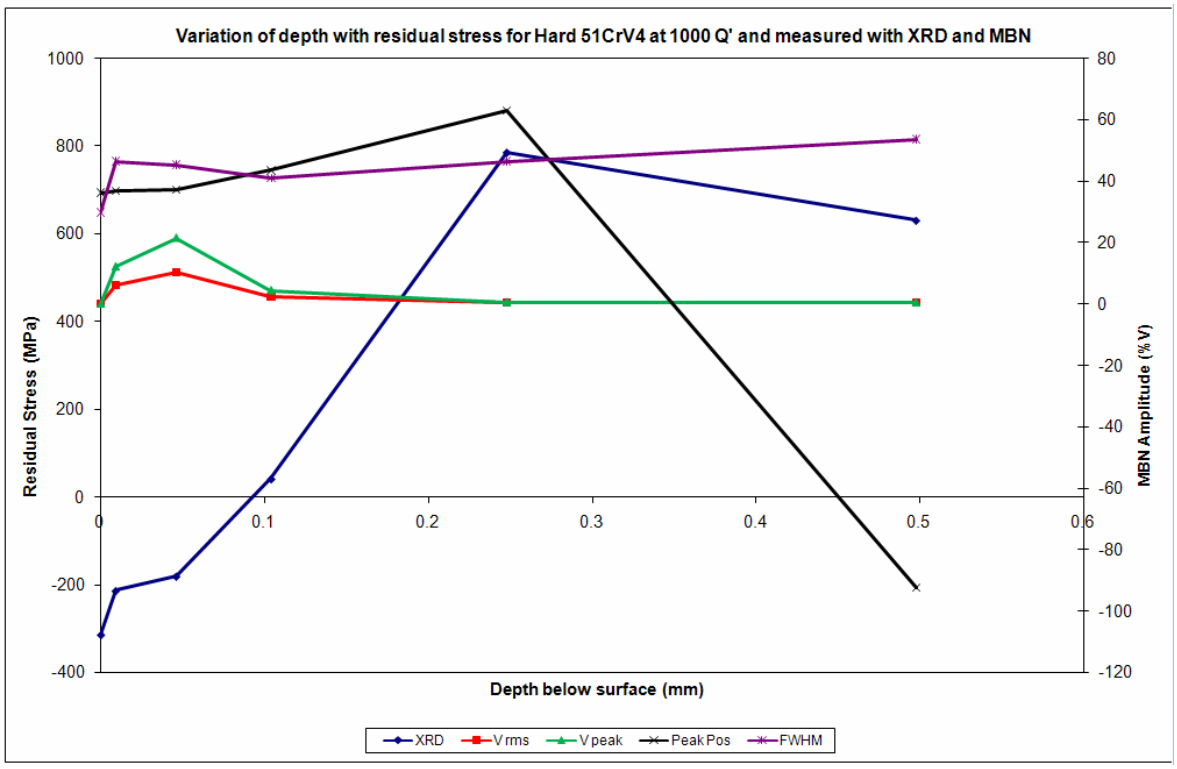

Figure 67: Variation of depth with residual stress of hard 51CrV4 using MBN and XRD techniques for Q'w of 1000 mm3/mm.s

The hard 5 Q'w sample had compressive stresses throughout the depth of the analysed depth. The Vrms and Vpeak produced a very good correlation with the XRD.

The hard 500 Q'_w also had a good correlation between the XRD and the Vrms and Vpeak with the residual stresses changing from compressive to tensile residual stresses. The peak position also had a good correlation as the compressive stresses changed to tensile stresses. The FWHM also showed a little increase and decrease at the point of change from compressive to tensile stresses (Figure 67).

The hard 1000 Q'_w sample had a very good correlation between XRD and Vrms and Vpeak. The peak position also shifted as the compressive residual stresses changed to tensile stresses (Figure 67).

Chapter 5 DISCUSSION

5.1 Burn Threshold Analysis

The calibration experiments using the MBN technique and mechanical tensile tests gave us a tool in documenting the effect of the MBN signal during elastic and plastic deformation. For all the tensile samples used, it was found that the MBN peak voltage (V peak) and the MBN Vrms (root mean squared) voltage were the most sensitive to applied stress. This corresponded to previous studies using steels where the amplitude of the MBN signal increased with increasing applied tensile stress and decreased with decreasing compressive stresses. However, this was only valid in the elastic region. When the tensile samples (SG05, SG06, HG11 and HG12) were strained beyond their elastic limit, it was found that their MBN V peak and V rms values stayed fairly constant. This also tied in with studies by Stefanita et al. (2000) that showed the onset of macroscopic yielding was the cause of the saturation of the MBN signal at higher applied stress values.

Stefanita et al (2000) also found that whereas MBN behavoiur in the elastic deformation region influenced the MBN signal by changes in the interatomic spacing (which in turn affected the magnetic behaviour of the material through magnetoelastic energy), in the plastic deformation region it occurred through slip processes.

The amplitude of the MBN signal was larger for the hard samples than it was for the soft. The hard 51CrV4 sample is characterised by small grain sizes and the soft 51CrV4 with large grain sizes (Figure 68).

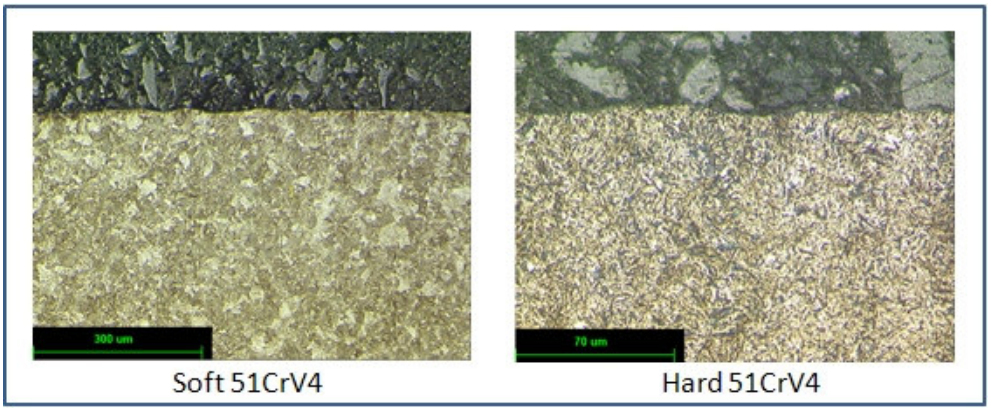

Figure 68: Hard 51CrV4 with fine grain structure and soft 51CrV4 with coarser grain structure

The large grain sizes act as pinning sites for the magnetic domains and hence produces smaller movements of the domain walls. The smaller grains on the other hand have a small dislocation density and thus produce less obstruction to the movement of the domain walls (Ng et al. 2003). This trend was also confirmed by Gatelier-Rothea et al., 1998 when they investigated the effect of MBN signals on pure iron samples with different grain sizes (50, 120 and 300µm). Since MBN signals are proportional to the number of unpinning events of domain walls, the hard samples of 51CrV4, which has the smaller grain size, will produce bigger MBN signals compared to that of the soft 51CrV4 sample. This also explains why the MBN signal is more sensitive to the hard 51CrV4 sample than the soft 51CrV4 (The slopes of the MBN versus applied stress for the hard 51CrV4 are bigger than the soft 51CrV4).

As a result of the linear behaviour of the MBN signal in the elastic deformation region, a working limit was imposed (Figure 69). The relationship between the MBN signal and stress was not linear in the plastic deformation region. For the soft sample, this was between -200MPa to and +200MPa and for the hard samples -400MPa to +400MPa. However, the viability of the predictive model for the soft 51CrV4 was tested, it was found that the working limit could be extended from -250MPa to +250MPa.

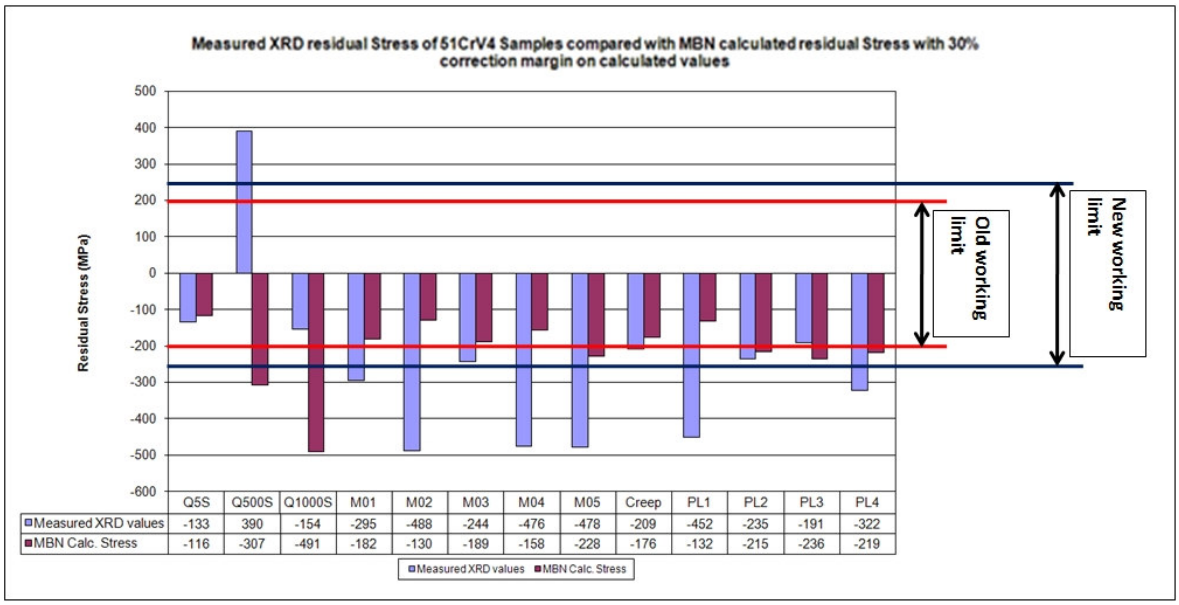

Figure 69: Working limits of the soft 51CrV4 predictive model

Within the old working limits, the biggest error margin between the measured XRD residual stress and the calculated was 20%. With the new working limits, though it included more samples, the error margin rose to 24%. The Q1000S sample with an error margin was ignored as it had undergone re-hardening burn and hence the large error (1468%) associated with it. This was confirmed from micrograph of the sample that showed resisted to nital etching and showed a white surface layer. The white layer was an untempered martensite (UTM) and below this layer was a layer of overtempered martensite (OTM).

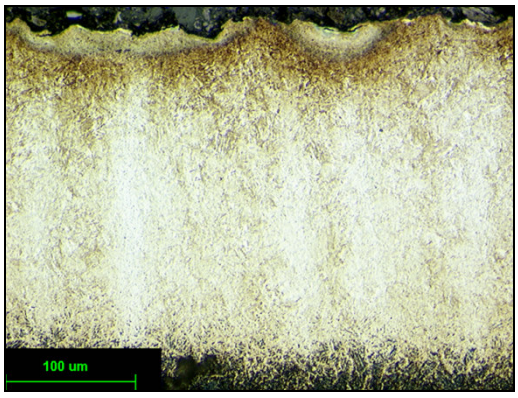

Figure 70: Micrograph of the Q1000S sample showing the white layer.

The samples outside of the limits had a large error margin because of their high stress magnitudes (compressive or tensile). In the direction of increasing Q'_w the sample being ground will first increase in compressive residual stress before it starts to increase in the tensile residual stress direction (Figure 71). A predictive

model as the one presented here will be invaluable as a quality control tool if the error margins could be reduced to make it more effective. Perhaps a more sensitive and rigorous calibration test will eliminate measurement sources of error and decrease the error margins. The model could then be used after the parts had been ground to ascertain their levels of residual stress and whether they had undergone plastic deformation or not.

The onset of grinding burn is normally accompanied by a change of residual stresses from compressive to tensile (Brinksmeier and Minke, 1993; Guptha et al., 1997; Chen et al., 2000). This was the principle factor that was to be used to detect grinding burn in this study. Badger and Torrance (2000) also stated that the residual tensile stresses caused during grinding burn were a result of thermal expansion beyond the yield stress of a material. Chen et al. (2000) found that during grinding, the resultant residual stress was a combination of compressive stresses due to mechanical deformation and tensile stress due to thermal effects. Since tensile stress are harmful for the integrity of the component being ground, keeping thermally induced stresses below the material yield stress would mean that permanent plastic deformation is avoided in the workpiece and tensile residual stresses are avoided (Chen et al., 2000).

Figure 71 (Brinksmeier and Minke, 1993) best describes the different mechanisms which results in the surface residual stress that a sample has after a grinding process.

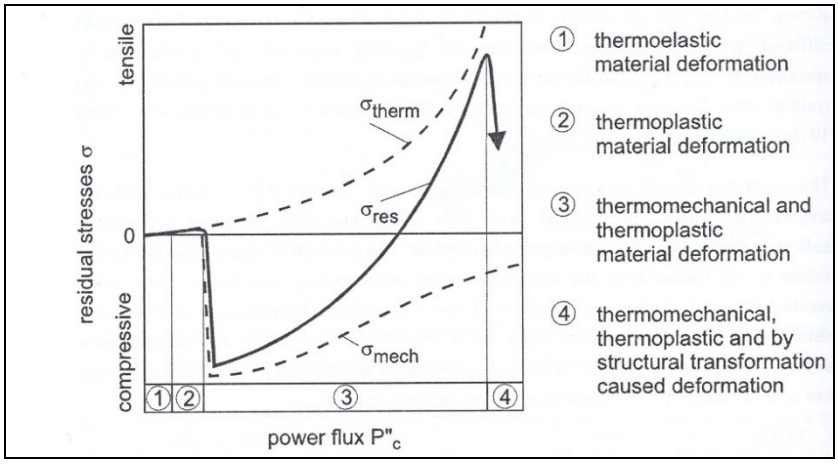

Figure 71: Different residual stress changing mechanisms during a grinding process (Brinksmeier and Minke, 1993)

As the change from compressive to tensile stress signals the start of grinding burn, this can be used to detect grinding burn before it happens. Figure 72 shows the change in MBN Vrms and with increasing grinding force which would equate to increasing residual stresses (changing from compressive to tensile).

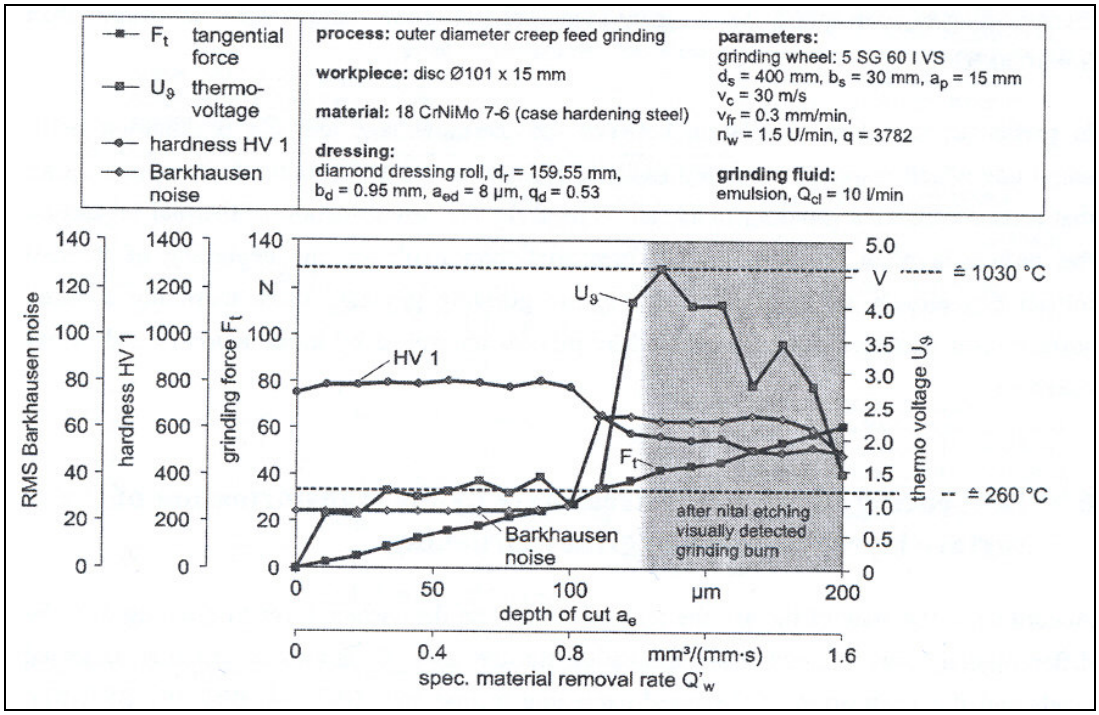

Figure 72: Change in MBN with yield (Brinksmeier and Minke, 1993).

Though the analysis was done with hardness, the results will be similar to that of residual stress. Inferring from the results of their work, the relationship shown in Figure 73 can be assumed.

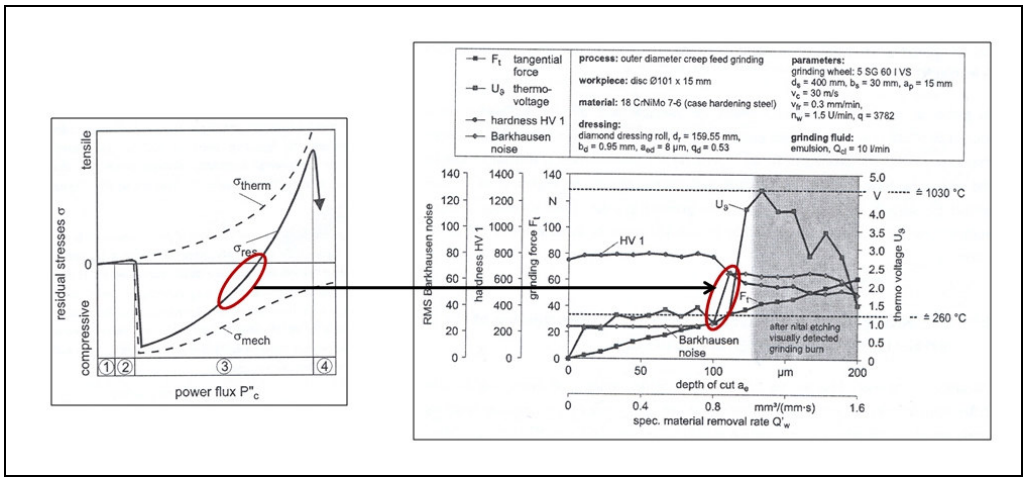

Figure 73: Change from compressive to tensile stress and equivalent change in MBN V rms (Brinksmeier and Minke, 1993).

In fact, the work of Guptha et al. (1997) produced the same results. As grinding burn was introduced into the workpiece as a result of different flow rates of the fluid (coolant), the decrease in microhardness togther with change in residual stress in the direction of tensile stress from compressive stress produced a big increase in MBN Vpeak (Figure 74).

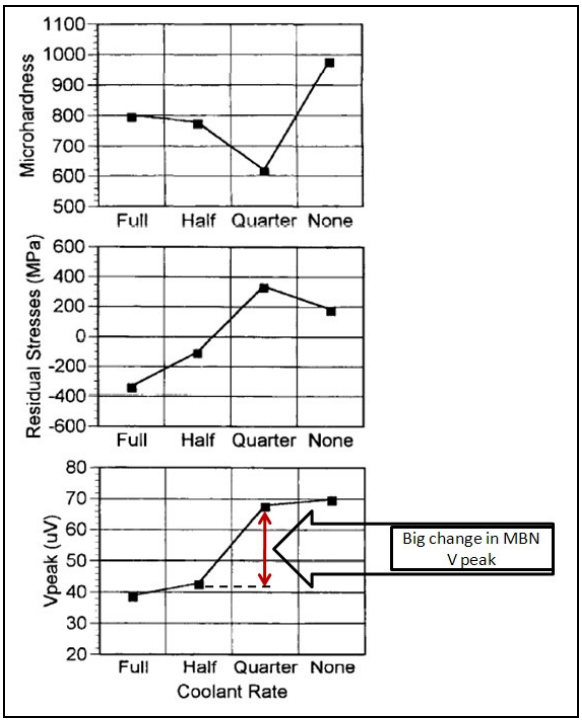

Figure 74: Variation of hardness and residual stress with MBN Vpeak as coolant rate is decreased (Guptha et al. (1997)).

Comparing these works to the results of the calibration would explain the sudden increases in V rms and V peak just before the change from compressive to tensile stress in the results (Figure 75).

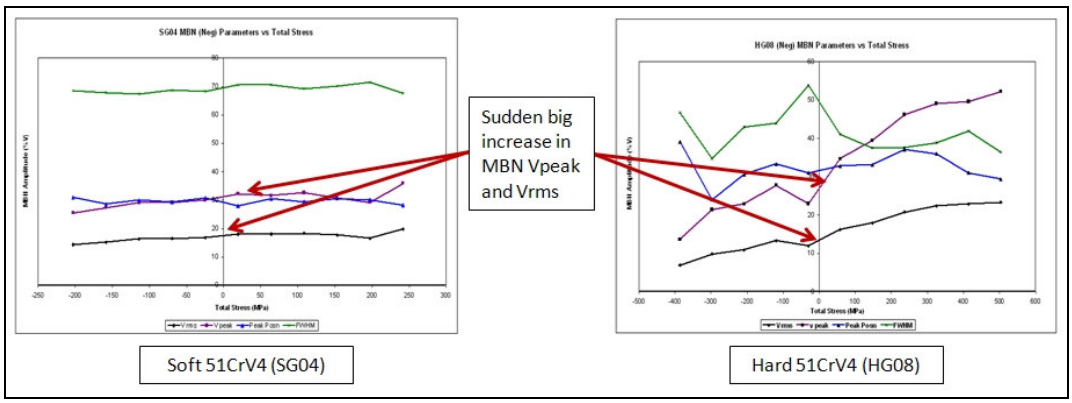

Figure 75: Examples of a hard and soft 51CrV4 sample showing sudden increases in MBN Vpeak and Vrms

The sudden increase of MBN Vpeak and Vrms though very indicative of the onset of grinding burn, is not easy to identify. This is because during the linear increase of the MBN signal with decreasing compressive and increasing tensile stress, there is a number of tiny increases and decreases. This is a result of different mechanisms that take place when increasing stress (applied or residual or both) from compressive to tensile. Moorthy, et al. 1999 split the effect of the stress-strain on the magnetic parameters into four stages. That is;

1. Perfectly elastic: The MBN signal stayed fairly constant as in the virgin state of the sample.
2. Microplastic yielding: There was a significant decrease in the MBN V peak as a result of dislocation pile-ups reducing the mean free path of the domain wall displacement.
3. Macroyielding: A sharp increase of the MBN signal amplitude, and
4. Progressive plastic deformation: A fairly linear decrease of the MBN signal as a result of the combinational effect of the introduction of compressive residual stresses on the surface and the increase of dislocation density during plastic deformation.

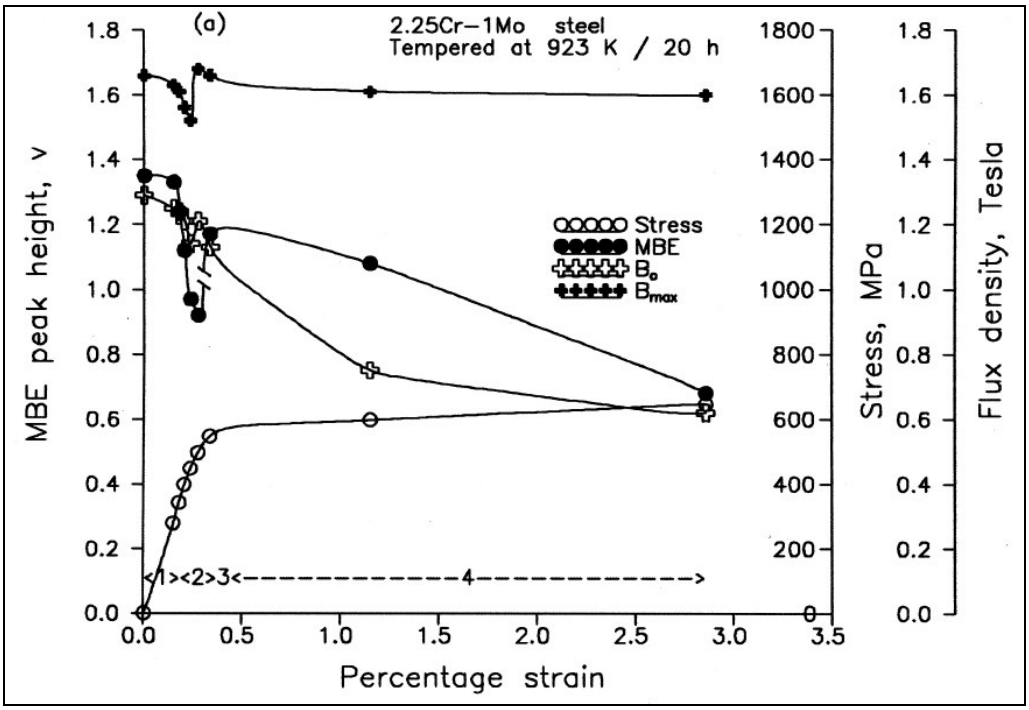

Figure 76: Variation of MBN Vpeak with the stress-strain curve showing 4 mechanisms.

Hence by detecting any sharp sudden increases of MBN V rms or V peak during grinding, the sample can be monitored for grinding burn. As the steepness of this increase would depend on the microstructure of the material being investigated it may not be the easiest to implement and the specific metal will have to be calibrated to ascertain this.

5.2 Stress Depth Analysis

From the results of the stress depth analysis, it was found that the measured MBN peak voltage (V peak) and the rms voltage (V rms) gave the best correlation, following the trend of the X –ray diffraction measured residual stress until a depth of about 30% of the calculated depth. This corresponded to results from Jiles and Suominen (1994) and Moorthy et al. (2003). Moorthy et al. (2003) explained that the difference in actual depth and calculated depth was due to the eddy current damping that opposed the attenuation of the MBN signal which depended on the frequency of the signal.

The trend of the Peak position and the FWHM parameters of the MBN signal were fairly steady for the samples with low specific material removal rates until microstructural changes at high specific removal rates. This tied in with the work Gupta et al. (1997) did, concluding that the FWHM was related to the microstructure of the material with changes pinning the magnetic Bloch walls and obstructing the movement thus influencing the signal.

It was also found that the Peak position also remained fairly steady at low removal rates and increased sharply at high removal rates. Again, this is due to the microstructural changes that occur at high removal rates due to the high temperatures associated with it. Phase changes occur at high metal removal rates due to the formation of overtempered martensite and untempered martensite. These tie in with the work by Moorthy et al. (1997).

5.2.1 Soft 51CrV4

The soft samples of 51CrV4 used for the depth analysis at a specific material removal rate of Q'_w' of 5mm^3/mm.s had been exposed to a gentle grind and thus the residual stresses present were all compressive due to mechanical plastic deformation. They were more compressive at the surface since the resultant effect was the plastic deformation of the surface layer by the grinding wheel. This tied in with the work by Brinksmeier (2003). At very low specific material removal rates, the peak position and the FWHM which are related to the microstructure (Gupta et al., 1997) of the material also stayed fairly steady since the thermal load associated is not high enough to cause any change n the microstructure.

For a 500mm^3/mm.s, the soft sample had still not undergone any microstructural changes though the stresses present in the material were tensile through to the calculated depth of 200 µm. The tensile stresses were a result of the thermomechanical and thermoplastic plastic deformations. Again, the V peak and the V rms of the MBN signal follow the trend of the measured XRD residual stress until a depth of about 50 µm, where they had a gentle decreasing slope despite an increase of residual stress in the compressive region. The peak position and the FWHM of the MBN signal also remain fairly steady showing no change in microstructure.

For the 1000mm^3/mm.s, the soft sample of 51CrV4 had undergone a phase change and this is evident from the peak position and the FWHM parameters. The FWHM parameter decreases sharply after a depth of 300 µm. There is a surface layer of untempered martensite with a hard brittle nature followed by a softer layer of untempered martensite. Also at very high removal rates, it is known from Brinksmeier (2003) that the tensile stresses change back into compressive stresses as a result of thermoplastic, thermomechanical and structural transformation caused deformation. Since hardness and stress are both being changed at the same time, the correlation between the MBN signal parameters and the XRD measured stress is poor.

5.2.2 Hard 51CrV4

The trends of the MBN peak and rms for the removal rate of 5mm^3/mm.s was the same for the soft 51CrV4 following that of the XRD measured residual stress. The slopes of the changes were sharper and higher for the hard samples than for the soft. This is due to the microstructural difference between the two materials. The hard samples of 51CRV4 have a smaller grain size which means that their dislocation densities are smaller and thus the domain walls move more freely compared to the soft samples. The peak position and the FWHM remain fairly constant also signifying no change in the microstructure through the surface of the material.

With the hard 51CrV4, it was seen that phase changes occurred with samples of material removal rate of 500 and 1000 mm^3/mm.s unlike with the soft sample where phase transformations only occurred at 1000mm^3/mm.s. Both samples also have stress depth profiles consistent with abusive grinding. The surface layers having a compressive layer at the surface which quickly rises below the surface into tensile before tending to decrease again back into the compressive region. In terms of the microstructure, the main difference between the two removal rates is with the peak position. The peak position of the 500 mm^3/mm.s hard sample shifts as depth increases. The sample of the hard 1000 mm^3/mm.s sample increases and then decreases sharply at a depth of about 250 µm. The differences can be attributed to the phase transformations. From the micrographs it is known that the 500 mm^3/mm.s has over temper burn and thus it is softer at the surface of the material whereas the 1000 mm^3/mm.s sample has untempered martensite and thus has a hard brittle layer at the surface. It has a softer layer of overtempered martensite layer underneath the hard brittle layer in the bulk of the material.

Chapter 6 CONCLUSIONS

This study looked at characterising the onset of grinding burn using the Magnetic Barkhausen Noise technique by monitoring the change in residual stresses present in the hard and soft samples of 51CrV4. The quick change of initially induced compressive stresses towards tensile stress is used as it is the most dependable sign that a material is at the onset of thermal damage. The conclusions of this research are;

1. A linear relationship between the MBN Vrms and Vpeak readings and the residual stress measurements was shown to occur in the soft 51CrV4 samples within the limits of -200MPa and +200MPa. This region relates to the elastic deformation of the sample.
2. The hard sample of 51CrV4 also showed the same linear relationship however, the region of elastic deformation was between -400MPa and +400MPa.
3. A correlation was also found between calculated stress values (from the linear relationship of residual stress and MBN Voltage) and the measured X-ray diffraction residual stress values of soft 51CrV4 samples ground with different parameters. The correlation was very good in the terms of the direction of the residual stress (compressive or tensile) and poor in terms of the magnitude.
4. Where a significant deviation in magnitude and direction was observed, the sample had undergone grinding burn and therefore the predictive model was unable to calculate the residual stresses present in the sample as a result of microstructural changes that had occurred.
5. The MBN parameters V peak and FWHM showed a sharp change in values just before the change from compressive to tensile stress. This can therefore be used to determine the onset of grinding burn.
6. The MBN technique is applicable to a coarse surface roughness of (R_a 0.15 µm) and large depths especially when compared to the X-ray diffraction technique. This correlation was also consistent with the results of the stress depth analysis up to a depth of about 30% of the calculated depth. In spite

of this, the MBN technique is still advantageous compared to its peers in the field of non – destructive evaluation. It is quick, easy to implement and portable.

Future work developing from this study can look to examine how the MBN readings compare between a rough surface and a polished surface. An in-depth study into how the predictive model will compare when using the hard samples of 51CrV4 will also be invaluable.

The Magnetic Barkhausen Noise technique is a quick non – destructive that can be applied to detecting the onset of grinding damage. This will benefit the grinding industry immensely as production rates linked with material removal rates can be increased without compromising the surface integrity of the manufactured component.

References

American Society of Mechanical Engineers. (1996). *Surface Texture (Surface Roughness, Waviness, and Lay): An American Standard.* New York.

Badger, J. A., & Torrance, A. (2000, December). Burn Awareness. *Cutting Tool Engineering Magazine , 52* (12).

Brandes, C. R., & Brook, G. B. (1992). *Smithells Metal Reference Book* (7th Edition ed.). Reed Educational and Professional Publishing.

Brinksmeier, E. (2003). Influence of Process Design on Residual Grinding Stresses. *1st European Conference on Grinding.* Aachen, Germany.

Brinksmeier, E., & Minke, H. (1993). High Performance Surface Grinding: The influence of Coolant on the Abrasive Process. *Annals of the CIRP , 42* (1), 367.

Brundle, C. R., Evans, C. A., & Wilson, S. (1992). *Encyclopedia of Materials Characterization: Surfaces, Interfaces Thin Films.* Butterworth.

Ceurter, J. S., Smith, C., & Ott, R. (1999). The Barkhausen Noise Inspection Method for Detecting Grinding Damage in Gears. *2nd International Conference on Barkhausen Noise and Micromagnetic Testing*, (pp. 53-64). Newcastle, UK.

Chen, X., Rowe, W. B., & Cai, R. (2002). Precision grinding using CBN wheels. *International Journal of Machine Tools and Manufacture , 42* (5), 585-593 .

Chen, X., Rowe, W. B., & McCormack, D. F. (2000). Analysis of the Transitional temperature for Tensile Residual Stresses in Grinding. *Journal of Materials Processing Technology , 107* (1-3), 216-221.

Degarmo, P., Black, J. T., Kohser, R. A., & Klamecki, B. E. (2003). *Materials and processes in Manufacturing* (9 edition ed.). John Wiley and Sons.

Desvaux, S., Duquennoy, M., Gualandri, J., & Ourak, M. (2004). The evaluation of surface residual stress in aeronautic bearings using the Barkhausen noise effect. *NDT & E International , 37*, 9-17.

Dhar, A., Clapham, L., & Atherton, D. L. (2001). Influence of Uniaxial Plastic Deformation on Magnetic Barkhausen Noise. *NDT & E , 34* (8), 507-514.

Donzella, G., Flammini, A., Sardini, E., Sisinni, E., & Solazzi, L. (2003). Multiparametric Barkhausen Noise Measurements for Stress and Microstructure Evaluation. *4th International Conference on Barkhausen Noise and Micromagnetic Testing*, (pp. 19-29). Brescia, Italy.

Engineers Edge. (2007). *Surface Grinding Machines and Process.* Retrieved August 29, 2007, from EngineersEdge: http://www.engineersedge.com/manufacturing/surface-grinding-process.htm

Fields, M., & Kahles, J. F. (1971). Review of Surface Integrity of Machined Components. *Annals of the CIRP , 20* (1), 107-108.

Freimuth, T., & Mandrysch, T. (1999). Micromagnetic in-process surface integrity analysis of ground workpieces. *2nd International Conference of Barkhausen Noise and Micromagnetic Testing*, (pp. 101-113). Newcastle, UK.

Gatelier-Rothea, C., Chicois, J., Fougeres, R., & Fleischmann, P. (1998). Characterization of pure iron and (130 p.p.m.) carbon-iron binary alloy by Barkhausen noise measurements: study of the influence of stress and microstructure. *Acta. Mater. , 46* (14), 4873-4882.

Gauthier, J., Krause, T. W., & Atherton, D. L. (1998). Measurement of residual stress in steel using the magnetic Barkhausen noise technique. *NDT & E International , 31* (1), 23-31.

Griffiths, B. (2001). *Manufacturing Surface Technology - Surafce Integrity and Functional Performance.* Penton Press.

Guptha, H., Zhang, M., & Parakka, A. P. (1997). Barkhausen Effects in Ground Steels. *Acta Mater , 45* (5).

Jiles, D. C. (1988). Review of Magnetic Methods for Non-destructive Evaluation. *NDT International , 21* (5), 311-319.

Jiles, D. C., & Suominen, L. (1994). Effects of surface stress on Barkhausen effect emissions: Model predictions and comparison with X-ray diffraction studies. *IEEE Transactions on Magnetics , 30* (6), 4924-4926.

Kandil, F. A., Lord, J. D., Fry, A. T., & Grant, P. V. (2001). *A Review of Residual Stress Measurement Methods - A guide to technique selection.* National Physics Laboratory, UK.

Karpuschewski, B. (1998). Introduction to Micromagnetic Techniques. *1st International Conference on Barkhausen Noise and Micromagnetic Testing*, (pp. 85-99). Hannover, Germany.

Karpuschewski, B., & Mandrysch, T. (1998). Micromagnetic in-process surface integrity analysis of ground workpieces. *1st International Conference on Barkhausen Noise and Micromagnetic Testing* (pp. 111-124). Hannover: Stresstech Oy.

King, R. I., & Hahn, R. S. (1986). *Handbook of modern Grinding Technology.* New York: Chapman and Hall.

Kleber, X., & Vincent, A. (2004). On the role of residual internal stresses and dislocations on Barkhausen noise in plastically deformed steel. *NDT & E International , 37*, 439-445.

Koshal, D. (1993). *Manufacturing Engineer's Reference Book.* Oxford: Elsevier.

Koster, W. P., Field, M., & Fritz, L. J. (1970). *Surface Integrity of Machined Structural Components* . Wright-Patterson Air Force Base, Materials Laboratory . Ohio: Wright-Patterson AFB.

Kutz, M. (2002). *Handbook of Material Selection.* John Wiley and Sons.

Kutz, M. (1998). *Mechanical Engineer's Handbook* (2nd Edition ed.). New York: John Wiley and Sons.

Marinescu, J. D., Rowe, W. B., Dimitrov, B., & Inasaki, I. (2004). *Tribology of Abrasive Machining Processes.* William Andrew Publishing.

Metcut Research Associates. (1980). *Machining data Handbook* (3rd Edition ed.). Cincinnati, Ohio.

Moorthy, V., Vaidyanathan, S., Jayakumar, T., Raj, B., & Kashyap, B. P. (1999). Effects of Tensile Deformation on Micromagnetic Parameters in 0.2% Carbon Steel and 2.25Cr-1Mo Steel. *Acta Mater , 47* (6), 1869-1878.

Ng, D. H., Cho, K. S., Wong, M. L., Chan, S. L., Ma, X. Y., & Lo, C. C. (2003). Study of microstructure, Mechanical Properties and Magnetization Process in Low Carbon Steel Bars by Barkhausen Emission. *Material Science and Engineering , A358* (1-2), 186-198.

Ng, D. H., Cho, K. S., Wu, C. N., Ng, H. T., & Ma, X. Y. (1999). The Effect of Residual Stress and Continuous Tensile Stress on Barkhausen Emission in Mild Steels. *Magnetics Conference 1999. Digest of INTERMAG 99.* IEEE International.

Physique & Industrie. (2003). *Physique & Industrie*. Retrieved from http://www.physiqueindustrie.com/residual_stress.php

Shaw, B. A., Hyde, T. R., & Evans, J. T. (1998). Detection of grinding damage in Hardened Gear Steels Using Barkhausen Noise Analysis. *1st Conference on Magnetic Barkhausen Noise and Micromagnetic Testing* (pp. 187-196). Hannover: Stresstech Oy.

Shaw, M. C. (1996). *Principles of Abrasive Processing* . Oxford: Clarendon Press.

Smallman, R. E., & Bishop, R. J. (2003). *Modern Physical Metallurgy and Materials Engineering - Science, Process, Applications* (6th Edition ed.). Elsevier.

Smith, W. F. (1981). *Structure and Properties of Engineering Alloys.* USA: McGraw Hill Inc.

Snoyes, R., Maris, M., & Peters, J. (1972). Thermally induced damage in grinding. *Annals of the CIRP , 27* (2), 571-581.

Stefanita, C. G., Atherton, D. L., & Clapham, L. (2000). Plastic versus Elastic Deformation Effects on Magnetic Barkhausen Noise in Steel. *Acter Mater , 48* (13), 3545-3551.

Stewart, D. M., Stevens, K. J., & Kaiser, A. B. (2004). Magnetic Barkhausen Noise analysis of stress in steel. *Current Applied Physics , 4* (2-4), 308-311.

Tawakoli, T. (1993). *High Efficiency Deep Grinding: Technology, process planning and economic application.* Mechanical Engineering Publications.

Tonshoff, H. K., Karpuschewski, B., & Oberbeck-Spintig, I. (1998). Residual stress determination of ferromagnetic sheets. *1st International Conference on Barkhausen and Micromagnetic Testing* (pp. 141-168). Hannover: Stresstech Oy.

Walton, I. M., Stephenson, D. J., & Baldwin, A. (2006). The measurement of grinding temperatures at high specific removal rates. *International Journal of Machine Tools and Manufacture , 46*, 1617-1625.

Wojitas, A. S., Souminen, L., Shaw, B. A., & Evans, J. T. (1998). Detection of Thermal Damages in Steel Components after Grinding using Magnetic Barkhausen Noise Method. *7th European Conference on Non-Destructive Testing*, *3.* Copenhagen.

Appendix A: 51CrV4 Material Specification Sheet

saarstahl

Material specification sheet

Saarstahl - 51CrV4 (50CrV4)

Material No.:	Former brand name:	International steel grades:
1.8159	F2K	BS: 735A51, 735M50, 735H51 AFNOR: 50CrV4, 51CV4 SAE: 6150

Material group: Steel for quenching and tempering according to DIN EN 10083

Chemical composition: (Typical analysis in %)

C	Si	Mn	Cr	V	other
0,50	0,25	0,90	1,10	0,12	(Pb)

Application: Alloyed heat treatable steel with a typical tensile strength of 900 - 1200 N/mm². For automotive and mechanical engineering components as gear parts, pinions, shafts.

Hot forming and heat treatment:

Forging or hot rolling:	1050 - 850°C
Normalising:	870 - 900°C/air
Soft annealing:	680 - 720°C/furnace
Hardening:	820 - 860°C/oil
Tempering:	540 - 680°C/air

Mechanical Properties:

Treated for cold shearability +S:	See condition A
Soft annealed +A:	max. 248 HB

Quenched and tempered, +QT:

Diameter d [mm]	≤ 16	>16 – 40	>40 – 100	>100 – 160	>160 – 250
Thickness t [mm]	≤ 8	8<t<20	20<t<60	60<t<100	100<t<160
0,2% proof stress $R_{p0,2}$ [N/mm²]	min. 900	min. 800	min. 700	min. 650	min. 600
Tensile strength R_m [N/mm²]	1100 - 1300	1000 - 1200	900 - 1100	850 - 1000	800 - 950
Fracture elongation A_5 [%]	min. 9	min. 10	min. 12	min. 13	min. 13
Reduction of area Z [%]	min. 40	min. 45	min. 50	min. 50	min. 50
Notch impact energy ISO-V [J]	min. 30	min. 30	min. 30	min. 30	min. 30

(http://www.saarstahl.com/english/produkte/walzstahlsorten/PDF-Dokumente/8159_51CrV4.pdf)

Appendix B: Surface Roughness Profiles of Tensile specimen

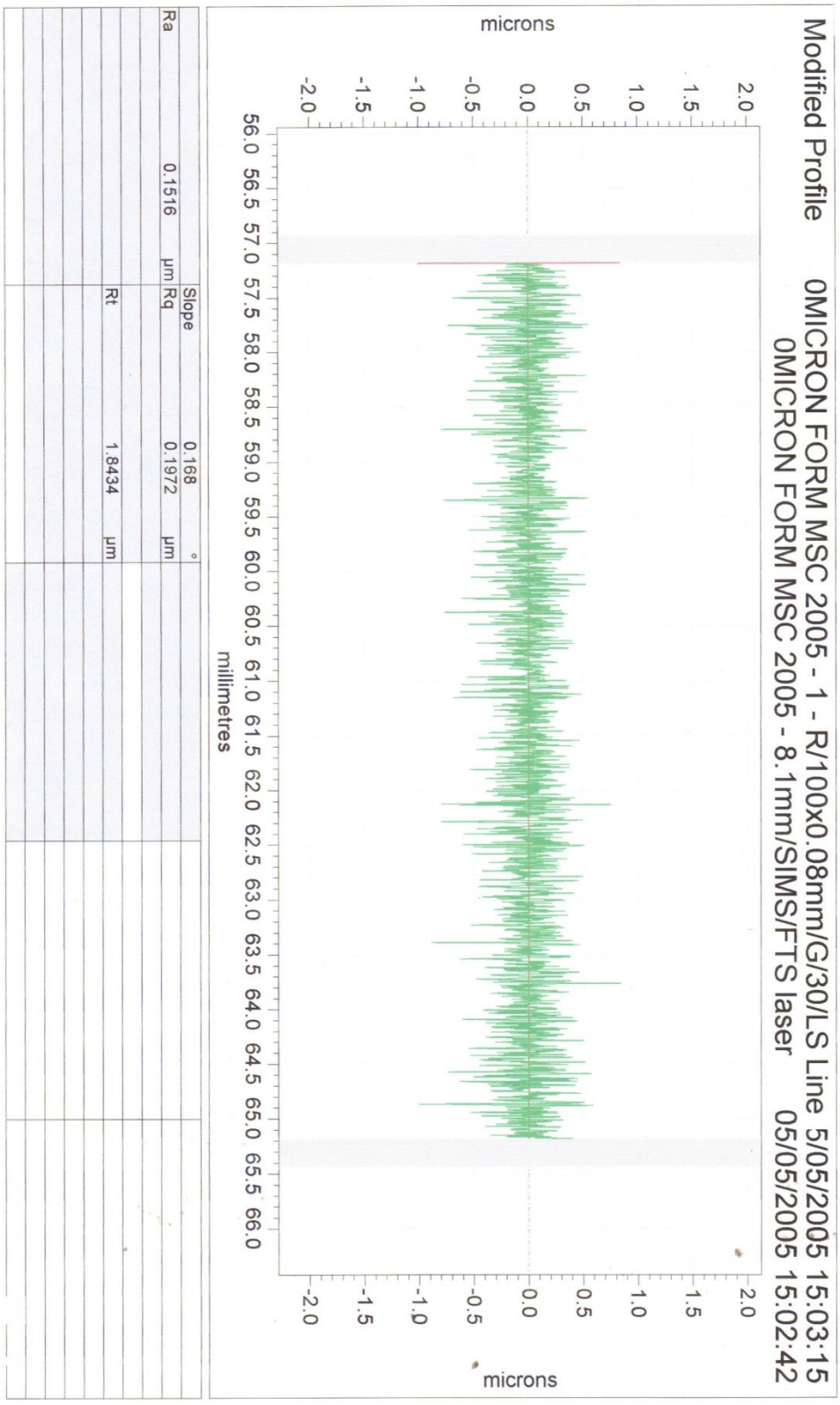

Figure 77: Surface roughness profile for ungrounded (as received) tensile specimen

Figure 78: Surface roughness profile for grounded tensile specimen

Appendix C: XRD Plots of Baseline Creep Ground Samples

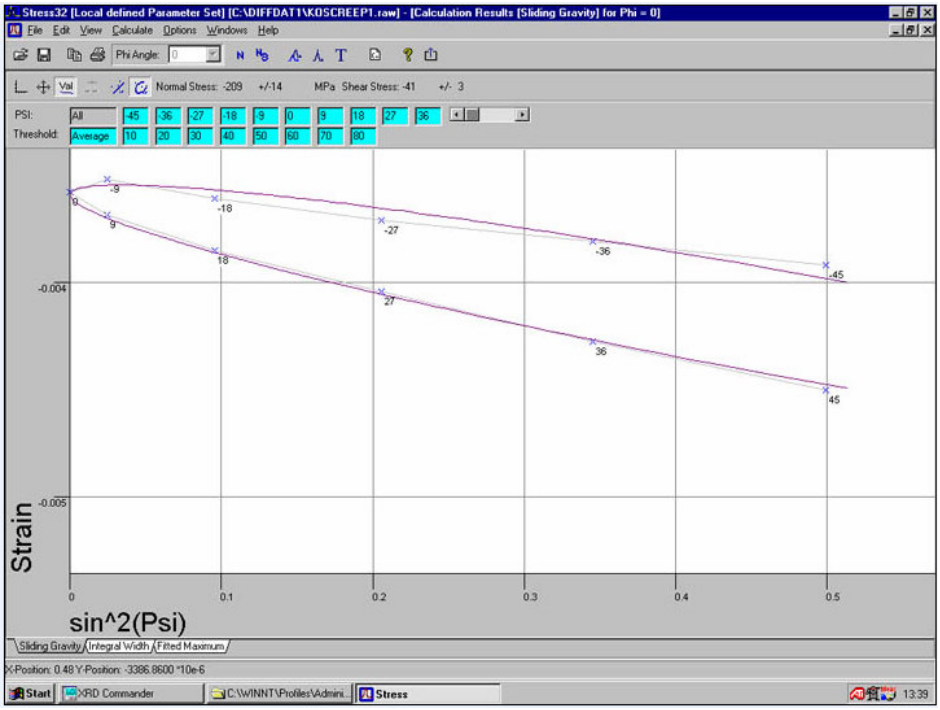

Figure 79: XRD Plot of Creep Ground 51CrV4 Soft sample (Representing a tensile specimen with a coarse surface on 1 side)

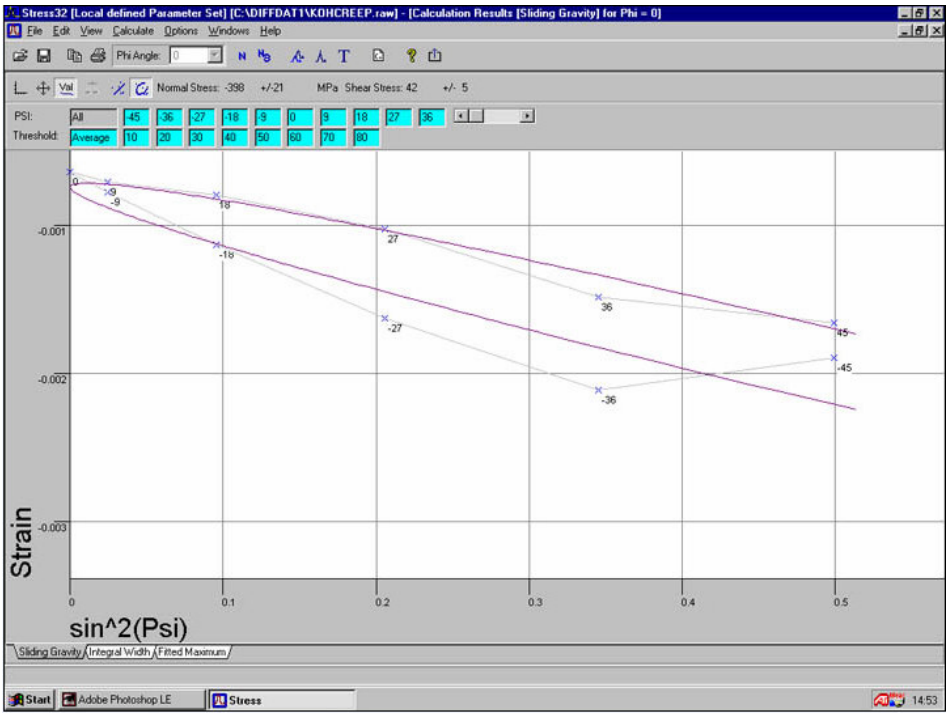

Figure 80: XRD Plot of Creep Ground 51CrV4 Soft sample (Representing a tensile specimen with a coarse surface on 1 side)

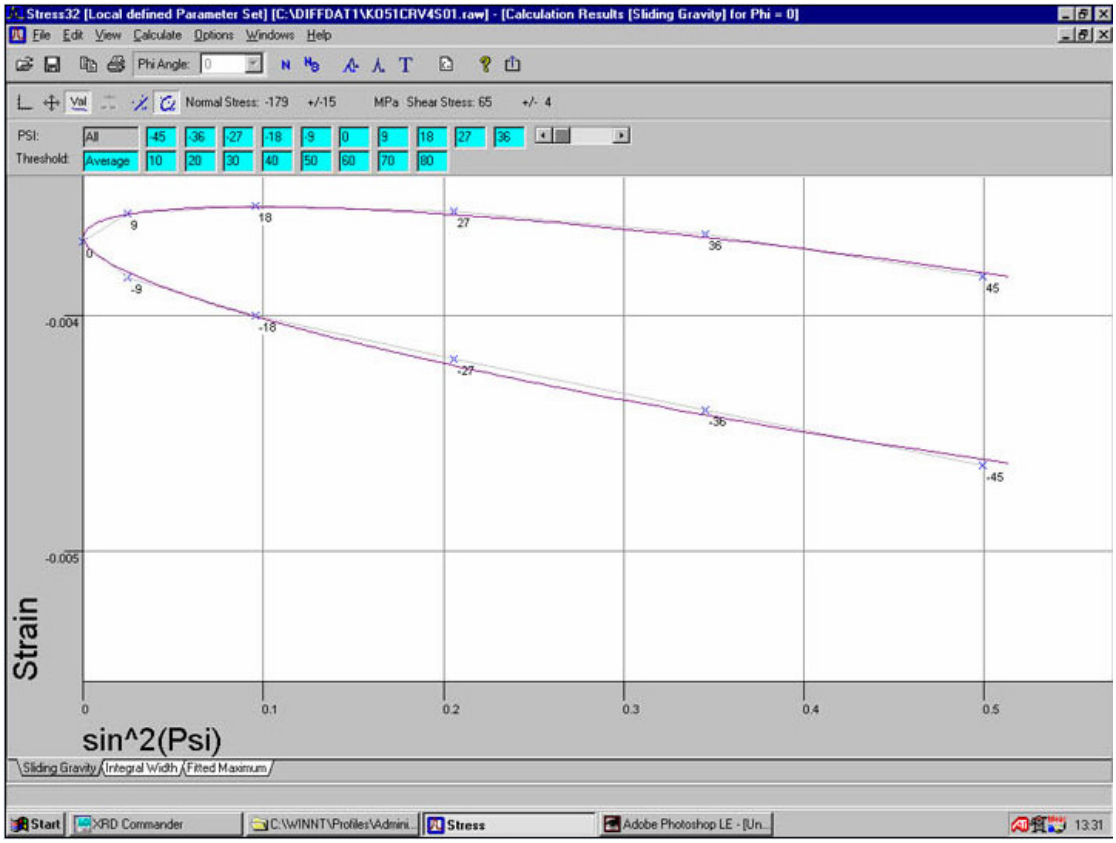

Figure 81: XRD Plot of as received 51CrV4 Soft sample (Representing an as received tensile specimen)

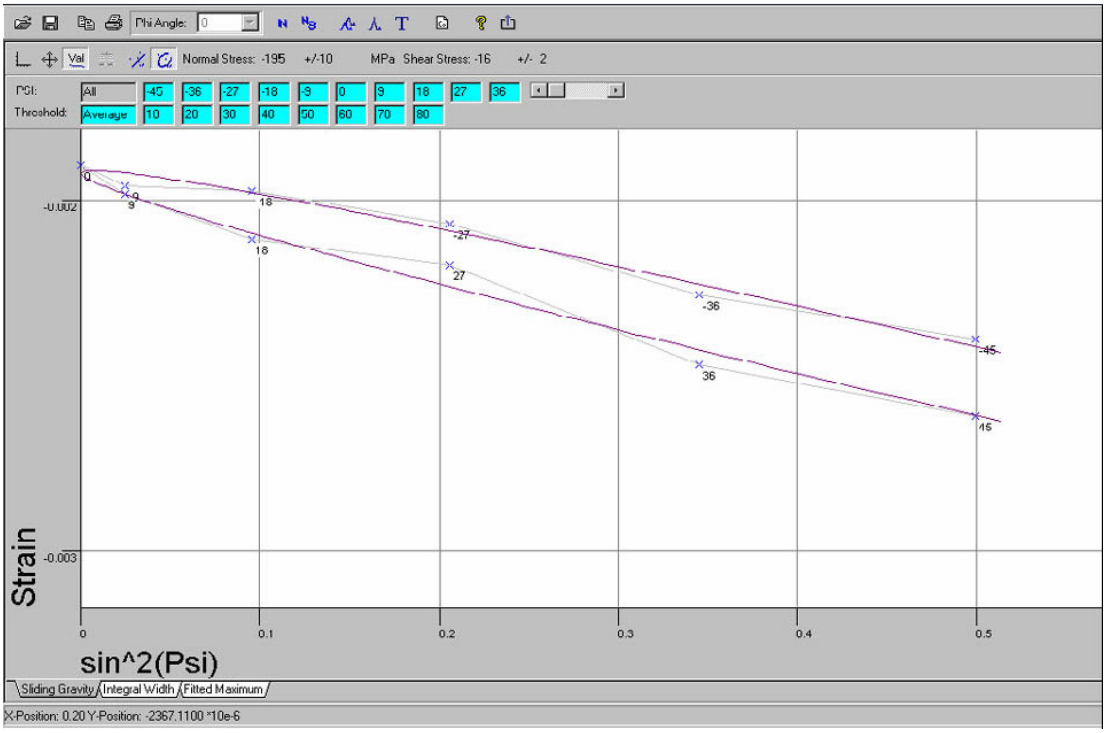

Figure 82: XRD Plot of as received 51CrV4 hard sample (Representing an as received tensile specimen)

Appendix D: SG04 Calibration Charts

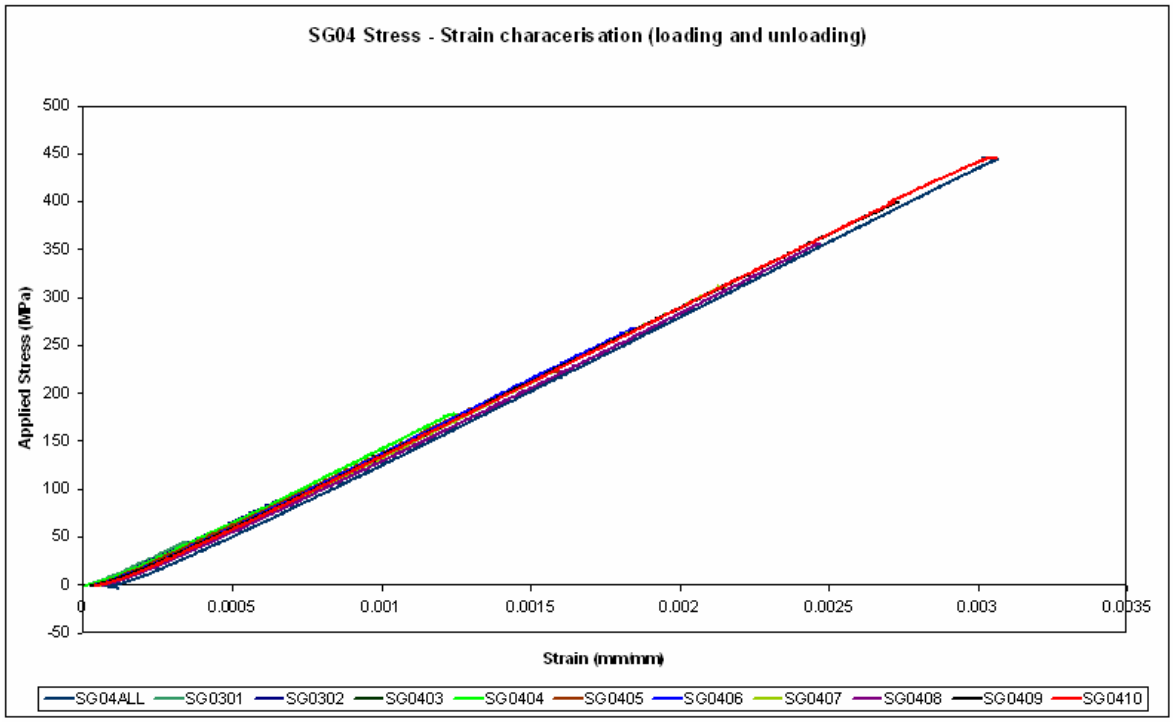

Figure 83: Stress - Strain chart for SG04 tensile sample, unloading after each load until 448 MPa

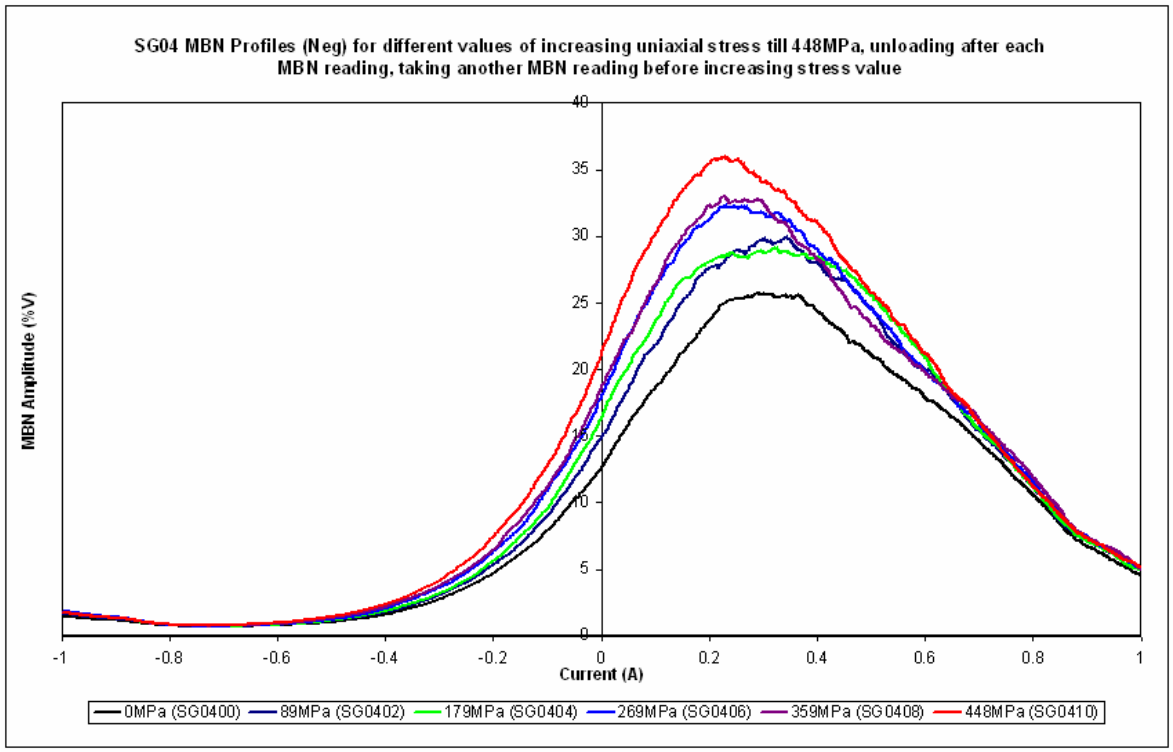

Figure 84: MBN Profiles of SG04 with increasing applied stress

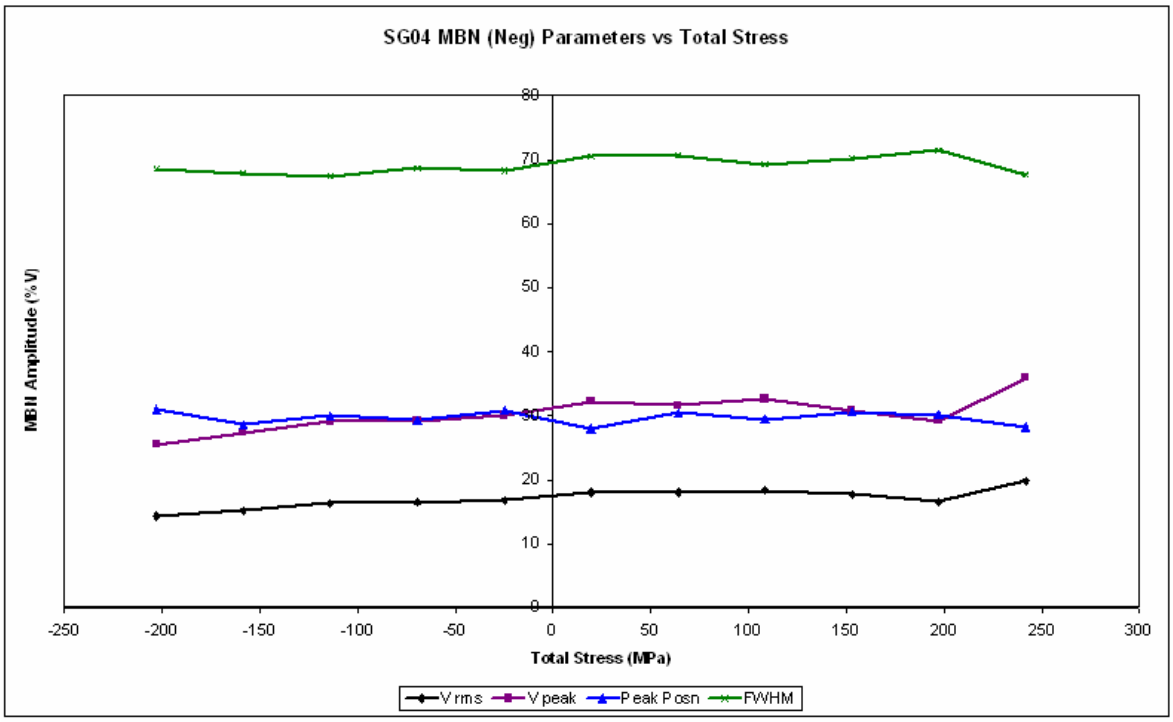

Figure 85: Total stress versus the MBN parameters for SG04

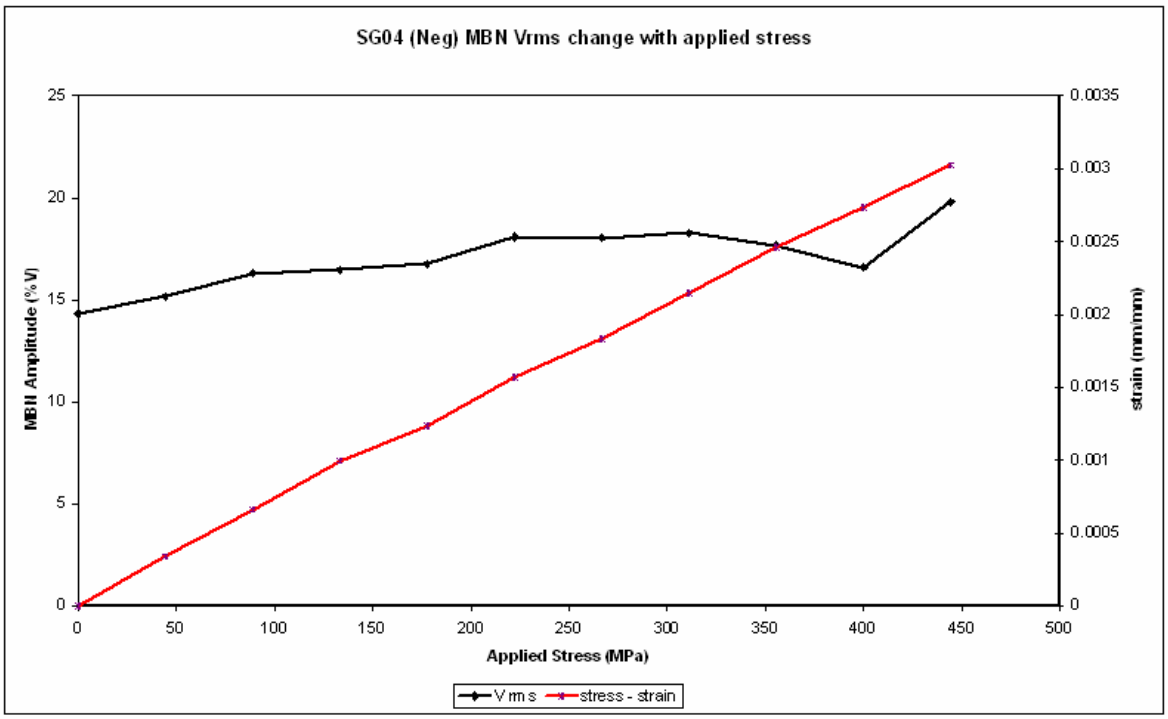

Figure 86: MBN Vrms variation as applied load increases for SG04

Appendix E: SG06 Calibration Charts

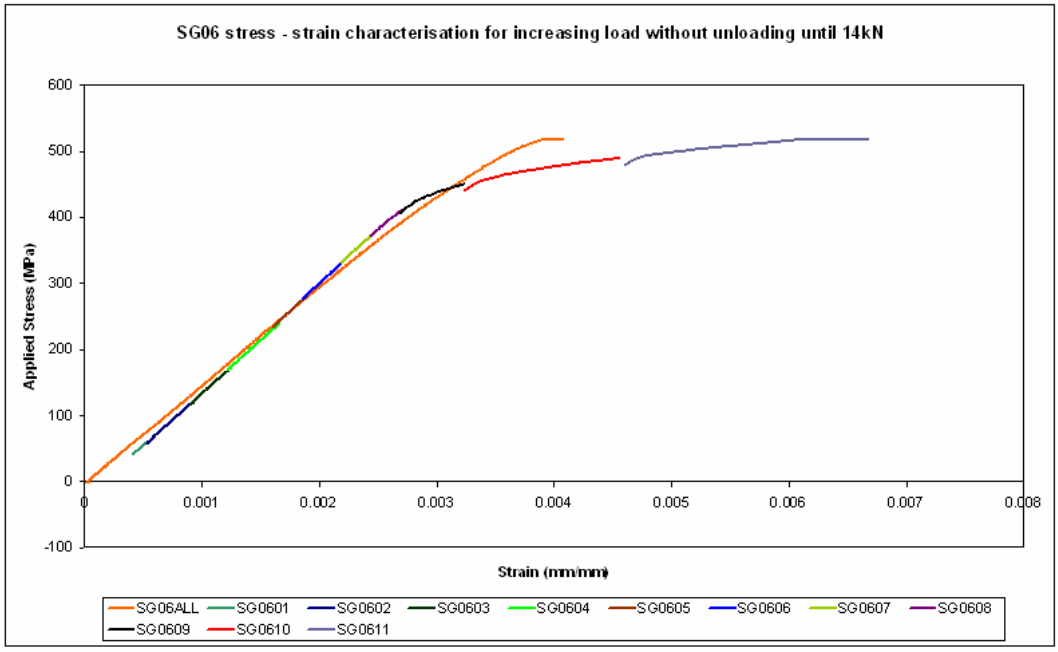

Figure 87: Stress - Strain chart for 51CrV4 Soft (SG06) tensile sample, unloading after each load until 518.5 MPa/14kN

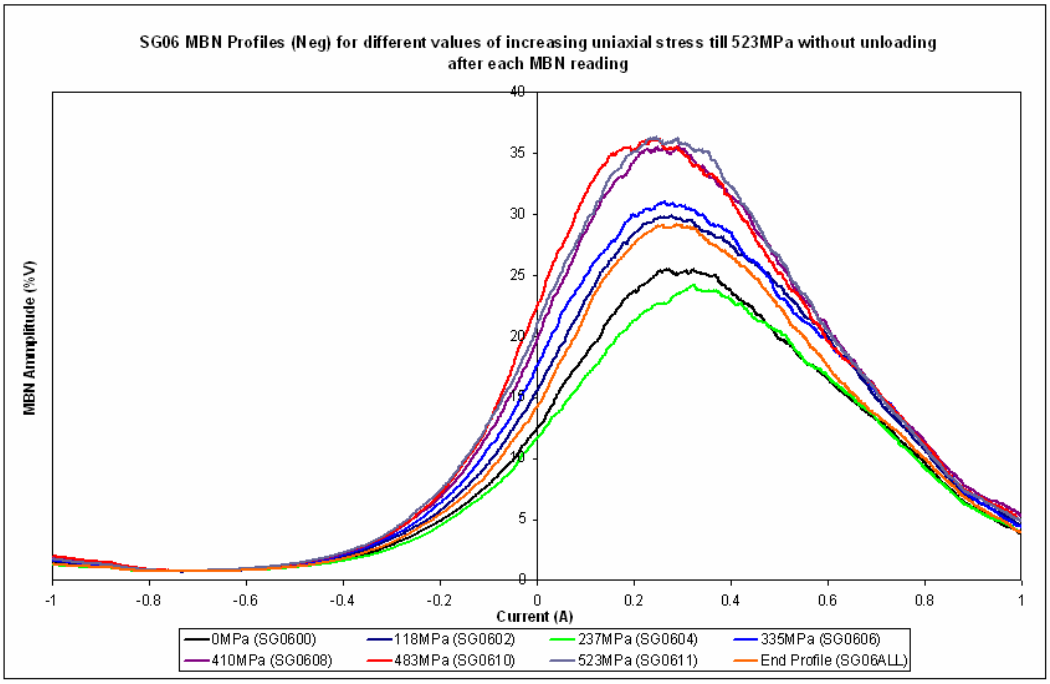

Figure 88: MBN profile envelope of SG06 tensile specimen loaded without unloading until 14kN

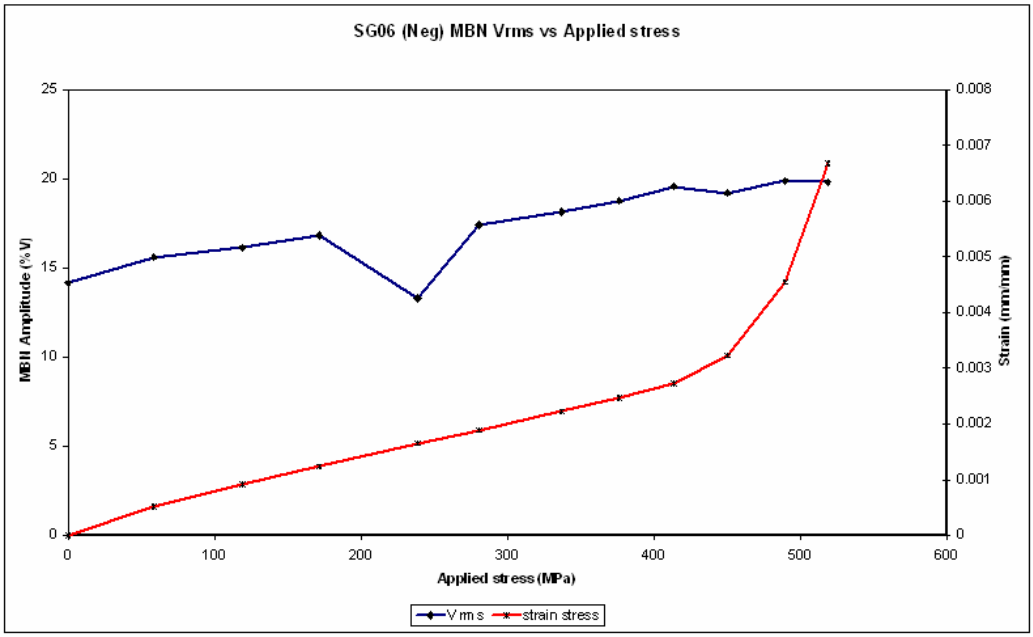

Figure 89: Variation of total stress with MBN Vrms for SG06

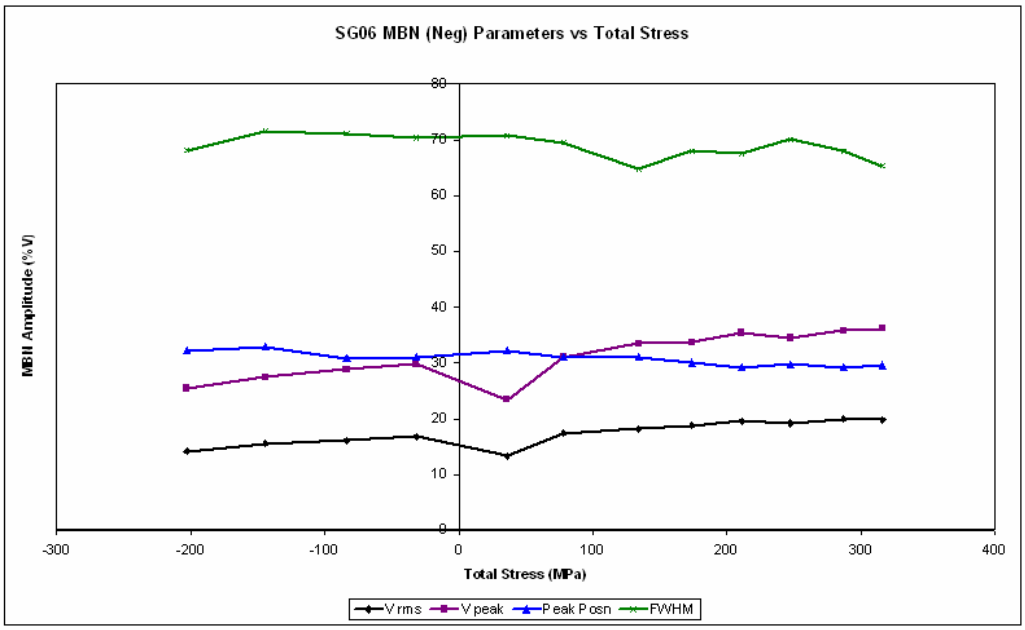

Figure 90: Total stress versus the MBN parameters for SG06

Appendix F: HG09 Calibration Charts

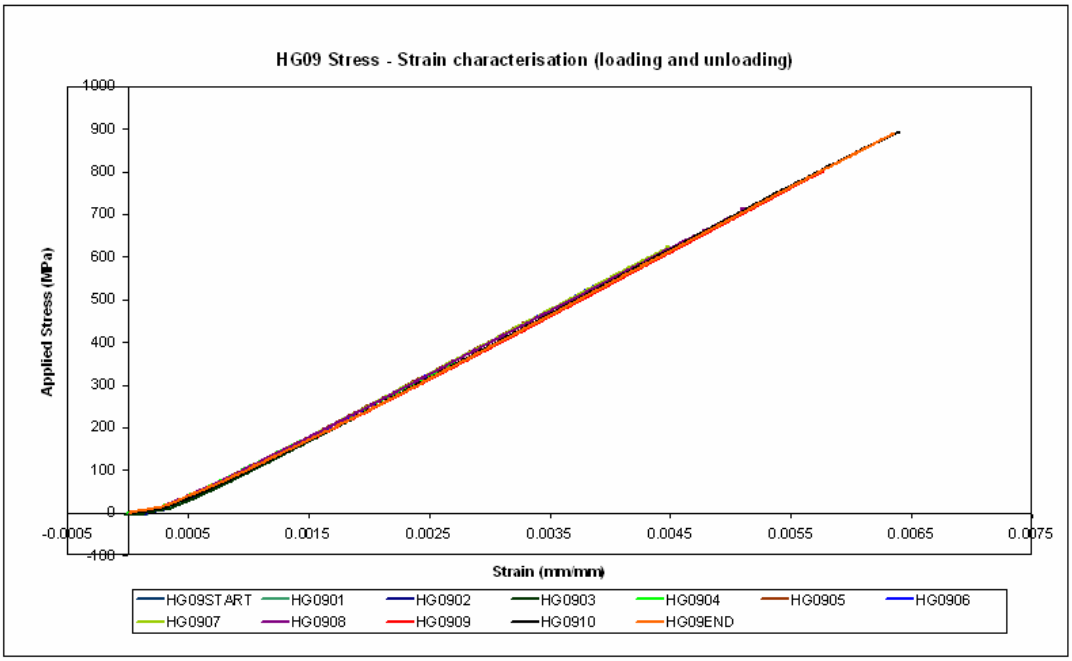

Figure 91: Stress - Strain curve for HG09 showing loading paths

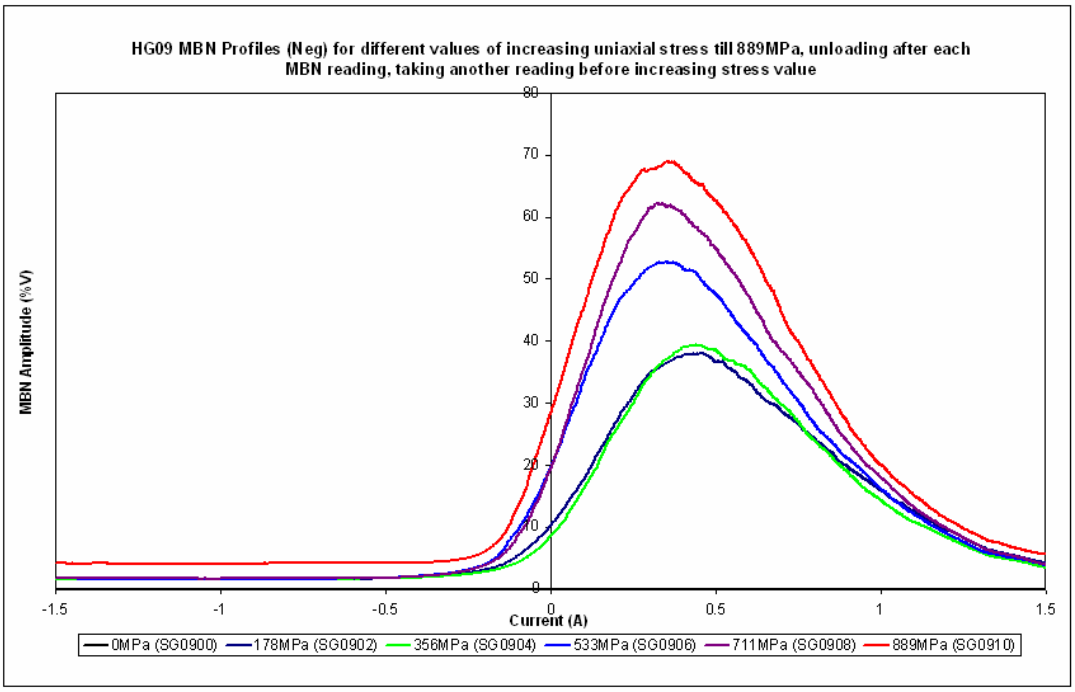

Figure 92: HG09 MBN profiles of selected load point of calibration test

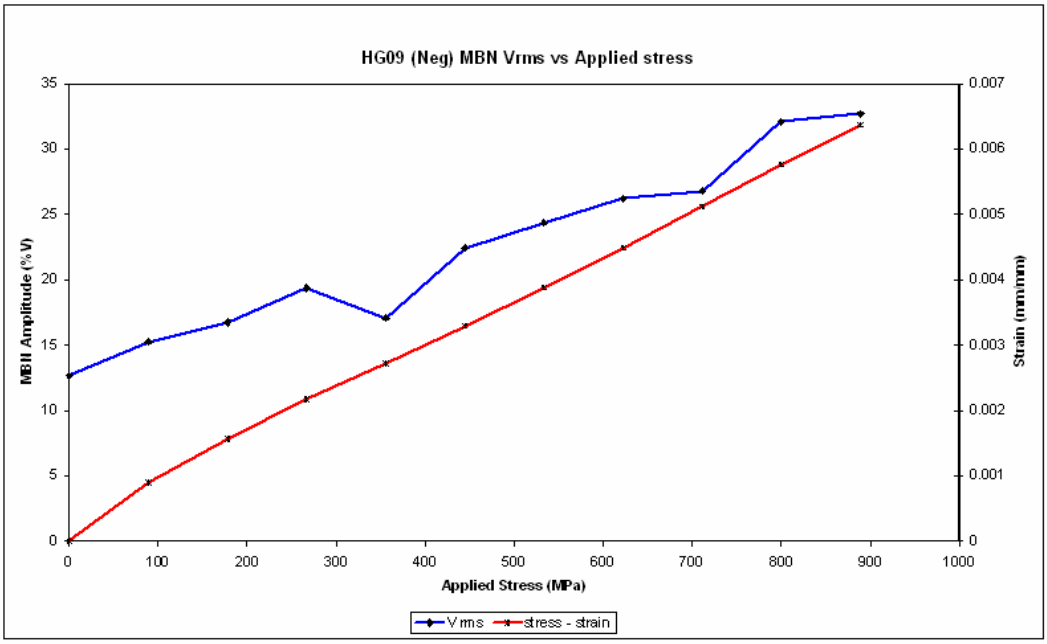

Figure 93: Variation of MBN Vrms with applied stress for HG09

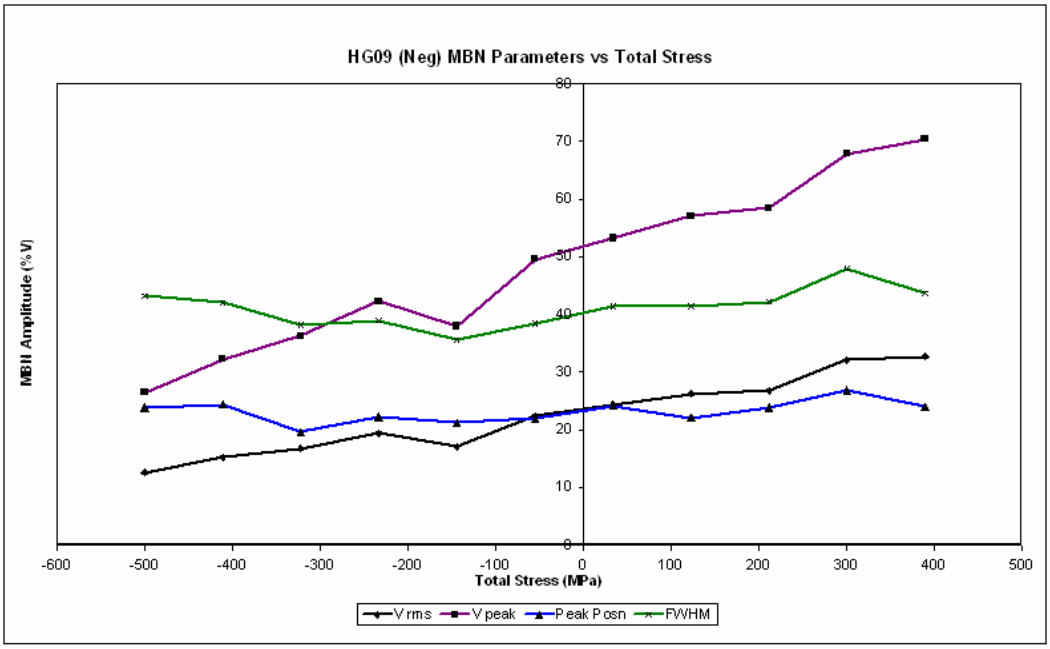

Figure 94: Variation of total stress with MBN parameters for HG09

Appendix G: Mineral Oil data

	m01		
	1st READING	2nd READING	AVERAGE
Vrms	41.44	20.4	30.92
Vpeak	73.19	37.29	55.24
PeakPos	30.25	29.13	29.69
FWHM	73.98	65.53	69.76
	m02		
	1st READING	2nd READING	AVERAGE
Vrms	22.2	21.51	21.86
Vpeak	43.52	40.56	42.04
PeakPos	27.14	29.91	28.53
FWHM	55.33	60.43	57.88
	m03		
	1st READING	2nd READING	AVERAGE
Vrms	20.26	20.13	20.20
Vpeak	37.48	36.1	36.79
PeakPos	30.17	34.06	32.12
FWHM	64.18	67.66	65.92
	m04		
	1st READING	2nd READING	AVERAGE
Vrms	24.06	25.02	24.54
Vpeak	46.28	48.25	47.265
PeakPos	25.43	25.69	25.56
FWHM	57.46	57.71	57.585
	m05		
	1st READING	2nd READING	AVERAGE
Vrms	18.98	19.18	19.08
Vpeak	33.47	33.98	33.725
PeakPos	32.32	30.87	31.60
FWHM	71.24	71.52	71.38

Appendix H: Water based fluid data

	PL01		
	1st READING	2nd READING	AVERAGE
Vrms	21.55	22.05	21.80
Vpeak	40.66	41.67	41.17
PeakPos	27.03	24.51	25.77
FWHM	59.73	59.96	59.85
	PL02		
	1st READING	2nd READING	AVERAGE
Vrms	19.13	19.74	19.44
Vpeak	34.91	35.97	35.44
PeakPos	24.09	25.8	24.95
FWHM	66.9	65.86	66.38
	PL03		
	1st READING	2nd READING	AVERAGE
Vrms	19.13	18.58	18.86
Vpeak	34.55	33.74	34.15
PeakPos	24.9	25.97	25.44
FWHM	65.86	65.95	65.91
	PL04		
	1st READING	2nd READING	AVERAGE
Vrms	19.75	18.92	19.34
Vpeak	37.54	35.69	36.62
PeakPos	29.91	31.51	30.71
FWHM	58.47	60.29	59.38